SYNTHESIS AND CHARACTERIZATION OF ZnO/SnO_2 NANOCOMPOSITE VIA A TWO STEP SPRAY PYROLYSIS ROUTE

Submitted By

WALIA BINTE TARIQUE

Roll No.: 0417142507F

Session: April, 2017

DEPARTMENT OF PHYSICS

BANGLADESH UNIVERSITY OF ENGINEERING AND TECHNOLOGY

DHAKA-1000, BANGLADESH.

SYNTHESIS AND CHARACTERIZATION OF ZnO/SnO_2 NANOCOMPOSITE VIA A TWO STEP SPRAY PYROLYSIS ROUTE

A dissertation submitted to the department of physics, Bangladesh University of Engineering and Technology, Dhaka in fulfillment of the requirement for the degree of master of Science (M.Sc.) in physics.

Submitted By

WALIA BINTE TARIQUE

Roll No.: 0417142507F

Session: April, 2017

DEPARTMENT OF PHYSICS

BANGLADESH UNIVERSITY OF ENGINEERING AND TECHNOLOGY

DHAKA-1000, BANGLADESH.

BANGLADESH UNIVERSITY OF ENGINEERING & TECHNOLOGY (BUET), DHAKA

DEPARTMENT OF PHYSICS

Certification of Thesis work

The thesis titled **"SYNTHESIS AND CHARACTERIZATION OF ZnO/SnO_2 NANOCOMPOSITE VIA A TWO STEP SPRAY PYROLYSIS ROUTE"** submitted by **Walia Binte Tarique**, Roll No-0417142507F, Session: April/2017, has been accepted as satisfactory in partial fulfillment of the requirement for the degree of **Master of Science** (M.Sc.) in Physics on 7th May, 2019.

BOARD OF EXAMINERS

1. **Dr. Jiban Podder (Supervisor)** — Chairman
Professor
Department of Physics, BUET, Dhaka

2. **Dr. Md. Forhad Mina** — Member (Ex-Officio)
Head
Department of Physics, BUET, Dhaka

3. **Dr. Muhammad Rakibul Islam** — Member
Assistant Professor
Department of Physics, BUET, Dhaka.

4. **Dr. Mohammed Abdul Basith** — Member
Professor
Department of Physics, BUET, Dhaka.

5. **Dr. Rabindra Chandra Sinha** — Member (External)
Professor
Department of Physics
Jahangirnagar University, Saver, Dhaka.

CANDIDATE'S DECLARATION

It is hereby declared that this thesis or any part of it has not been submitted elsewhere for the award of any degree or diploma.

Signature of the candidate

Walia

Walia Binte Tarique

DEDICATED

TO

MY BELOVED PARENTS

ACKNOWLEDGEMENTS

First of all I am very much grateful to Almighty God who has given me the strength and opportunity to complete this research work.

I would like to express my sincere appreciation to my honorable supervisor **Professor Dr. Jiban Podder** for his wonderful guidance and tremendous support during my M. Sc study and research. I especially wish to thank him for the generosity he showed with his time. It seemed I could knock on his door any time I needed to discuss anything, and he was always willing to talk. He is a wonderful advisor who helped me go through all the difficulties that I encountered in my study, research, and even life. He is a great materials scientist. It is my great honor to be his student. What I learned from him will benefit my whole life.

I am thankful to **Professor Dr. Farhad Mina**, Head, Department of Physics, BUET, for providing me necessary facilities to carry out this research work.

I am very much grateful to **Dr. Muhammad Rakibul Islam** and **Mrs Mehnaz Sharmin**, Assistant Professor, Department of Physics, BUET, for their valuable teaching efforts and suggestions that helped quite a great extent in writing this thesis and preparing the presentation.

I would like to express my sincere thanks to all of the faculty members of the Department of Physics for their heartfelt cooperation to my thesis work. I also express my cordial thanks to my friends, well-wishers and all the staff members of the Department of Physics, BUET.

I wish like to thank **Professor Dr. Md. Abdul Matin**, Head, Department of Glass and Ceramic engineering, BUET, Dhaka for allowing to perform FESEM and XRD study.

I am thankful to the authority of BUET for giving me necessary permission and providing financial support for this research work.

I am also thankful to the authority of Ministry of Science of Science and Technology for giving National Science and Technology fellowship 2018-2019 in the sake of elevating my research work.

I acknowledge with thanks to the Bangladesh University of Engineering & Technology for giving me necessary permission and providing financial support to this thesis work.

Finally, I would like to express my gratitude and love from my heart my parents and other family members for their constant support and encouragement during this research work.

Abstract

Zinc oxide (ZnO), tin oxide (SnO_2) and bilayer ZnO/SnO_2 thin films have been prepared by spray pyrolysis method on a glass substrate. The surface morphological, structural, optical and electrical properties of the as-deposited pure ZnO, pure SnO_2 and bilayer ZnO/SnO_2 thin films are studied in details. Tin oxide (SnO_2) and Zinc oxide (ZnO) thin films have been deposited at substrate temperature 450°C and 300°C respectively. Bilayer ZnO/SnO_2 thin films have been synthesized with four different thicknesses of SnO_2 layer (200 nm, 250 nm, 300 nm and 350 nm) but constant thickness of ZnO.

The SEM micrographs of as-deposited films show uniform surface with comprised of dense nanoparticles. It is also observed that the surface morphology of the films are strongly dependent upon the thickness of the SnO_2 bottom layer. Fibrous and non-fibrous shaped observed on the whole substrate of the as-deposited bilayer ZnO/SnO_2 thin film at 400 nm thickness. When the thickness is increasing then fibrous shape of the films disappear gradually. The crystalline structure of the as-deposited pure ZnO, pure SnO_2 and bilayer ZnO/SnO_2 thin films were studied by X-ray diffraction (XRD). From the XRD data it is clear that the pure ZnO, pure SnO_2 and bilayer ZnO/SnO_2 thin films are polycrystalline nature. Where pure ZnO shown hexagonal wurtzite type crystal structure, pure SnO_2 shown tetragonal rutile crystal structure and bilayer ZnO/SnO_2 thin films have shown mixed faces of hexagonal wurtzite of ZnO and tetragonal rutile crystal structure of SnO_2. For bilayer ZnO/SnO_2 thin films the crystalline size is increasing with inreasing the thickness of SnO_2 layer, the intensity of (110) peak of SnO_2 substantially increases indicating the good crystalline property of the double layered films.

It is also observed from AFM that the three dimensional view of the films shown the growth of the film takes place with closely placed sharp peaks and valleys. The surface roughness of the bilayer ZnO/SnO_2 film increases with increasing thickness of SnO_2 and the behavior is strongly reflected in the dependence of RMS values on the film thickness. The optical transmittance for pure ZnO is 92% and pure SnO_2 is 83%. In the case of bilayer ZnO/SnO_2 thin films the transmittance decrease with increasing the thickness of SnO_2 layer. The optical

direct band gap for pure ZnO is 3.38, for pure SnO_2 is 3.68 and for bilayer thin films bandgap varies from 3.47 to 3.64 eV.

Hall effect measurement has revealed that all of the films have n-type carrier concentration and in the case of bilayer thin films carrier concentration increase with increasing thickness of SnO_2 layer. The electrical study of the deposited films confirms that the temperature dependent resistivity's of the deposited bilayer ZnO/SnO_2 films are decreasing with with increasing thickness of SnO_2 layer and also showed its semiconducting nature in all the films. Moreover, the sheet resistance of the deposited bilayer ZnO/SnO_2 thin films are also decreasing with with increasing thickness of SnO_2 layer. This study reveals that bilayer ZnO/SnO_2 thin film can be used for gas sensing application and other opto-electronic devices more effectively.

Contents **Page No**

Declaration		ii
Dedication		iii
Acknowledgements		iv
Abstract		vi
List of figure		xi
List of tables		xiii
	CHAPTER-ONE: GENERAL INTRODUCTION	**(2-21)**
1.1	Introduction	2
1.2	Importance of transparent conducting oxides (TCO's)	3
1.3	Application of conducting oxides (TCO's) thin films	4
1.4	Zinc Oxide (ZnO)	6
	1.4.1 Physical properties of ZnO	6
	1.4.2 Crystal structure of ZnO	7
1.5	Tin (IV) Oxide (SnO_2)	8
	1.5.1 Physical properties of SnO_2	9
	1.5.2 Crystal structure of SnO_2	9
1.6	Multilayer thin film and its application	10
1.7	Literature reviews	13
	1.7.1 ZnO thin films	13
	1.7.2 SnO_2 thin films	14
	1.7.3 ZnO/SnO_2 bilayer thin films	15
1.8	Aim of the present work	17
1.9	Outline of this thesis	18
	References	19
	CHAPTER-TWO: THIN FILM DEPOSITION PROCESSES AND ITS FORMATION	**(23-49)**
2.1	Introduction	23
2.2	Classification of Thin Films Deposition Techniques	23
	2.2.1 Physical Techniques	25
	2.2.1.1 Evaporation	25
	2.2.1.2 Sputtering	27
	2.3.1.3 Physical Vapor Deposition (PVD)	29
	2.3.1.4 Pulsed Laser Deposition (PLD)	29
	2.2.2 Chemical deposition Techniques	31
	2.2.2.1 Atmospheric-Pressure CVD (APCVD)	31

2.2.2.2 Metal-Organic CVD (MOCVD) 31
2.2.2.3 Plasma-Enhanced CVD (PECVD) 31
2.2.2.4 Atomic Layer Deposition (ALD) 32
2.2.3 Wet Chemical Techniques 33
2.2.3.1 Chemical Bath Deposition (CBD) 34
2.2.3.2 Spin coating 36
2.2.3.3 Spray pyrolysis 37
2.3 Thin Film Formation 41
2.3.1 Thin Films Growth Modes 41
2.3.2 Condensation 43
2.3.3 Nucleation 44
2.3.4 Growth Stages 44
2.3.4.1 Nucleation stage 45
2.3.4.2 Island stage 45
2.3.4.3 Coalescence stage 46
2.3.4.3 Channel, hole and continuous film stages 46
2.3.5 Factors affecting the growth, structure and film properties 47
Reference 48

CHAPTER THREE: THIN FILM CHARACTERIZATION TECHNIQUES (52-83)

3.1 Introduction 52
3.2 Structural Characterization 52
3.2.1 X-ray diffraction 52
3.3 Surface Morphology 55
3.3.1 Scanning Electron Microscopy (SEM) 55
3.3.2 Principles of Scanning Electron Microscopy (SEM) 56
3.3.3 Atomic Force Microscopy (AFM) 59
3.4 Optical Characterization 61
3.4.1 UV-VIS spectroscopy 61
3.4.2 Optical characterization of thin films 62
3.4.3 Beer-Lambert law 63
3.4.4 Derivation of the Beer-Lambert law 64
3.4.5 Electronic transitions 65
3.4.6 Direct and indirect optical transition 68
3.4.7 Refractive index and extinction coefficient 69
3.4.8 Absorption coefficient 71
3.5 Thickness measurement of thin film 72

3.6	Electrical Characterization	74
	3.6.1 Direct method	74
	3.6.2 Two point probe method	75
	3.6.3 Four point probe method	75
	3.6.4 Van der pauw method	77
	3.6.5 Hall Effect Measurement	79
	3.6.6 Activation energy	81
	References	82

CHAPTER FOUR: EXPERIMENTAL DETAILS (85-95)

4.1	Preparations of Thin Films	85
4.2	Experimental details	85
	4.2.1 Preparation of masks	85
	4.2.2 Heater	86
	4.2.3 The design of the reactor	86
	4.2.4 The fume chamber	87
	4.2.5 Air compressor	87
	4.2.6 Spray nozzle	87
4.3	Substrate and Substrate Cleaning	88
4.4	Working Solution	89
4.5	Deposition Parameters	89
4.6	Rate of deposition	90
4.7	Thickness control	90
4.8	Steps of thin film processes	90
4.9	Sample Deposition	91
	References	94

CHAPTER FIVE: RESULTS AND DISCUSSION (97-125)

5.1	Introduction	97
5.2	Surface Morphology	97
	5.2.1 Pure ZnO	97
	5.2.2 Pure SnO_2	98
	5.2.3 Bilayer ZnO/SnO_2	98
5.3	X-ray Diffraction Analysis	102
5.4	Atomic Force Microscopy (AFM)	108
5.5	Optical Properties	112
	5.5.1 Transmittance	112
	5.5.2 Absorbance	113
	5.5.3 Absorption coefficient	114

5.5.4 Determination of optical band gap 115
5.5.5 Extinction coefficient 118
5.5.6 Refractive Index 119
5.6 Electrical Properties 120
5.6.1 Hall effect measurement 120
5.6.2 Variation of Resistivity and Conductivity with temperature 121
5.6.3 Variation of sheet resistance with temperature 123
References 124

CHAPTER 6: CONCLUSIONS AND SUGGESTION FOR FUTURE WORK **(127-129)**

6.1 Conclusions 127
6.2 Suggestions for future work 129

Fig. No **LIST OF FIGURES** **Page No**

1.1 The stable wurtzite structure of zinc oxide 8
1.2 Tetragonal rutile structure of SnO2 10
2.1 Schematic of thermal evaporation 27
2.2 A diagram of a sputtering system 28
2.3 A diagram of physical vapor deposition technique 29
2.4 A diagram of pulsed laser deposition system 30
2.5 A diagram of a Plasma Enhanced CVD (PECVD) system 32
2.6 A diagram of an Atomic Layer Deposition (ALD) system 34
2.7 A diagram of CBD method 35
2.8 A diagram of spin coating technique 36
2.9 A diagram of spray pyrolysis technique 38
2.10 Schematic illustration of the three different modes of growth 42
2.11 The stages of the film growth 45
2.12 Coalescence of two supercritical nuclei and Shape change during coalescence 46
3.1 Reflection of X-rays from two planes of atoms in a solid 53
3.2 Schematic diagram of a scanning electron microscope 57
3.3 A field emission scanning electron microscope set up 58

3.4	Block diagram of atomic force microscope	59
3.5	The components of a typical spectrometer	62
3.6	Absorption of light by a sample	64
3.7	Vibrational and rotational energy	66
3.8	Possible electronic transitions	66
3.9	Schematic presentation of direct and indirect transitions between valence and conduction band	68
3.10	Refraction of light at the interface between two different refractive indices media	69
3.11	Interferometer arrangement for producing refection Fizeau fringes of equal thickness	73
3.12	Electrical resistivity measurement by two point probe method	75
3.13	The arrangements of four probes that measure voltage (V) and supply current (I) to the surface of the crystal	76
3.14	experimental arrangements for measuring resistivity by using Van der Pauw method	77
4.1	Mask for the sample	85
4.2	Experimental setup of spray pyrolysis technique	87
4.3	Steps of thin film processes	91
4.4	Experimental set up of Spray Pyrolysis unit at the Department of Physics, BUET	92
4.5	Deposited single layer thin films (a) ZnO(200nm) (b) SnO_2 (200nm) (c) SnO_2 (250nm) (d) SnO_2 (300nm) and (e) SnO_2 (350nm)	93
4.6	Deposited bilayer thin films (a) ZnO/SnO_2 (400nm) (b) ZnO/SnO_2 (450nm) (c) ZnO/SnO_2 (500nm) (d) ZnO/SnO_2 (550nm)	93
5.1(a)	FESEM image (X10 k) of ZnO thin film deposited at the Ts of 300 °C	97
5.1(b)	FESEM image (X10 k) of SnO_2 thin film deposited at the Ts of 450 °C	98
5.2(a)	FESEM image (X10 k) of bilayer ZS1 (for ZnO=200 nm; SnO_2=200nm thicknesses) thin film	99
5.2(b)	FESEM image (X10 k) of bilayer ZS2 (for ZnO=200 nm; SnO_2=250nm thicknesses) thin film	100
5.2(c)	FESEM image (X10 k) of bilayer ZS3 (for ZnO=200 nm; SnO_2=300nm thicknesses) thin film	100
5.2(d)	FESEM image (X10 k) of bilayer ZS4 (for ZnO=200 nm; SnO_2=350nm thicknesses) thin film	101
5.3(a)	Cross-sectional FESEM image (×10 k) of bilayer ZS1 thin film	101
5.3(b)	Cross-sectional FESEM image (×10 k) of bilayer ZS2 thin film	102
5.4(a)	XRD pattern of pure ZnO	103
5.4(b)	XRD patterns of pure SnO_2 thin films	104
5.4(c)	XRD patterns of bilayer ZnO/SnO_2 thin films	105

5.5(a) Variations of grain size and strain with film thickness 107
5.5(b) Variations of grain size and dislocation density with film thickness 107
5.6.1 AFM image of pure ZnO 109
5.6.2 AFM image of pure SnO_2 109
5.6.3 AFM image of bilayer ZnO/SnO_2 for (ZnO=200; SnO_2=200) thickness 110
5.6.4 AFM image of bilayer ZnO/SnO_2 for (ZnO=200; SnO_2=250) thickness 110
5.6.5 AFM image of bilayer ZnO/SnO_2 for (ZnO=200; SnO_2=300) thickness 111
5.6.6 AFM image of bilayer ZnO/SnO_2 for (ZnO=200; SnO_2=350) thickness 111
5.7 Transmittance vs. wavelength of pure ZnO, pure SnO_2 and bilayer ZnO/SnO_2 thin films 113
5.8 Absorbance vs. wavelength of pure ZnO, pure SnO_2 and bilayer ZnO/SnO_2 thin films 114
5.9 Variation of absorption coefficient with wavelength for pure ZnO, pure SnO_2, and bilayer ZnO/SnO_2 thin films 115
5.10 Plots of $(\alpha h\upsilon)^2$ vs. $h\upsilon$ of pure ZnO, SnO_2 and bilayer ZnO/SnO_2 thin films 117
5.11 Variation of extinction coefficient with wavelength for pure ZnO, pure SnO_2 and bilayer ZnO/SnO_2 thin films 119
5.12 Variation of refractive index with wavelength for pure ZnO, pure SnO_2 and bilayer ZnO/SnO_2 thin films 120
5.13 Variation of resistivity with temperature for pure ZnO, pure SnO_2 and bilayer ZnO/SnO_2 thin films 122
5.14 Variation of resistivity with temperature for pure ZnO, pure SnO_2 and bilayer ZnO/SnO_2 thin films 122
5.15 Variation of sheet resistance with temperature for pure ZnO, pure SnO_2 and bilayer ZnO/SnO_2 thin films 123

List of Tables **Page No**

Table 1.1 Application of (TCOs) Thin Film 4
Table 5.1 Structural parameters of pure ZnO, pure SnO_2, bilayer ZnO/SnO_2 thin films 108
Table 5.2 Roughness vaues of pure ZnO, pure SnO_2, bilayer ZnO/SnO_2 thin films 112
Table 5.3 Bandgap of pure ZnO, pure SnO_2 and bilayer ZnO/SnO_2 thin films 118
Table 5.4 Hall effect measurement of pure ZnO, pure SnO_2 and bilayer ZnO/SnO_2 thin films 121

CHAPTER ONE

GENERAL INTRODUCTION

CHAPTER ONE

GENERAL INTRODUCTION

1.1 Introduction

The development of modern society purely depends on the advancement of technology, which in turn is not possible without technological progress in the field of thin films science. Thin film technology is the basis of outstanding development in solid state electronics in modern technology. Thin film studies have exploited the unique characteristics in the terms of thickness, structure and geometry of the thin films. Experimental work on thin films has been continued in different parts of the world for successful applications of their properties in scientific, engineering and industrial purposes. The increasing demands for microelectronics and micro structural components in different branches of science and technology have greatly expanded the sphere of thin film research [1-2].

A thin film is a layer of material ranging from fractions of a nanometer (monolayer) to several micrometers in thickness. When a thin layer of solid material is formed on a solid substrate and if the layer thickness becomes comparable in magnitude with a mean free path of the conduction electrons of solid material then is termed as "thin film". Thin films behave differently from bulk materials of the same chemical composition in several ways. For instance, thin films are sensitive to surface properties while bulk materials generally aren't. Thin films are also relatively more sensitive to thermo-mechanical stresses [3]. Additional functionality in thin films can be achieved by depositing multiple layers of different materials. The multilayer thin films can behave as completely new engineered materials, unknown in bulk form. When multiple layer in is combined with the lithographic pattern in the plane of the films, then a variety of microstructure can be constructed (e.g. Basic technology of IC technology industry, optical waveguide, micromechanical devices etc.) [4]. Thin films have a number of applications in various fields. Few of them are A.R. coating, interference filters, polarisers, narrow band filters, solar cells, photoconductors, IR detectors, waveguide coatings. Temperature control of satellites, photo thermal solar coatings such as black chrome, nickel, cobalt etc., magnetic films, superconducting films,

anticorrosive films, microelectronics devices, diamond films, reduction of fabrication through coating or surface modification i.e. epitaxy and heterostructure films, high temperature wear resistance films, hard coatings etc.

Transparent conducting oxides (TCOs) are a special class of materials that can simultaneously be both optically transparent and electrically conducting and, as such, are a critical component in almost all thin-film photovoltaic devices. TCOs are generally based on a limited class of metal oxide semiconductors such In_2O_3, ZnO, SnO_2 and CdO, which are transparent due to their large band gap. Studies of these highly conducting semiconductors have attracted the interest of many researchers because of their wide applications in both industry and research. The present research work is aimed at the production of uniform, conductive bilayer ZnO/SnO_2 nanocomposite thin films by a low cost technique using a precursor solution of $Zn(CH_3COO)_2.2H_2O$ and $SnCl_2.2H_2O$ respectively.

1.2 Importance of transparent conducting oxides (TCOs)

An oxide material exhibits both transparent and conducting properties is known as the transparent conducting oxides (TCOs). The basic electromagnetic theory does not permit a material to be transparent and conducting simultaneously. Maxwell's electromagnetic theory demands that no material can be both transparent and conducting simultaneously. For example, copper or silver cannot be transparent, NaCl, CaF_2, In_2O_3 cannot conduct. So, in order to get a material which is to be a transparent conductor, mix a metal oxide with a metal.

Researchers have explored the use of TCO which exhibit unique properties, including excellent carrier mobilities, mechanical stress tolerance, compatibility with organic dielectric and photoactive materials, and high optical transparency. Transparent conducting oxide films play an important role in the construction of solar cells. They act as a window layer as well as conducting electrodes. The widely used transparent conducting oxide films for various types of solar cells are SnO_2, In_2O_3, Cd_2SnO_4, CdO and ZnO. The first transparent conducting oxide thin film was reported by Badeker [5] in 1907; cadmium oxide

(CdO) prepared by thermally oxidizing a vacuum sputtered film of cadmium metal. Since then, TCOs have received a great attention because of their various technological applications. Post-oxidation of evaporated metal films to form the metal oxide was one of the earliest deposition methods for TCOs. Tin oxide (SnO_2) was deposited by Baur in the year 1937. Transparent conductive indium oxide was first prepared by post-oxidation of metal thin films in 1954. The co-existence of electrical conductivity and optical transparency in these materials depends on the nature, number and atomic arrangements of metal cations in crystalline or amorphous oxide structures, on the resident morphology and on the presence of intrinsic or intentionally introduced defects [6].

1.3 Application of (TCOs) thin films

Thin films are deposited onto bulk materials (substrate) to achieve properties unattainable or not easily attainable in the substrates alone. Table 1.1 divides these properties into five basic categories and gives examples of typical applications within each category.

Table 1.1 Application of (TCOs) Thin Film

Thin film property category	Typical application
Optical	• Antireflection coatings ("Multicoated optics"). • Highly reflecting coatings (laser mirrors). • Interference filters. • Beam splitter and thin film polarizers.

Engineering/processing	• Tribological Applications: Protective coatings to reduce wear corrosion and erosion, low lriction coatings. • Hard coatings for cutting tools • Surface passivation • Protection against high temperature corrosion • Self-supporting coatings of refractory metals for rocket nozzles, crucibles, pipes. • Decorative coatings • Catalyzing coatings
Optoelctronics	• Photodetectors • Image transmission • Optical memories • LCD/TFT
Electronics	• Passive thin film elements (Resistors, Condensers, Interconnects) • Active thin film elements (Transistors, Diodes) • Integrated Circuits (VLSI, Very Large Scale Integrated Circuit) • CCD (Charge Coupled Device)
Magnetic Applications	• Audio, video and computer memories • Magnetic read/write heads
Sensor application	• Data acquisition in aggressive environments and media Telemetry • Biological Sensors.

Biomedicine	• Biocompatible implant coatings • Neurological sensors • Claddings for depot pharmacy
Alternative Energies	• Solar collectors and solar cells • Thermal management of architectural glasses and foils • Thermal insulation (metal coated foils)
Cryotechnics	• Superconducting thin films, switches, memories • SQUIDS (Superconducting Quantum Interference Devices)

1.4 Zinc Oxide (ZnO)

Zinc oxide (ZnO) nanoparticles are semiconducting oxide, dielectric, transparent, piezoelectric material with a direct band gap of 3.37 eV at room temperature and a large excitation binding energy (60 meV), that is 2.4 times the effective thermal energy (K_BT =25 meV) and de-excitation vitality is 15 meV. This is one of the important parameters that exhibits near UV discharge and resistance to high temperature electronic degradation. It is generally utilized as a catalyst, piezoelectric traducer and photonic material. Also, it is utilized as an element for a variety of applications such as heat resisting glass, spacecraft defensive coating, a constituent of cigarette channels, color in paints with UV-defensive and fungistatic properties, an added substance for elastic and plastics, recovering unguents and an optical waveguide etc. [7].

1.4.1 Physical properties of ZnO

The standard values relating to the physical properties of ZnO are mentioned below:-
(a) Others names: Zinc white, calamine, philosopher's wool, Chinese white, flowers of zinc
(b) Chemical formula: ZnO, Inorganic
(c) Molar mass: 81.38 g/mol

(d) Appearance: White solid

(e) Density: 5.606 g/cm^3

(f) Melting point: 1,975°C

(g) Band gap: 3.37 eV (Direct bandgap)

(h) Crystal structure: Wurtzite

(i) Refractive index: 2.0041

1.4.2 Crystal structure of ZnO

ZnO has three possible crystal structures: hexagonal wurtzite, cubic zinc blende or cubic rock salt. Under ambient conditions, the wurtzite structure is the most thermodynamically stable (Fig. 1.1).The lattice constants are a = 3.25 and c = 5.2 and the ratio c:a is approximately 1.60 which is close to the ideal value for hexagonal cell c:a = 1.633. The bonding in ZnO is largely ionic. This is consistent with the fact that most group II-VI materials show large ionic bonding in oxides. The radii are about 0.074 nm for Zn^{2+} and 0.140 nm for O^{2-} in case of ZnO. This large ionic bonding property is responsible for the stable wurtzite structure rather than zinc blende. The strong piezoelectricity of ZnO is also the result of large ionic bonding. Stable ZnO wurtzite structure which can be used to generate highly ordered materials; allowing growth along the c-axis to create a three-dimensional array of highly oriented ZnO nanorods. These nanorods provide a continuous electron channel that improves charge transport. These kinds of nanoscale oxides are strong electron acceptors with high electron affinities and electron mobilities [8]. Crystal growth along the (002) orientation is preferred because the (002) plane possesses the minimum surface energy. Preferential growth of the (101) and (100) orientations has however also been reported. Intrinsic ZnO is typically a n-type semiconductor due to oxygen vacancies.

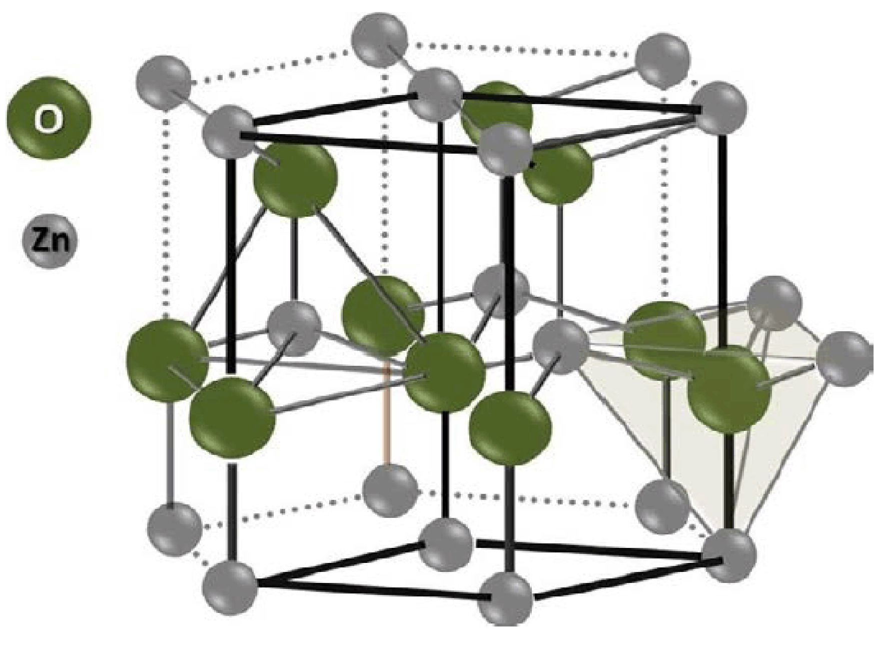

Figure 1.1: The stable wurtzite structure of zinc oxide

1.5 Tin (IV) Oxide (SnO_2)

Tin (IV) oxide (stannic oxide), SnO_2, is probably the simplest of the TCOs and the most attractive since tin is less expensive and more abundant than others. Furthermore, SnO_2 is environmentally stable and has good mechanical strength. Another property of SnO_2 is that although it is transparent in the visible, it is reflective for infrared light. This property is responsible for the use of SnO_2 as an energy conserving material. SnO_2 is a n-type wide bandgap semiconducting material with wide direct bandgap energy of 3.6 eV and indirect bandgap of 2.6 eV, where inherent oxygen vacancies act as an n-type dopant. This properties of SnO_2 makes it an excellent material for transparent electrodes, solar cells, anodes for lithium ion batteries and other important applications [9].

1.5.1 Physical properties of SnO_2

The standard values relating to the physical properties of SnO_2 are mentioned below:-

(a) Others names: Stannic oxide, Stannic Anhydride, Flowers of tin, Cassiterite

(b) Chemical formula: SnO_2, Inorganic

(c) Molar mass: 150.71 g/mol

(d) Appearance: White or light gray powder

(e) Density: 6.95 g/cm^3 (20°C)

(f) Melting point: 1,630°C

(g) Band gap: 3.6 eV (Direct bandgap)

(h) Crystal structure: Rutile tetragonal

(i) Refractive index: 2.006

1.5.2 Crystal structure of SnO_2

SnO_2 is also called Cassiterite and the most common form of SnO_2 is tetragonal rutile. It possesses the same rutile structure as many other metal oxides, e.g. TiO_2, RuO_2, GeO_2, MnO_2, VO_2, IrO_2, and CrO_2. The rutile structure has a tetragonal unit cell with a space-group symmetry of $P4_2/mnm$. The unit cell contains two tin atoms and four oxygen atoms with lattice constants $a = b = 4.737$ Å and $c = 3.185$ Å, where $\alpha = \beta = \gamma = 90$. Each tin atom is surrounded by six oxygen atoms which are coordinated in an octahedral manner and each oxygen atom is neighbored by three tin atoms, essentially forming an equilateral triangle (Fig:1.2). Thus, the structure has 6:3 coordination. The ionic radii for Sn^{4+} and O^{2-} are 0.69 Å and 1.24 Å, respectively. In its stoichiometric form SnO_2 is an insulator, thus its conductivity arises due to non-stoichiometry. SnO_2 can also be doped with various elements to improve its functional properties such as Sb or F to enhance its conductivity, and Ag or Pd to improve its gas sensitivity [10].

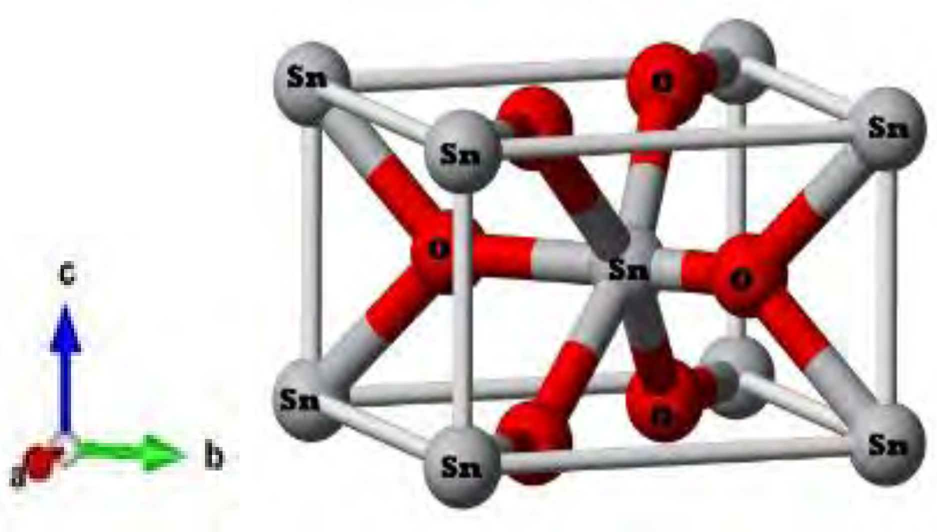

Figure-1.2: Tetragonal rutile structure of SnO_2

1.6 Multilayer thin film and its applications:

Multilayer thin films consist of alternating layer of two different materials. In case of bilayers, the first layer appears as a substrate for the second layer. The multilayer structure typically contains several times repeats of a bilayer unit cell that is characterized by a spatial repeat length or period of a nanometer or greater. Multilayers have been widely studied because their properties differ from those of their bulk constituents owing to the two dimensional structure of the film, the high density of interfaces, and the possibility of interactions between the layers. Unlike the doped semiconductors, multilayer films have a broad wavelength tunability which gives an optical response that is desired for a particular application. They consist of a stack of alternating layers of materials having high and low refractive index respectively and operate on the basis of optical interference. Its reflectance usually depends on the constructive or destructive interference of light reflected at successive boundaries of different layers of the stack. The interface formed between the alternating layers has a great influence on the performance of the multilayer devices [11]. Therefore the appropriate sequencing of the layers of suitable materials and their thicknesses is crucial for achieving the desired spectral response and application. Multilayer

thin films are widely used in today's technology and their applications are expected to be even more widespread in the future. Some application of the multilayer thin film in the present time is given bellow:-

a) Optical coatings

An optical coating is composed of a combination of thin film layers that create interference effects used to enhance transmission or reflection within an optical system. The performance of an optical coating is dependent upon the number of layers, the thickness of the individual layers and the refractive index difference at the layer interface. Many common types of coating are used in precision optics, including anti-reflection (AR) coating, high reflective (Mirror) coating, beam splitter coating, and filter coating such as shortpass, longpass, and notch filters. Anti-reflection coatings are included on most refractive optics and are used to maximize throughput or across a broad range of wavelengths and are most often used to create mirrors. The beam splitter coatings are used to divide incident light into known transmitted and reflected light outputs. Filters are found in a large number of life science and medical applications and are used to transmit, reflect, absorb, or attenuate light at specific wavelengths.

b) Solar cell

Solar energy can be utilized in various ways either in stored energy in the forms of fossil fuels and nuclear power (called non-renewable energy), or directly from sources such as wind, tidal, photovoltaic/thermal, biomass and hydro-power (called renewable energy). Renewable energies are clean, environmentally friendly and endless in supply. Among all the renewable energies, photovoltaic (PV) technology is the best because it converts the sun's rays directly into electricity without involvement of moving parts or emitting pollutants. TCO materials play an integral part of the photovoltaic industry as they serve as the transparent electrode for thin film solar cells such as amorphous silicon solar cells, dye synthesized solar cells (DSSCs) and organic based photovoltaic devices. Multilayer thin films are particularly useful in that they are transparent to visible light and thin layers are easily fabricated on a large scale via online processes. The absorption of light can be increased efficiently by using multi-layered cells. It is reported that a theoretical conversion

efficiency of 86.6% can be achieved using a multi-layer structure. Efficiencies of 32.6% and 43.5% have been achieved using two and three junction solar cells respectively [12]. Materials with different bandgaps are used, with each layer absorbing a different range of energies of photons. High energy photons are absorbed at the front of solar cell structure which is made of wide bandgap energy and at the rear of this structure absorption of lower energy photons take place. Two ways of getting this structure are by connecting them in series or parallel respectively

c) Gas sensor

Gas sensing technologies can be broadly classified into electrochemical, optical and chemoresistive. While optical sensing TCOs has received some interest, the affordability and simplicity in manufacture, have accounted for the widespread use of chemoresistive multilayer based sensors. The multilayer gas sensor works on the principle that a measurable change in the resistivity or electrical conductivity occurs on exposure of the thin layer films to a target gas which acts as either a donor or an acceptor of electrons [13]. The most common solid state metal oxide gas sensors are based on the materials: SnO_2, ZnO, TiO_2, Cr_2O_3 and WO_3 with sensitivities as low as ppm and even ppb for some gases.

d) Heat control filters

One type of multilayer mirror, called a cold mirror, is used to reflect the visible light and transmit the infrared. The cold mirror reflects the visible light towards the film, but permits the heat in the infrared to pass out the back. This system is even more efficient if a heat reflector is inserted between the arc and the film. This reflector which has a high transmission in the visible spectral region but a high reflectivity in the infrared, reflects the heat away from the film but permits the visible light to pass through to the film with little attenuation. Another type of heat control filter is the cover glass which is placed over solar cells which are used to power a space vehicle. These cover glasses are designed to reflect the radiant energy at wavelengths longer than 1.2µ. The radiant energy from the sun in the wavelength range from 1.2µ to 2.5µ does not generate power, but only increase the temperature of the solar cells, thereby decreasing its efficiency.

1.7 Literature reviews

1.7.1 ZnO thin films

Islam et. al.[14] have found High purity ZnO films of different thicknesses were prepared using a Spray Pyrolysis deposition system at relatively low temperature (200 °C) and studied the effect of surface morphology and optical properties of the as deposited thin films . From SEM study was observed nano fiber structure the undoped ZnO thin films. Sahay et al [15] were prepared ZnO thin films by spray pyrolytic decomposition of zinc acetate onto glass substrate. These films were analyzed for the optical and electrical properties. Optical studies show that in these films the electronic transition is of the direct transition type. The optical energy gap for the film of different thicknesses is estimated to be in the range 2.98-3.09 eV. Electrical studies indicate that the films exhibit thermally activated electronic conduction and the activation energies are found to be dependent on the film thickness. The complex impedance measurement was carried out over a wide range of frequencies at room temperature. All the impedance spectra contain only a single arc, but the arc has a non-zero intersection with the real axis in the high frequency region. Also, the arc has its center lying below with the real axis which indicates the multi-relaxation behavior of the films. Kumar et al. [16] prepared polycrystalline ZnO thin films on glass substrate at the substrate temperature of 250 °C using aqueous solution of zinc acetate by SPT. The result of XRD clearly revealed polycrystalline nature of ZnO films with hexagonal wurtzite structure with the (0 0 2) preferential orientation. The films exhibited excellent optical properties with transmittance of about 80 %, low absorbance and reflectance in the visible region. Refractive index, extinction co-efficient and energy band gap were calculated and the developed films had a direct band gap value of 3.2 eV. Godbole et. al. [17] prepared ZnO thin films on glass substrates by SPT at the substrate temperature of 400 °C. They characterized ZnO thin films of different thicknesses by X-ray diffraction (XRD) and atomic force microscopy (AFM). They found polycrystalline nature of the thin films in XRD analysis. The grain size decreased and roughness of the film increased with the increase the film thickness. From the resistivity-temperature measurements they found that the activation energy decreased with the increase in thickness of the film. Ilican S. et al. [18] have found polycrystalline of ZnO thin films using sol-gel spin coating. They have

reported grain size in the range of 25-32 nm. The interesting thing about this paper is that they have calculated I-V characteristics of ZnO thin films in dark and under UV light. Results showed that ZnO thin films are sensitive to UV light and hence can be used as window materials in photovoltaic applications.

1.7.2 SnO_2 thin films

Antonaia A. et al. [19] have found device quality, tin oxide polycrystalline layers deposited by spray pyrolysis technique have been characterized in terms of morphological, electrical and transport properties. The set of the investigated samples exhibit high values of the mobility (ranging between 30 and 70 cm^2V^{-1} s^{-1}). The behaviour of the mobility, reported as a function of the carrier concentration and of the size of the crystallites, reveals a transport governed by the processes at the grain boundaries. Furthermore, the behaviour of the mobility with the temperature strongly suggests a transport mechanism determined by tunneling of the potential barrier existing between the grains, and rules out the importance of the thermionic emission process. Allag Abdelkrim et al. [20] prepared tin oxide (SnO_2) thin films on glass substrates by using a home-made spray pyrolysis system. Effects of film thickness on the structural, optical, and electrical film properties are investigated. The films are characterized by several techniques such as x-ray diffraction (XRD), atomic force microscopy (AFM), ultravioletvisible (UV–Vis) transmission, and four-probe point measurements, and the results suggest that the prepared films are uniform and well adherent to the substrates. X-ray diffraction (XRD) patterns show that SnO_2 film is of polycrystal with cassiterite tetragonal crystal structure and a preferential orientation along the (110) plane. The calculated grain sizes are in a range from 32.93 nm to 56.88 nm. Optical transmittance spectra of the films show that their high transparency average transmittances are greater than 65% in the visible region. The optical gaps of SnO_2 thin films are found to be in a range of 3.64 eV–3.94 eV. Figures of merit for SnO_2 thin films reveal that their maximum value is about 1.15×10^{-4} Ω^{-1} at 550 nm. Moreover, the measured electrical resistivity at room temperature is on the order of 10^{-2} Ω-cm. Suresh Sagadevan et al.[21] prepared Zinc doped Tin oxide (SnO_2) nanoparticles by co-precipitation method. The formation of Zn-doped SnO_2 nanoparticles was confirmed by X-ray diffraction. The average crystallite sizes of pure and Zn-doped SnO_2 nanoparticles were found to be 11 and 14 nm.

The SEM revealed the morphology of the synthesized samples and it showed that Zn-doped SnO_2 nanoparticles were spherical in shape. Optical properties of the Zn-doped SnO_2 nanoparticles were investigated by using UV–Visible absorption spectrum. UV-visible absorption studies showed that the decrease of particle size was accompanied by decrease of the band gap value from 3.6 eV for SnO_2 down to 3.5 eV for Zn doping. Moholkar, A.V. et. al. [22] studied. Transparent conducting F:SnO_2 thin films have been prepared from $SnCl_4$ precursor solution on glass substrates of different thickness by the simple and low-cost spray pyrolysis technique. The film thickness varies from 740 to 1525 nm. The material in thin film form is polycrystalline with tetragonal structure and highly textured. The preferred orientation is in (2 0 0) direction and the grain sizes are calculated. It is also found that the lattice parameters remained unaffected with the substrate thickness. The average grain size is approximately 44 nm. The maximum texture coefficient for the typical thin film is 6.19. The lowest sheet resistance of 7.48 **Ω** is obtained for F:SnO_2 film. The figure of merit is of the order of 1.93×10^{-3} Ω^{-1} for the sample on 4mm thick substrate. The maximum conductivity of the order of 11.9 Ω^{-1} cm^{-1} is achieved for the same sample. The hall mobility of the order of 10 cm^2V^{-1} s^{-1} is obtained for 4mm substrate. The increasing trend of the standard deviation with an increase in substrate thickness suggests the increased number of grains along the preferred direction.

1.7.3 ZnO/SnO_2 bilayer thin films

Liu, J. et al. [23] studied the ZnO/SnO_2 heterostructure composites with a hollow structure were successfully synthesized through a solution phase route. The structural and morphological of the materials synthesized above were characterized by several technical methods. The results revealed that ZnO nanoparticles were dispersed homogeneously on the surface of SnO_2 hollow spheres. Such novel composites were utilized to fabricate promising gas sensor and it turned out to be an excellent sensing material with high response and low detection limits (even ppb-level) to ethanol. Moreover, the fabricated sensor showed commendable long-stability which gave the key evidence for the materials being applied in practices. The plausible gas-sensing mechanism was also discussed. R.A. Zargar et al. [24] have found ZnO/SnO_2 thick film has successfully fabricated by low-cost synthesis and the study of optical properties shows direct transition was performed from the optical

spectrum, variation of the optical constants with photon energy indicates that some interactions between photons and electrons in the films are produced in energy range studied. Reports suggests that this material might be practically useful for optoelectronic devices. Also, this novel structure may find utilizations where the environmental remediation can be totally implicated with clean energy. Omondi C A et al. [25] prepared bilayer configurations of nanocrystalline SnO_2 and ZnO thin films grown on ITO (Indium tin oxide) coated glass substrates by Spray Pyrolysis technique. The X-ray diffraction confirmed complete phase formation with tetragonal phase for both SnO_2 and ITO substrate. ZnO layer indicated Hexagonal (Wurtzite) phase. Scanning Electron Microscopy revealed a crystalline growth of bilayers and of individual films with particle sizes. Nonlinear behaviour was observed in ITO-ZnO-SnO_2 as well as in ITO-ZnO and ITO-SnO_2. This was due to p-n junction diode or Schottkey characteristics. Both ZnO and SnO_2 plays an important role in nonlinear behaviour of the bilayers and the bilayer shows a good photo-response since resistance decreased from dark to short UV, a quality which can be exploited in light sensing. Yaxin Cai et al. [26] have found Hierarchical and hollow cylinder comb-like nanostructures with ZnO backbones and SnO_2 branches which were successfully prepared by an ultrasonic spray pyrolysis process. A hollow cylinder comb consists of SnO_2 nanobranches and ZnO backbones with an overall thickness of about 500 nm. The time-dependent morphology evolution of ZnO/SnO_2 samples was studied in detail in order to explore the formation mechanism of such a novel structure. Moreover, the gas-sensing properties of our hierarchical ZnO/SnO_2-based sensor were tested, exhibiting high and quick response to ethanol at 275 °C. This suggests a simple method of making hetero-junctions between nanorods and nanowires for gas sensors. R. Anandhi et al. [27] prepared Fluorine doped tin oxide (SnO_2:F – FTO) layer over fluorine doped zinc oxide layer (ZnO:F – FZO) so as to get FTO/FZO bilayers with varying thickness proportions of the two layers using a simplified spray pyrolysis technique. The FTO/FZO film with thickness proportions 456:309 nm (≈3:2) is found to have least sheet resistance (2.6 Ω/m), which is two orders less than that of FZO films. The optical transparency is also reasonable (80%) for this case. The quality factor for this FTO/FZO double-layered film is $4.24 \times 10{-}2$ $(\Omega/m)^{-1}$, which is nearly three order greater than that of FZO films.

1.8 Aim of the present work

The spray pyrolysis method for the deposition of thin solid films is a good method for the preparation of thin films suitable for scientific studies and for many applications in technology and industry. This method is used for the preparation of thin films of the important semiconductors II-VI. In the recent years, the II-VI binary semiconductor nanomaterials have attracted much attention due to their potential technological applications such as storage devices, highspeed electronics, nanoelectronics, opto-electronic and solar cell devices. The knowledge of optical constants of materials is frequently of great interest in the design and analysis of materials to be used in optoelectronics. Moreover, optical measurements are extensively used for characterization of composition and quality of the materials. So, it is essential to have an insight into the optical properties, which include the optical band gap, reflectivity, absorption coefficient, the dielectric constant and the refractive index as a prerequisite in using the suitable material for device applications. The objectives of the present study are to synthesize ZnO, SnO_2 and ZnO/SnO_2 bilayer thin films by locally fabricated SP system and to characterize those thin films by using various experimental techniques. The effective combination of two different TCO layers and the variation of thickness SnO_2 layer on the structural, optical and electrical properties of the thin films is to be studied elaborately. It is expected that optically transparent and homogeneous thin films can be synthesized by using this low cost technique. These thin films may have expected electrical and optical properties to find applications in sensors, electronic and optoelectronic devices, etc.

1. To synthesize ZnO, SnO_2 and ZnO/SnO_2 bilayer thin films with different thickness of SnO_2 layer.
2. To study the surface morphology of the deposited thin films is to be studied by scanning electron microscopy field emission SEM (FESEM).

3. To analyze the structure of the deposited films by XRD.

4. To study surface roughness of the deposited films by atomic force microscopy (AFM)

5. To determine transmittance, absorbance, optical absorption coefficient, optical band gap, refractive index, dielectric constants etc. from UV-visible spectroscopy.

6. To determine the carrier concentration, mobility, conductivity etc. from hall effect measurement.

7. To measure DC electrical conductivity by liner four point probe method.

1.9 Outline of this thesis

This thesis contains six chapters. The general introduction of the thin films and materials with relevant literature survey is given in chapter 01. Thin film deposition processes and its formation are discussed in Chapter 02. The theoretical principle of thin film characterization and film thickness measurement are discussed in Chapter 03. In chapter 04, the fabrication steps of bilayer ZnO/SnO_2 thin films by spray pyrolysis technique have been given. Experimental results and their possible discussions are presented in Chapter 05. Finally, the conclusion of the present work and suggestion for Future Work are discussed in Chapter 06.

References

[1] Kumar, A., Chung, Y. W., Moore, J. J., and Smugeresky, J. E., "Surface Engineering Science and Technology", The Minerals, Metals & Materials Society, Warrendale, 1999.

[2] Gloker, D. A., and Shah, S. I., "Hand Book of thin film process Technology", Institute of Physics Publishing, Bristol and Philadelphia, 1998.

[3] Chopra, K. L., "Thin Film Phenomena", McGraw Hill, New York, 1969.

[4] Miller, D. A. B., Gerken M., "Multilayer thin film coatings for optical communication systems", Optical Society of America.

[5] Fortunato, E., Ginley D., Hosono H., and Paine D. C., "Transparent Conducting Oxides for Photovoltaics", MRS Bulletin, vol. 32, pp. 242-247, 2007.

[6] Tadatsugu, M., "Transparent conducting oxide semiconductors for transparent electrodes", Semiconductor Science and Technology, vol. 20 (4), pp. S35, 2005.

[7] Coleman, V. A.; Jagadish, C., "Chapter 1 - Basic Properties and Applications of ZnO. In Zinc Oxide Bulk", Thin Films and Nanostructures; Elsevier Science Ltd: Oxford, pp. 1-20, 2006.

[8] Liu, Y.; Li, Y.; Zeng, H., "ZnO-Based Transparent Conductive Thin Films: Doping, Performance, and Processing", Journal of Nanomaterials, vol. 2013, pp. 9, 2013.

[9] Jarzebski, Z. M.; Marton, J. P.,"Physical Properties of SnO_2 Materials: II. Electrical Properties", Journal of The Electrochemical Society, Vol. 123 (9), pp. 299C-310C, 1976.

[10] Singh, A. K.; Janotti, A.; Scheffler, M.; Van de Walle, C. G., "Sources of Electrical Conductivity in SnO_2", Physical Review Letters, Vol. 101 (5), pp. 055502, 2008.

[11] Mele, P., End, T., Arisawa, S., Li, C., and Tsuchiya, T., "Oxide Thin Films, Multilayers and Nanocomposite", Springer International Publishing, Swizerland, 2015.

[12] Khanna, K. M., Ekai, R., Ronno, C. K., Rotich, S. K., & Torongey, P. K.," Theory of multilayer solar cells", Indian Journal of Pure & Applied Physics, Vol. 43, pp. 432-438, 2005.

[13] Dibattisa, M., Patel, S. V., Wise, K. D., Gland, J. L., Mansfieldt, J. F., Schwank, J. W.," Characterization of Multilayer Thin Film Structures for Gas Sensor Applications", Materials Research Society ,Vol. 382, pp. 477, 1995.

[14] Islam, M. R., and Podder, J., "Optical Properties Of ZnO Nano Fiber Thin Films Grows by Spray Pyrolysis of Zinc Acetate Precursor", Cryst. Res.Techno.Vol. 44, pp. 286-292, 2009.

[15] Sahay, P. P., Tewari, S. and Nath, R. K., "Optical and Electrical Studies on Spray Deposited ZnO Thin Films", Cryst. Res. Techn., Vol. 42, pp. 723-729, 2007.

[16] Kumar, R. A., Manivannan, V., Krishnaraj, S., "Growth and Characterization of ZnO Nano thin films using Spray Pyrolysis", Int. J. Res. Pure Appl. Phys., vol. 3(4), pp. 39-42, 2013.

[17] Godbole, B., Badera, N., Shrivastava, S., Jain, D., Ganesan, V., "Growth Mechanism of ZnO Films Deposited by Spray Pyrolysis Technique", Mater. Sci. Appl., vol. 2, pp. 643- 648, 2011.

[18] Ilician, S., Caglar, Y., Caglar, M., "Preparation and characterization of ZnO thin films deposited by sol-gel spin coating method", J. Optoelectron. Adv. M., vol. 10 (10), pp. 2578 – 2583, 2008.

[19] Antonaia, A., Menna, P., Addonizio, M.L., and Crocchiolo, M., "Transport properties of polycrystalline tin oxide films", Solar Energy Materials and Solar Cells, vol. 28, pp. 167-173, 1992.

[20] Abdelkrim, A., Rahmane, S., Abdelouahab, O., Hafida, A., and Nabila, K., "Optoelectronic properties of SnO_2 thin films sprayed at different deposition times", Chin. Phys. B vol. 25, pp. 046801, 2016.

[21] Sagadevan, S., and Podder, J., "Investigation on Structural, Surface Morphological and Dielectric Properties of Zn-doped SnO_2 Nanoparticles", International Journal of Nanoparticles Vol. 8, pp. 289 – 301, 2015.

[22] Moholkar, A.V., Pawar, S.M., Rajpurea, K.Y., Patil, P.S., Bhosale, C.H., "Properties of highly oriented spray-deposited fluorine-doped tin oxide thin films on glass substrates of different thickness", Journal of Physics and Chemistry of Solids, vol. 68, pp. 1981–1988, 2007.

[23] Liu, J., Wang, T., Wang, B., Sun, P., Yang, Q., Liang, X., Song, H., Lu, G., "Highly sensitive and low detection limit of ethanol gas sensor basedon hollow ZnO/SnO_2 spheres composite material" Sensors and Actuators B, vol. 245, pp. 551–559, 2017.

[24] Zargar, R.A., Bhat, M.A., Parrey, I.R., Arora, M., Kumar, J., Hafiz, A.K., "Optical properties of ZnO/SnO_2 composite coated film" Optik, vol. 127, pp. 6997-7001, 2016.

[25] Omondi, C. A., Sakwa, W. T., Ayodo, Y. K., and Wafula, H. B., "BILAYER METAL OXIDE THIN FILMS FOR UV – VISIBLE LIGHT SENSING", Eastern Africa Journal of Engineering Science & Technology, vol. 1, pp. 67-73, 2012.

[26] Cai, Y., Li, X., Liu, Y., Du, S., Cheng, C., Liu, F., Shimanoe, K., Yamazoe, N., and Lu, G., "Hollow cylinder ZnO/SnO_2 nanostructures synthesized by ultrasonic spray pyrolysis and their gas-sensing performance", Cryst. Eng. Comm. vol. 16, pp. 6135, 2014.

[27] Anandhi, R., Ravichandran, K., Mohan, R., "Conductivity enhancement of ZnO:F thin films by the deposition of SnO_2:F over layers for optoelectronic applications", Materials Science and Engineering B, vol. 178, pp. 65– 70, 2013.

CHAPTER TWO

THIN FILM DEPOSITION PROCESSES AND ITS FORMATION

CHAPTER TWO

THIN FILM DEPOSITION PROCESSES AND ITS FORMATION

2.1 Introduction

The Material Science and Engineering community's ability to visualize the novel materials with extraordinary combination of chemical, physical and mechanical, properties has changed the modern society. Thin film technology is the basics of amazing development in solid state electronics. Thin films science and technology, a branch of material science, plays an important role in the today's high-tech industries. The beginning of Thin-Film can possibly start from the observation of Grove, who noted that metal films were formed by sputtering of cathode with high energy positive ions [1]. The continued production of thin films for device purposes is the development of past 40 years. Thin films as a two dimensional systems are of great importance to many real world problems. Their material costs are very little as compared to the corresponding bulk material and they perform the same function when it comes to surface processes. Thus, knowledge and determination of the nature, functions and new properties of thin films have been used for the development of new technologies for future applications. With more and more of today's technologies entering miniaturization to the levels of the single atom and demand for precision reaching tolerances which only can be read by an electron microscope. Thin film technology is rapidly branching out to new industries every day. 'Films' can be mathematically defined as homogenous solid material between two planes and extended in two directions but restricted along third direction perpendicular to XY plane. Their magnitude varies from 50-100Å (ultra thin), 100-1000Å (thin) and >1000Å (thick films) [2-3].

2.2 Classification of thin-film deposition techniques

The number of thin film materials, their deposition processing and fabrication techniques are used to produce the devices. It is possible to classify these techniques in two ways.

- Physical Techniques
- Chemical Techniques

Physical method covers the deposition techniques which depend on the evaporation or discharge of the material from a source, i.e. evaporation or sputtering, on the substrate by chemical reaction of vapor phase chemicals that contain the required constituents. Structure-property relationships are the key features of electronic devices and basis of thin film technologies. Underlying the performance and economics of thin film components are the manufacturing techniques on a specific chemical reaction. Thus chemical reactions may depend on thermal effects, as in vapor phase deposition and thermal growth. However, in all these cases a definite chemical reaction is required to obtain the absolute film.

- **Physical Techniques**
  - Evaporation Method
  - Sputtering
  - Epitaxial growth
  - Physical vapor deposition
  - Pulsed laser deposition (PLD)
  - Electrohydrodynamic deposition

- **Chemical Techniques**
  - Atmospheric-pressure CVD (APCVD)
  - Low-pressure CVD (LPCVD)
  - Metal-organic CVD (MOCVD)
  - Plasma-enhanced CVD (PECVD)
  - Atomic layer deposition (ALD)
  - Laser-induced CVD (LCVD)

  - **Wet Chemical Techniques**
    - Chemical Bath Deposition (CBD)
    - Electroplating
    - Spin coating
    - Spray pyrolysis

2.2.1 Physical Techniques

Physical deposition techniques conduct mechanical, electromechanical or thermodynamic means to produce a thin film of solid. The material to be deposited is placed is an energetic, entropic environment, so that particles of material escape its surface. Facing this source is a cooler surface which draws energy from these particle as they arrive, allowing them to from a solid layer. The whole system is kept in a vacuum deposition chamber, to allow the particles to travel as freely as possible. Since particles tend to follow a straight path, films deposited by physical means are commonly directional, rather than conformal [4].

2.2.1.1 Evaporation

In the process of evaporation, heat enters into the source material (often called the charge, which may be an elemental metal, an alloy, a mixture or a compound) to create a plume of vapor which travels in straight line paths to the substrate. The atoms, molecules, and clusters of molecules condense from the vapor phase to form a solid film, upon arrival at the substrate. The heat of condensation is absorbed by the substrate [5]. On a microscopic scale the localized heating from this process can be huge. In the development of metal coating techniques for thin cross section plastic parts, it is common, to melt substrates during the initial deposition runs. Monitoring of source-to-substrate distances and deposition rates will allow coating of temperature sensitive substrates without melting. There are several methods by which heat can be delivered to the charge to cause vaporization: induction heating, electric resistance heating, and electron beam heating. Deposition of thin films by laser ablation and cathodic arc could be grouped in this section with thermal processes. The laser source is located outside the evaporation system and the beam penetrates through a window and is focused onto the evaporate material, which is generally fine powder form.

Thermal evaporation

Thermal evaporation is a common method of thin-film deposition. The source material is evaporated in a vacuum. The vacuum allows vapor particles to travel directly to the target object (substrate), where they condense back to a solid state. Thermal evaporation is used in micro-fabrication to make electrical contacts. In thermal evaporation resistive coil or boat

is used that contains charge in solid bar or powder form. A large DC current passed through resistive coil/boat to acquire high melting points of respective metals, where metal gets evaporated and attain to substrate in high vacuum conditions. The low melting points materials can be deposited by this technique specially [6]. Evaporation takes place in a vacuum, i.e. vapors other than the source material is almost entirely removed before the process begins. The thermal evaporation chamber is pumped by diffusion pump to create high vacuum. The material that is to be deposited is placed in heater or the crucible that is heated by giving DC power supply. As the crucible or heater gets heated the charge gives off vapor that reaches to substrate and sticks on the surface. In high vacuum (with a long mean free path), evaporated particles can travel directly to the deposition target without colliding with the background gas. Hot objects in the evaporation chamber, such as heating filaments, produce unwanted vapors that limit the quality of the vacuum. The schematic of thermal evaporation system is shown in figure 2.1. The issues with conventional evaporation are:

a) Purity of the deposited film depends on the quality of the vacuum, and on the purity of the source material.

b) At a given vacuum pressure the film purity will be higher at higher deposition rates as this minimizes the relative rate of gaseous impurity inclusion.

c) The thickness of the film will vary due to the geometry of the evaporation chamber. Collisions with residual gases aggravate non-uniformity of thickness.

d) Wire filaments for evaporation cannot deposit thick films, because the size of the filament limits the amount of material that can be deposited.

e) In order to deposit a material, the evaporation system must be able to melt it. This makes refractory materials such as tungsten hard to deposit by methods that do not use electron-beam heating.

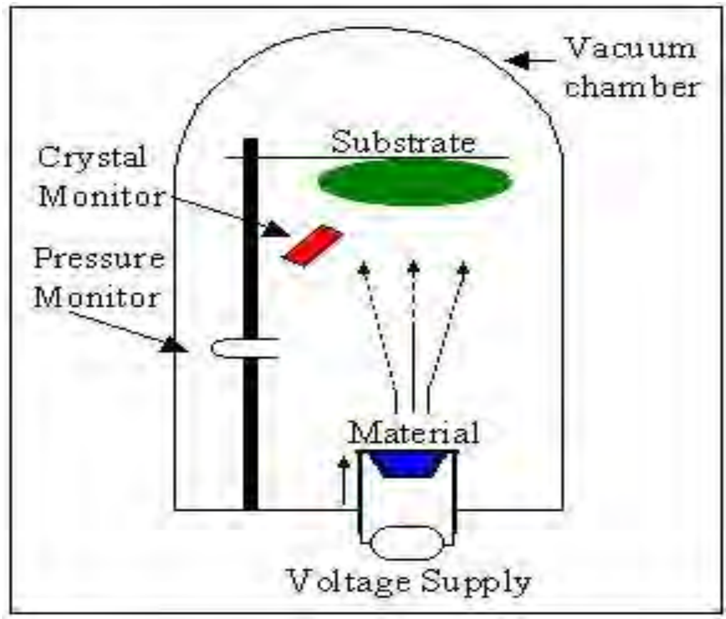

Figure 2.1: Schematic of thermal evaporation.

E-Beam evaporation

EBE is a technique suitable for the fabrication of nanometer scale structures. In EBE a target anode is bombarded with an electron beam given off by a charged tungsten filament under high vacuum. The electron beam causes atoms from the target to transform into the gaseous phase. These atoms then precipitate into solid form, coating everything in the vacuum chamber with a thin layer of the anode material [7].

2.2.1.2 Sputtering

Sputtering is a process whereby atoms are ejected from a solid target material due to bombardment of the target by energetic ions and is commonly used for thin-film deposition, etching and analytical techniques. Sputter deposition is a method of depositing thin films by sputtering material from a target which is then deposited onto a substrate. Atoms can be ejected from the target by momentum exchange between the sputtering ions and the target atoms, due to collisions. The average number of atoms ejected from the target per incident ion is called the sputter yield. The sputtering yield from the target is thereby one of the main parameters for sputter deposition of thin films and depends on the ion incident angle, the

energy of the ion, the masses of the ion and target atoms, and the surface binding energy of atoms in the target. Sputtered atoms and ions ejected from the target have a wide energy distribution, whereas the sputtered ions can ballistically fly from the target in straight lines and impact energetically on the substrates or vacuum chamber (causing resputtering) [8]. However, the sputtered ions could also collide with gas atoms which act as moderator or as necessary growth reactant. Typically an inert gas is used for sputtering (for example argon or xenon). The sputtering further classified into:

1) DC sputtering

2) RF sputtering

3) Magnetron sputtering

4) Reactive sputtering

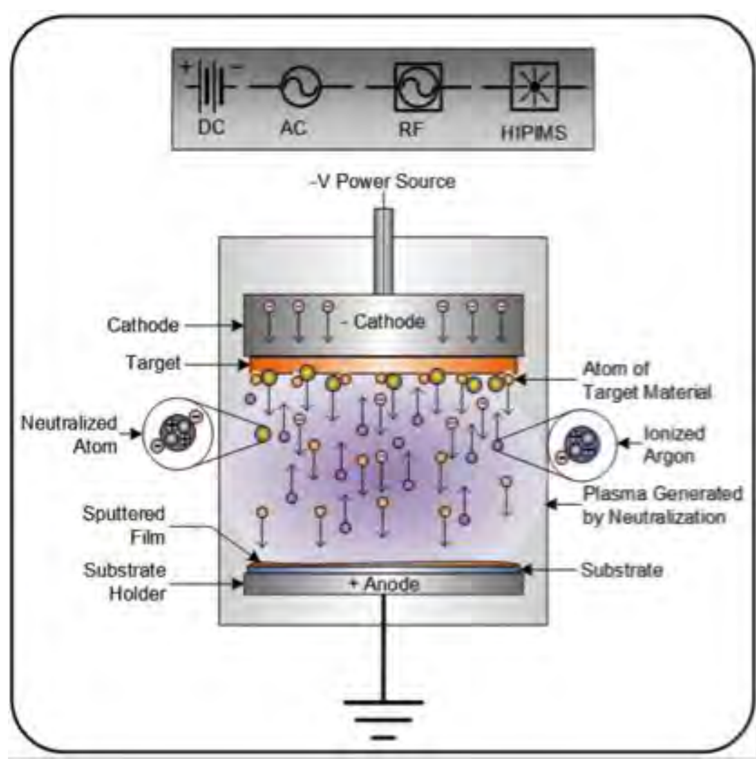

Figure 2.2: A diagram of a sputtering system.

2.2.1.3 Physical Vapor Deposition (PVD)

Physical Vapor Deposition (PVD) describes a variety of vacuum deposition methods which can be used to produce thin films and coatings. PVD is characterized by a process in which the material goes from a condensed phase to a vapor phase and then back to a thin film condensed phase. The coating method involves purely physical processes such as high temperature vacuum evaporation rather than involving a chemical reaction at the surface to be coated as in chemical vapor deposition. The most common PVD processes are sputtering and evaporation. It is far more common than CVD for metals since it can be performed at lower process risk and cheaper in regards to materials cost. The quality of the films is inferior to CVD, which for metals means higher resistivity and for insulators more defects and traps. The step coverage is also not as good as CVD.

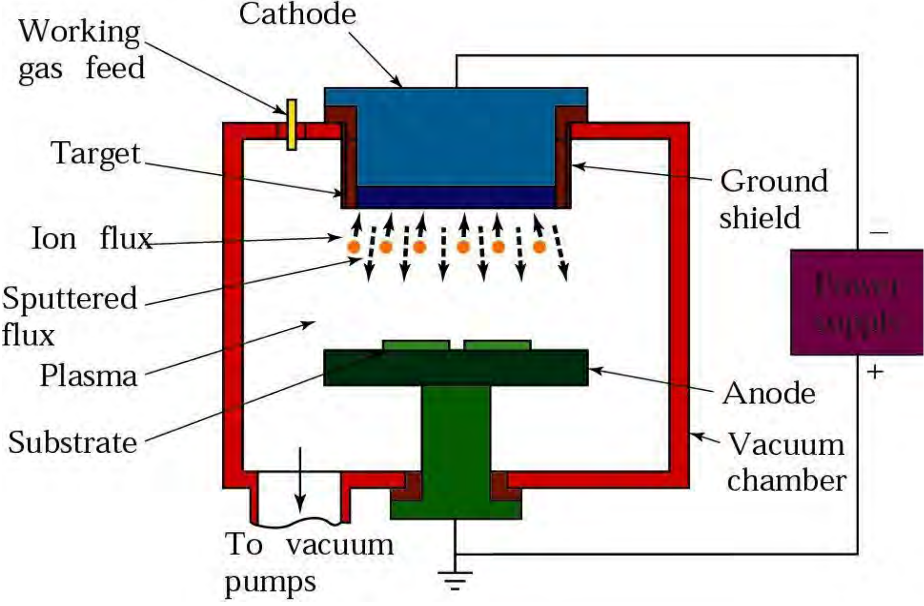

Figure 2.3: A diagram of physical vapor deposition technique

2.2.1.4 Pulsed Laser Deposition (PLD)

Pulsed Laser Deposition (PLD) is a physical vapor deposition (PVD) technique where a high-power pulsed laser beam is focused inside a vacuum chamber to strike a target of the material that is to be deposited. This material is vaporized from the target (in a plasma plume) which deposits it as a thin film on a substrate. This process can occur in ultra high

vacuum or in the presence of a background gas, such as oxygen which is commonly used when depositing oxides to fully oxygenate the deposited films. In laser deposition, a high-power pulsed laser (1 J/shot) is irradiated onto the target of source materials through a quartz window. A quartz lens is used to increase the energy density of the laser power on the target source. Atoms that are ablated or evaporated from the surface are collected on nearby substrate surfaces to form thin films [9].

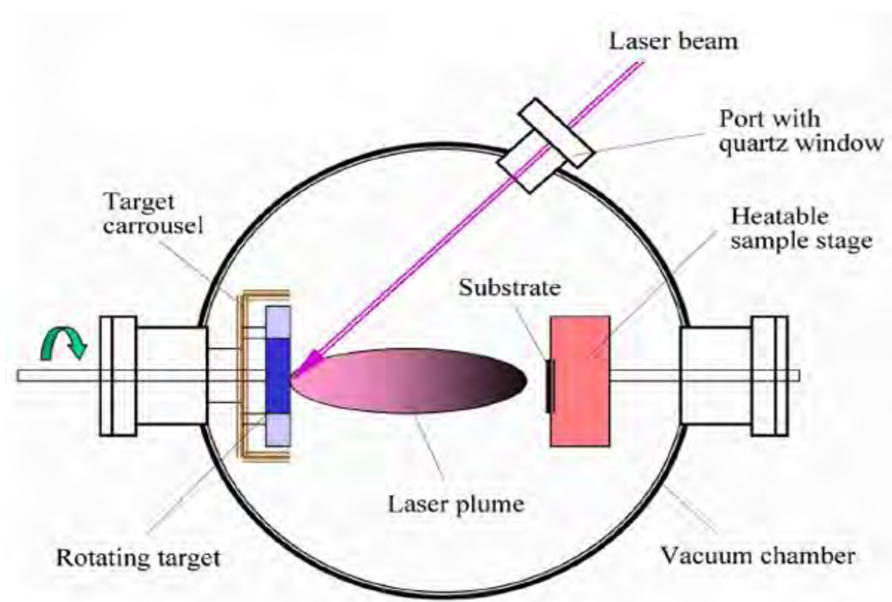

Figure 2.4: A diagram of pulsed laser deposition system

The target material is locally heated to the melting point, melted, and vaporized in a vacuum. The laser pulse may also provide photo-emitted electrons from the target to make a plasma plume and the evaporation mechanism may be complex since the process includes the thermal process and the plasma process. By optimizing various parameters such as ablation energy, base vacuum level, background oxygen pressure, distance between target and substrate and the temperature of substrates, one can have desired deposition rate and structure quality.

2.2.2 Chemical Deposition Techniques

Here, a fluid precursor undergoes a chemical change at a solid surface, leaving a solid layer. An everyday example is the formation of soot on a cool object when it is placed inside a flame. Since the fluid surrounds the solid object, deposition happens on every surface, with little regard to direction; thin films from chemical deposition techniques tend to be conformal, rather than directional [10].

2.2.2.1 Atmospheric-Pressure CVD (APCVD)

APCVD is a CVD method at normal pressure i.e. atmospheric pressure which is used for deposition of doped and undoped oxides. The deposited oxide has a low density and the coverage is moderate due to a relatively low temperature. The surface reaction on the heated wafer, typically at 400°C, grew films in the 2000 to 3000 Å/min range [11-12]. The low temperature simple reactor design and high wafer throughput is a big advantage of this process. APCVD suffers from poor step coverage, fast precursor flow, particle contamination, frequent cleaning. With a better understanding of the reaction mechanisms and the injection of reactants, some of these step coverage problems could be minimized. Various new reactors have been built around these enhancements and are used today. Because of improved tools, the APCVD undergoes regeneration [13].

2.2.2.2 Metal-Organic CVD (MOCVD)

MOCVD (metal organic chemical vapor deposition) is a technique that is used to deposit very thin layers of atoms onto a semiconductor wafer. In MOCVD ultra pure gases are injected into a reactor and finely dosed to deposit a very thin layer of atoms onto a semiconductor wafer. It is used to produce single or polycrystalline thin films. It is a highly complex process for growing crystalline layers to create complex semiconductor multilayer structures [14-15].

2.2.2.3 Plasma-Enhanced CVD (PECVD)

In this method of CVD, plasma is added in the deposition chamber with reactive gases to create the desired solid surface on the substrate. The plasma is any gas in which a significant

percentage of the atoms or molecules are ionized and is energetic and disposes on the surface. The PECVD takes place at 250 to 350 °C. Due to low temperatures the process gases cannot be decomposed thermally. The plasma is created by RF (AC) frequency or DC discharge between two electrodes, the space between which is filled with the reacting gases. Because metallization, such as aluminum, cannot be exposed to high temperatures, the PECVD is used for SiO2 and Si3N4 deposition on top of metal layers. PECVD becomes alternative that is low temperature and low pressure technique having plasma as energy input. The conformity is not as good as in LPCVD (0.6 to 0.8), however, the deposition rate is much higher (0.5 microns per minute). The process parameters like gas flow rates, power input, chamber pressure, reactor geometry, inter electrode spacing; substrate temperature etc. can be controlled to achieve the desired quality films [16]. Advantages of PECVD include the low temperature, higher film density for higher dielectric and more compression, and ease of cleaning the chamber. Disadvantages include the expense of the equipment and the stress of plasma bombardment [17].

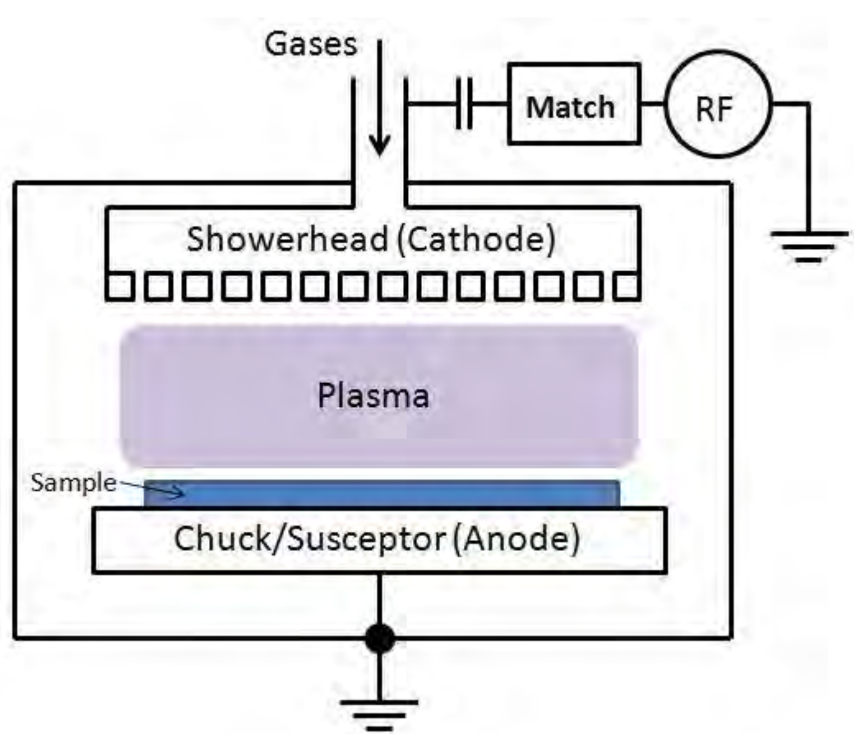

Figure 2.5: A diagram of a Plasma Enhanced CVD (PECVD) system.

2.2.2.4 Atomic Layer Deposition (ALD):

Atomic Layer Deposition (ALD) is a modified CVD process to manufacture thin films. The process uses several gases which are led into the process chamber alternating. It is a thin film deposition technique that is based on the sequential use of a gas phase chemical process. Each gas reacts in such a way that the current surface is saturated, and therefore the reaction comes to a standstill. The alternative gas is able to react with this surface in the same way. Between the reactions of these gases the chamber is purged with an inert gas, like nitrogen or argon. A simple ALD process could look like this:

i. self-limiting reaction at the surface with first gas

ii. purging with an inert gas

iii. self-limiting reaction at the surface with second gas

iv. purging with an inert gas

Due to the characteristics of self-limiting and surface reactions, ALD film growth makes control at atomic scale. ALD is similar in chemistry to CVD, except that the ALD reaction breaks the CVD reaction into two half-reactions, keeping the precursor materials separate during the reaction. By keeping the precursors separate throughout the coating process, atomic layer control of film growth can be obtained as fine as ~0.1 Å (10 pm) per cycle. Separation of the precursors is accomplished by pulsing a purge gas (typically nitrogen or argon) after each precursor pulse to remove excess precursor from the process chamber and prevent 'parasitic' CVD deposition on the substrate [18].

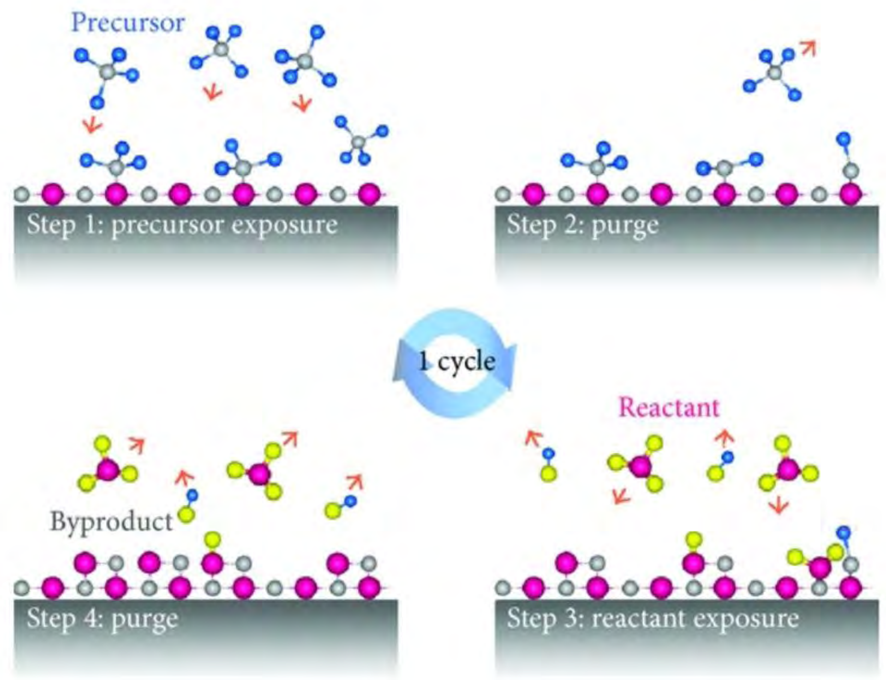

Figure 2.6: A diagram of an Atomic Layer Deposition (ALD) system.

2.2.3 Wet Chemical Techniques

In these techniques liquid solution is coated on the substrate and then dried to form the thin solid film.

2.2.3.1 Chemical Bath Deposition (CBD)

Chemical Bath Deposition (CBD) is a method to deposit thin films and nonmaterials; it can be employed for large-area batch processing or continuous deposition. It is also known as Chemical Solution Deposition (CSD). It is not a new technique as early as in 1835 Liebig reported the first deposition of Silver, the silver mirror deposition using a chemical solution technique.

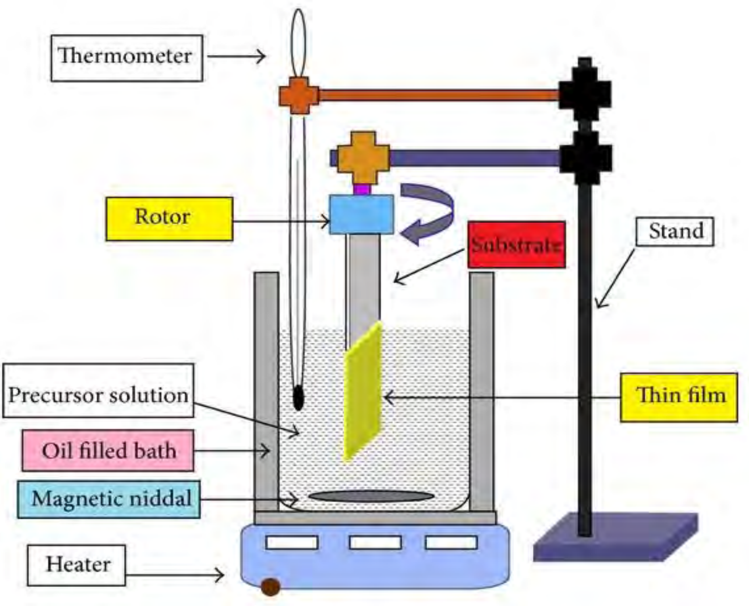

Figure 2.7: A diagram of CBD method**.**

The only requirements of these methods are a vessel to contain the solution (usually an aqueous solution of chemicals) and the substrate on which deposition is to be carried out. In addition to this various complications such as some mechanism for stirring and a thermo started bath to maintain a specific and constant temperature are options that they may be useful [19]. CBD is a method of growing thin film of certain materials on a substrate immersed in an aqueous bath containing appropriate reagents at temperature ranging from room temperature to 100 ^{0}C. Figure 2.6 shows the diagram of a CBD process. CBD involves two steps, nucleation and particle growth. It also involves the controlled precipitation from solution of a compound on a suitable substrate. The technique offers many advantages over the more established vapor phase synthetic routes to semiconductor materials, such as CVD and MBE etc. varying the solution pH , temperature and reagent concentration allies factors such as control of film thickness and deposition rate with the ability of CBD to coat large areas in a reproducible and low cost process. In CBD two processes are traditionally used for growth: single dip, where the substrate is immersed in the reaction both only once, and multiple dips, where the same substrate is repeatedly coated to obtain thicker film [20].

2.2.3.2 Spin coating

Spin coating is a procedure used to apply uniform thin films to flat substrates. A typical process involves depositing a small puddle of a fluid resin onto the center of a substrate and then spinning the substrate at high speed (typically around 3000 rpm) (Mitzi et al. 2004).Centrifugal force will cause the resin to spread to, and eventually off, the edge of the substrate leaving a thin film of resin on the surface.

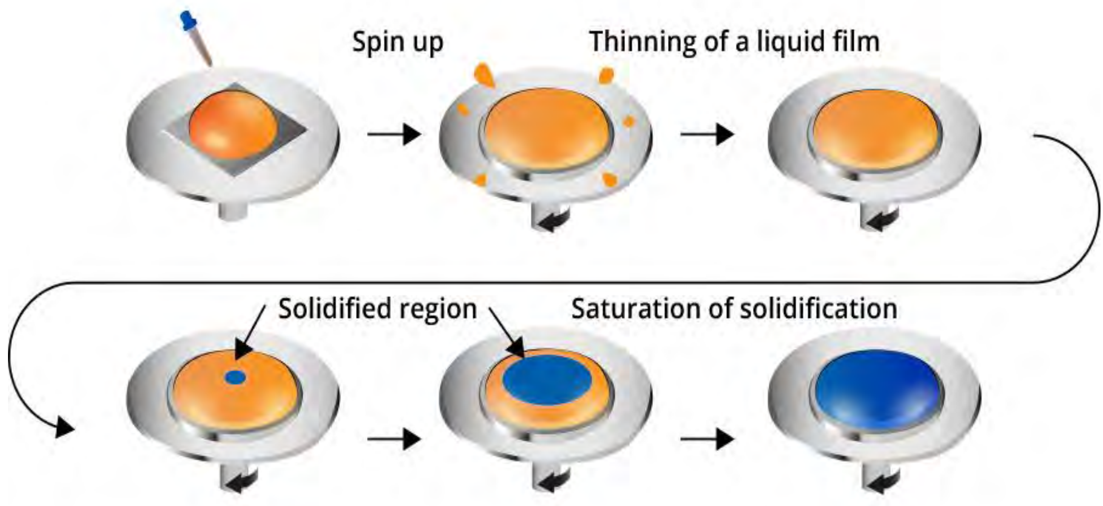

Figure 2.8: A diagram of spin coating technique

Final film thickness and other properties will depend on the nature of the resin (viscosity, drying rate, percent solids, surface tension, etc.) and the parameters chosen for the spin process. A machine used for spin coating is called a spin coater, or simply spinner. Rotation is continued while the fluid spins off the edges of the substrate, until the desired thickness of the film is achieved. The applied solvent is usually volatile, and simultaneously evaporates. So, the higher the angular speed of spinning, the thinner the film. The thickness of the film also depends on the concentration of the solution and the solvent (Hellstrom 2007). Spin coating is widely used in micro-fabrication, where it can be used to create thin films with thicknesses below 10 nm [21-22].

2.2.3.3 Spray pyrolysis

Spray pyrolysis is a simple and low-cost technique that has been used to prepare the thin film on a variety of substrates like glass, ceramic or metallic. These films were used in various devices such as solar cells, sensors, and solid oxide fuel cells. Due to the simplicity of the apparatus and the good productivity of this technique on a large scale, it offered a most attractive way for the formation of thin films of metal oxides. This technique is the most popular today because of its applicability to produce a variety of conducting and semiconducting materials and devices [23].

The basic principle involved in spray pyrolysis technique is pyrolytic decomposition of salts of a desired compound to be deposited. Every droplet of spray reaching the surface of the hot substrate undergoes pyrolytic (endothermic) decomposition and forms a single crystalline or a cluster of crystallites as a product. The other volatile by-products and solvents escape in the form of vapor phase. The substrates provide thermal energy for the thermal decomposition and subsequent recombination of the constituent species, followed by sintering and crystallization of the clusters of crystallites and thereby resulting in coherent film. The required thermal energy is different for the different materials and also for the different solvents used in the spray process. The atomization of the spray solution into a spray of fine droplets also depends on the geometry of the spraying nozzle and the pressure of a carrier gas [24].

The spray pyrolysis mainly consists of spray nozzle, rotor for spray nozzle, liquid level monitor, hot plate, gas regulator value and airtight fiber chamber**.**

1) Spray nozzle

'Spray nozzle' is used to carry the gas whose film is to be deposited. It is made up of glass and consists of the solution tube surrounded by the glass bulb. At the tip of the nozzle the vacuum is created, and the solution is automatically sucked in the solution tube and the spray process starts. The Rotor controls the linear simple harmonic motion of the spray nozzle over the required length of the hot plate.

2) Liquid level monitor:

The spray rate at a fixed air pressure depends upon the height of the solution measured with respect to the tip of the nozzle. The arrangement for the change in height of the solution forms the liquid level monitor system.

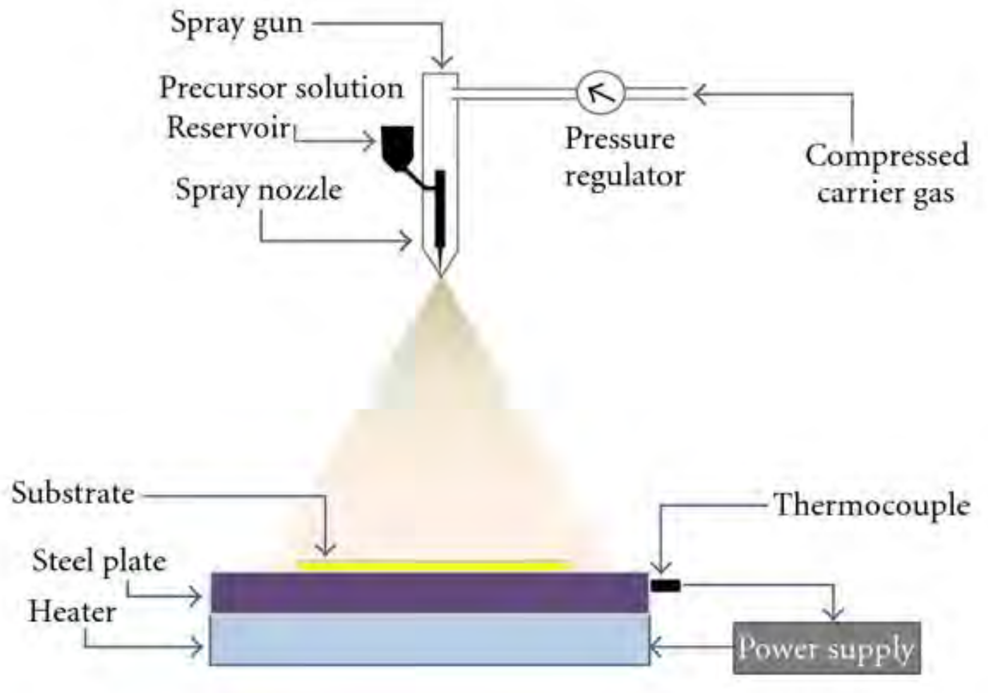

Figure 2.9: A diagram of spray pyrolysis technique

3) Hot plate:

The iron disc (with diameter 16 cm and thickness 0.7 cm along with 2000 Watt heating coil is fixed) served as a hot plate. Maximum temperature of 600 ± 5ºC can be achieved with this arrangement. The chromel-alumel thermocouple is used to measure the temperature of the substrates. It is fixed at the center of the front side of the iron plate. The temperature of the hot plate is monitored with the help of temperature controller.

4) Gas regulator valve:

The gas regulator valve is used to control the pressure of the carrier gas flowing through the gas tube of the spray nozzle. A glass tube of length 25 cm and of diameter 1.5 cm is

converted into gas flow meter. Since air pressure depends upon the size of the air flow meter, the air flow meter should be calibrated from nozzle to nozzle.

5) Air tight fiber chamber:

Since the number of toxic gases is evolved during the thermal decomposition of sprayed solution, hence it is necessary to fix the spraying system inside with airtight fiber chamber. This chamber of the size (60 cm x 60 cm x 60 cm) was fabricated. The fiber avoids the corrosion of the chamber. The outlet of chamber is fitted to exhaust fan to remove the gases evolved during thermal decomposition. In spray pyrolysis, the process parameters like precursor solution, atomization of precursor solution, aerosol transport and decomposition of precursor are important factors while studying the structural, electrical & optical properties, morphology and crystallinity of the thin films. These parameters are discussed in the following section.

a) Precursors

A precursor solution plays a vital role in the formation of thin film of various compounds. The true solutions, colloidal dispersions, emulsions and sols can be used as aerosol precursors. Aqueous solutions are usually used due to case of handling safety, low cost and availability of a wide range of water soluble metal salts. The solute must have a high solubility which increases in particle yield of the process. Increasingly, alcoholic and organic solutions have been studied due to the interest in the synthesis of organic materials from metal organic and undergo polymerization and for the synthesis of non-oxide ceramic solutions.

b) Atomization

A variety of atomization techniques have been used for solution aerosol formation, including pneumatic, ultrasonic and electrostatics. These atomizers differ in droplet size, rate of atomization and droplet velocity. The velocity of the droplet when it leaves the atomizer is important because, it can determine heating rate and residence time of the droplet during spray pyrolysis. The sizes of the droplet products with pneumatic or pressure nozzles

decreases when the pressure difference across the nuclei is increased. For a specific atomizer the droplet characteristics depend on the solution density, viscosity and surface tension.

c) Evaporation

In first stage of spray pyrolysis, evaporation of the solvent from the surface of the droplet, diffusion of the solvent vapor away from the droplet in the gas phase, change in droplet temperature and diffusion of solute towards the center of the droplet have important role concerns with the stoichiometry of films. The factors controlling the particle growth and ultimately film formations of well adherent surface is due to

1. Evaporation of liquid droplets
2. Evaporation from solution droplets
3. Temperature of liquid droplets
4. Temperature of solution droplets
5. Solute diffusion in a droplet
6. Solute condensation.

Apart from its simplicity, the spray pyrolysis technique has a number of advantages as follows:-

- Spray pyrolysis is a simple and low cost technique for the preparation of thin films.
- It has capability to produce large area, high quality adherent films of uniform thickness.
- Does not require vacuum at any stage.
- Spray pyrolysis does not require high quality targets or substrates.
- The deposition rate and the thickness of the films can be easily controlled over a wide range thereby changing the spray parameters.
- It operates at low temperature.
- It offers an extremely easy way to dope films with virtually any elements in any proportion, just by adding it in some form to the spray solution.
- By changing composition of the spray solution during the spray solution during the spray process, it can be used to make layered films and films having composition gradients throughout the thickness [25].

2.3 Thin Film Formation

Thin films are fabricated by the deposition of individual atoms on a substrate. Sufficient time interval between the two successive deposition of atoms and also layers are required so that these can occupy the minimum potential energy configuration. Three major steps that constitute a typical thin-film deposition process are [26]:

(i) production of the appropriate atomic, molecular, or ionic species

(ii) transport of these species to the substrate through a medium

(iii) condensation on the substrate, either directly or via a chemical and/or electrochemical reaction, to form a solid deposit.

2.3.1 Thin Films Growth Modes

Because thin films are widely used in electronic industry, the growth of thin films has been studied increasingly since the 1970s. Scientists and researchers use a wide range of analytical techniques, including transmission electron microscopy (TEM), scanning electron microscopy (SEM), low-energy electron microscopy (LEEM), reflection high-energy electron diffraction (RHEED), medium-energy electron diffraction (MEED), spot profile analysis low-energy electron diffraction (SPALEED) and scanning tunneling microscopy (STM); with such techniques, the goal is to detect the behavior of growing material during the growth of thin films[27]. At the same time, theory and computational simulations are also used in studying and understanding fundamental phenomena controlling thin film growth. A summary of thin film growth modes based on surface energies theorem is presented below. Most thin film growth experiments observe one of three different growth modes. A decisive period of thin film growth is the nucleation at the very early stages of the growth. The mechanisms of these three growth modes are still not well understood. However, it is widely accepted by researchers that the equilibrium shape of nucleation depends on the magnitudes of the respective free surface and interface energies. Depending on such factors three different modes of film growth are distinguished as follows:-

(1) Volmer-Weber mode: This is also known as “3D island growth mode”. In Volmer-Weber (V-W) growth mode, atoms deposit on favored sites of substrate and form initial

islands. As atoms continuously deposit on the substrate, they attach to existing islands, which grow larger until neighboring islands start to merge or coalesce together. After initial islands coalesce, depositing atoms fill channels and voids between islands. The thickness of the continuous film does not increase until depositing atoms fill up the channels between islands and a flat film surface is formed.

(2) Frank-Van der Merwe mode: In this growth mode, atoms wet the entire surface of the substrate at the very beginning and the film grows in a layer by layer fashion. This growth mode can be viewed as "2D island growth mode". It goes through network stage, fills in remaining 2D channels and then forms a continuous layer before growing the next layer. These are analogous steps to what are seen in 3D Volmer- Weber mode.

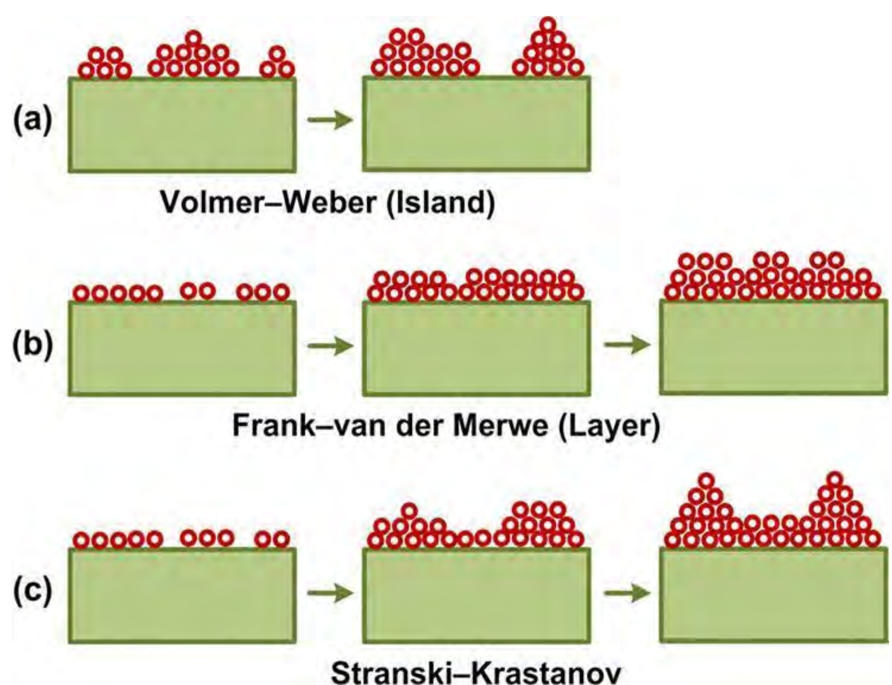

Figure 2.10: Schematic illustration of the three different modes of growth.

(3) Stranski-Krastanov mode: This growth mode occurs through a combination of Frank-Van der Merwe and Volmer-Weber mode. Stranski-Krastanov growth mode follows two steps: initially, complete films, up to several monolayers" thick, grow in a layer by layer

fashion on the surface of substrate. Beyond a critical layer thickness, growth continues through the nucleation and coalescence of discrete islands in an island growth mode.

2.3.2 Condensation:

Condensation simply means the transformation of a gas into a liquid or solid. The condensation of a vapor atom is determined by its interaction with the impinged surface in the following manner. The impinging atom is attracted to the surface by the instantaneous dipole and quadruple moments of the surface atoms. As a result, the atom loses its velocity component normal to the surface in a short time, provided the incident kinetic energy is not too high. The vapor atom is then physically absorbed (called “adatom”), but it may or may not be completely thermally equilibrated. It may move over the surface by jumping from one potential well to the other because of thermal activation from the surface and /or its own kinetic energy parallel to the surface. The atom has a finite stay or residence time on the surface during which it may interact with other adatoms to form a stable cluster and be chemically absorbed with the release of the heat of condensation. If not absorbed, the adatom reevaporates or desorbs into the vapor phase. Therefore, condensation is the net result of equilibrium between the adsorption and desorption processes. The probability that an impinging atom will be incorporated into the substrate (surface) is called the “condensation” or “sticking coefficient”. It is measured by the ratio of the amount of material condensed on a surface to the total amount impinged. In fact, often the sticking coefficient is so small that observation is not observable by ordinary techniques. On the other hand, the sticking coefficient is found to be strongly dependent on the total time during which the substrate was subject to impingement, and also on the substrate temperature. A non unity sticking coefficient is usually explained in terms of monomers re-evaporation from the areas on the substrate which are outside the capture zones around each stable nucleus [28]. Langmuir and Frenkel formulated condensation model (This model considers vapor solid transformation. At high deposition temperatures, a vapor-liquid (amorphous)-solid condensation mode may occur. Semenoff suggested that heterogeneous nucleation always proceeds by formation of an amorphous film followed by nucleation of crystallites within the amorphous film in which the absorbed atoms move over the surface during their lifetimes to form pairs which, in turn, acts as condensation centers for other atoms.

2.3.3 Nucleation

The first stage in the process of depositing thin films on substrates is the formation of adsorbed monomers of one or more atoms which in the second phase, under the action of forces similar to surface tension, or capillarity combine to form small clusters. These clusters are called nuclei and the process of cluster formation is called nucleation. There are two types of nucleation occurs during the formation of a thin film:

(1) homogeneous nucleation

(2) heterogeneous nucleation.

(1) Homogeneous nucleation: Homogeneous nucleation refers to the spontaneous creation of a new phase from a metastable phase. The phase change can be from the vapor to a condensed phase (condensation), from a condensed phase to the vapor phase (cavitations), or from a solution phase to solid phase. Here the total free energy is used in the formation of a cluster of atoms.

(2) Heterogeneous nucleation: Particular shapes of clusters are formed by collisions of atoms on the substrate surface, and in the vapor phase its super saturation is sufficiently high. They initially developed within increase in free energy until a critical size is reached above which growth continues with a decrease in free energy. In atomistic theory, in low substrate temperature or very high super saturations, the critical nucleus may be a single atom which will form a pair with another atom by random occurrence to become a stable cluster and grow spontaneously.

2.3.4 Growth Stages

There are several stages in the growth process from the initial nucleation of the deposits to the final continuous three dimensional film formation states. These stages of film growth have been observed by many workers from their electron microscopic and other studies. These are valid not only for deposits condensing from the vapor phase but also for others, i.e. for solutions, by electro deposition, chemical reactions anodic oxidation, etc. There are four stages of the growth process based on the electron microscope observations [29]. They are:-

- Nucleation stage
- Island stage
- Coalescence stage
- Channel, hole and continuous film stages

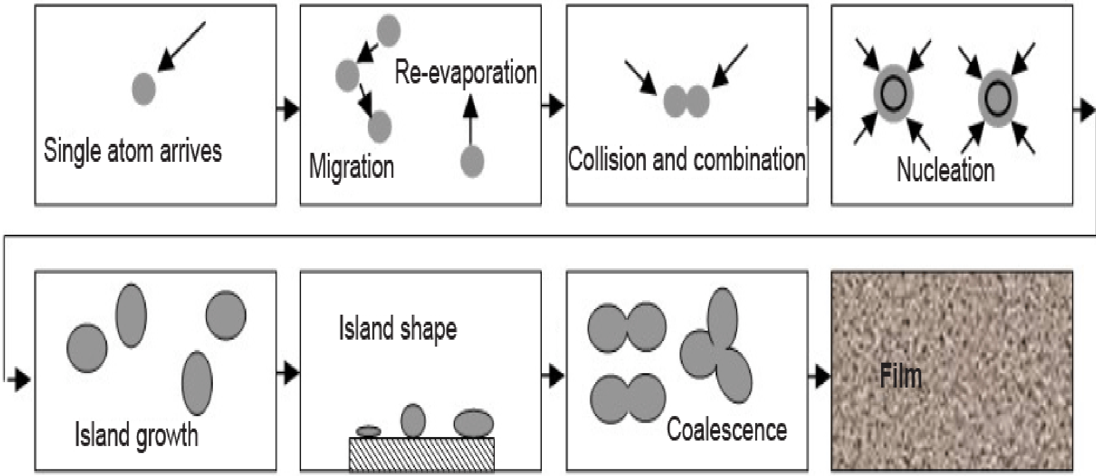

Fig.2.11: The stages of the film growth.

2.3.4.1 Nucleation stage

Thin film formation involves the deposition of the appropriate atomic, ionic or molecular species, atom by atom (or molecule by molecule) and layer by layer on to the substrate. The atoms or molecules impinging onto the substrate move over the surface of the substrate and interact with other species to form clusters. The assemblages of atoms or molecules formed at certain sites on the substrates are called nuclei. These nuclei then grow up to a critical size by combining with new adsorbed species. This first step which involves the formation of the critical sized, thermodynamically stable nuclei is known as the nucleation stage.

2.3.4.2 Island stage

The critical-sized nuclei then grow both parallel and perpendicular to the substrate due to the arrival of new species. These larger nuclei or embryos are three dimensional in nature

with their height much less than their lateral dimensions. These larger nuclei appear as islands onto the substrate with lot of unoccupied space between them and hence this stage is called island stage.

2.3.4.3 Coalescence stage

In this stage of thin film growth, the islands are combined with the neighboring ones to form larger islands. The phenomenon of formation of larger islands from the smaller ones is called agglomeration or coalescence. This coalescence stage involves the transfer of mass between islands by diffusion and hence small islands disappear rapidly. The time of coalescence is very short, of the order of about 0.1 second for the small nuclei. In addition, nuclei having well-defined crystallographic shapes [18] before coalescence become rounded during the event. The composite island takes on a crystallographic shape again if left for a sufficiently long time before interacting with its neighbors.

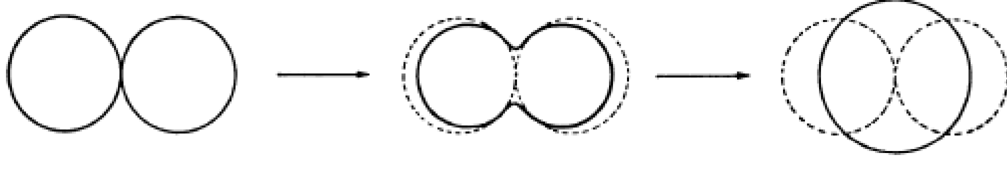

Fig.2.12: Coalescence of two supercritical nuclei and Shape change during coalescence.

2.3.4.4 Channel, hole and continuous film stages

As a consequence of the arrival of more and more species on the substrate, the coalescence continues, resulting in a network of the deposited areas with channels (void spaces) in between. These channels last only for a small time, as some secondary nuclei begin to grow within these void spaces. Further deposition of the material leads to the diminishing or even vanishing of these voids resulting in an eventually continuous film, even though some pores may be present in some cases. To obtain a perfectly continuous film, a minimum thickness is needed which depends upon the nature of the deposited material, method of deposition and the deposition parameters involved in that particular deposition technique [30].

2.3.5 Factors affecting the growth, structure and film properties

Various factors affect the growth, structure and properties of a deposited film. They are: (i) nature of the substrate, (ii) substrate temperature, (iii) source temperature, (iv) presence of gas inside the chamber, (v) annealing, (vi) contamination by impurities and presence of defects on the substrate surface, (vii) presence of electrostatic charges etc. The temperature of the substrate and thickness of the film are two very important parameters affecting its properties. The mobility of the just deposited adatoms on the substrate surface can be enhanced by increasing the temperature of the substrates during the deposition process. Higher mobility of the adatoms give the adatoms more chance to grow together in ordered manner leading to formation of thin films with large crystallites. Low mobility on the other hand leads to the formation of a film of amorphous nature. Lower temperature and higher gas phase concentration are actually favorable in forming polycrystalline film. If the substrate is the face of a single crystal, periodic forces of cohesion induce an oriented growth called the epitaxial growth. Thus a thin film can be deposited in crystalline, polycrystalline and amorphous form.

References

[1] Ohring, M., “Materials Science of thin films”, Academic Press, San Diego, CA, 2nd edition, 2002.

[2] Seshan, K., “Handbook of Thin-Film Deposition Processes and Techniques”, 2nd Ed. Noyes Publications, 2002.

[3] Chopra, K. L., “Thin Film Phenomena”, McGraw Hill, New York, 1969.

[4] Brown, R., Maissel, L. I. and Glang, R., “Handbook of Thin Film Technology”, McGraw Hill, NewYork, 1970.

[5] Campbell, S. A., “The Science and Engineering of Microelectronic Fabrication”, Oxford University Press NewYork, 1996.

[6] Ghandhi, S. K., “VLSI Fabrication Principles”, 2nd Ed. John Wiley & Sons, 2012.

[7] Smith, D. L., “Thin-Film Deposition principles and practice, McGraw-Hill”, Inc., 1995.

[8] Behrisch, R., “Sputtering by Particle Bombardment”, Springer, Berlin, 1981.

[9] Aziz, M. J., “Film growth mechanism in pulsed laser depositon”, Appl. Phys. A: Matter. Sci. Proc., Vol. 93(3), pp. 579-587, 2008.

[10] Dobkin, D. and Zuraw, M. K., “Principles of Chemical Vapor Deposition”, Springer, Science and Business Media, 2003.

[11] Jensen, K. F., “Chemical Vapour Deposition. Microelectronics Processing: Chemical Engineering Aspects”, D. W. Hess, K. F. Jensen, Eds. Washington, D.C.: Amer Chemical Society, 1989.

[12] Zhang, J., Li, J., Luo, L., Wo, Y., **“**Microstructure and morphology of SiOx film deposited by APCVD”, J. Alloys Comp., Vol. 2, pp. 14, 2008.

[13] Morales, C., Juarez, H., Diaz, T., et al., **“**Low temperature SnO2 films deposited by APCVD”, J. Microelect., Vol. 39, pp. 586-588, 2008.

[14] Yang, P. F., Jian, S. R., Lai, Y. S., et al., **“** Morphological, structural, and mechanical characterizations of InGaN thin films deposited by MOCVD”, J. Alloys Comp., Vol. 463, pp .533-538, 2008.

[15] Luo, W., Wang, X., Xiao, H., Wang, C., et al., **“**Growth and fabrication of AlGaN/GaN HEMT based on Si(111) substrates by MOCVD”, Microelectronics J., Vol. 39, pp. 1108-1111, 2008.

[16] von Rohr, P. R., Borer, B., " Plasma-Enhanced CVD for Particle Synthesis Using Circulating Fluidized Bed Technology", Chem. Vap. Deposition, Vol. 13, pp. 499-506, 2007.

[17] Wright, D. N., Marstein, E. S., Rognmo, A., Holt, A., " Plasma-enhanced chemical vapour-deposited silicon nitride films; the effect of annealing on optical properties and etch rates", Solar Energy Mater Solar Cells, Vol. 92, pp. 1091-1098, 2008.

[18] Miikkulainen, V.; Leskelä, M.; Ritala, M.; Puurunen, R. L.,."Crystallinity of inorganic films grown by atomic layer deposition: Overview and general trends". Journal of Applied Physics, Vol. 113 (2), pp. 021301, 2013.

[19] K.L. Chopra, R.C. Kainthla, D.K. Pandya and Thakoor, A.P., "In: Physics of Thin Films", Vol. 12, Academic Press, London, 1982.

[20] Lokhande, C. D., "A chemical method for preparation of metal sulfide thin films", Mater. Chem. Phys., Vol. 28(1), pp. 145-149, 1991.

[21] Hench, L. L. and West, J.K., "The sol-gel process", Chem. Rev., Vol. 90(1), pp. 33-72, 1990.

[22] Scriven, L.E, "Physics and applications of dip coating and spin coating". Better ceramics through chemistry III. pp.717–729, 1988.

[23] Ilican, Caglar, M. and Caglar, Y., "The effect of deposition parameters on the physical properties of CdxZn1-xs fims deposited by spray pyrolysis method", J. Optoelectr. and Adv. Mater., Vol. 9, pp.1414-1417, 2007.

[24] Chamberlin, R. R.and Skarman, J. S., "Chemical spray deposition process for inorganic films", J. Electrochem. Soc., Vol. 113(1), pp. 86-89, 1966.

[25] Perednis, D. and Gauckler, L. J., "Thin film deposition using spray pyrolysis", J. Electroceram., Vol. 14, pp.103-111, 2005.

[26] Zhang, Z. and Lagally, M. G., "Atomistic processes in the early stages of thin film growth", Science, Vol. 276, pp. 377-383, 1997.

[27] Chopra, K. L., "Nucleation, growth and structure of films", Thin Film Phenomena, McGraw Hill, New York, pp. 110-137, 1969.

[28] Tolman, R. C., "The Effect of Droplet Size on Surface Tension", J. Chem. Phys., Vol. 17, pp.118, 1949.

[29] Jensen, Havlin, P., "A fractal model for the first stage of thin film growth", Fractels, Vol. 4(3), pp. 321-329, 1996

[30] Ratsch, C. and Venables, J.A., "Nucleation theory and the early stages of thin Films growth", J. Vac. Sci. Technol. A, Vol. 21(5), pp. 96-109, 2003.

CHAPTER THREE

THIN FILM CHARACTERIZATION TECHNIQUES

CHAPTER THREE

THIN FILM CHARACTERIZATION TECHNIQUES

3.1 Introduction

The deposited ZnO, SnO_2 and ZnO/SnO_2 bilayer nanocomposite thin films are characterized for their surface morphological, structural, optical and electrical properties. X-ray diffraction (XRD) is used for studying the nature and structure, scanning electron microscopy (SEM) is used to identify the surface morphology and atomic force microscopy (AFM) is used to study of surface roughness of the prepared films. The optical parameters were analyzed from the transmittance and absorbance spectra obtained using UV- Visible spectrophotometer. Hall effect measurement used to identify the carrier concentration and carrier mobility. The Four point probe technique is employed to measure electrical resistivity of the films. The principle, functioning and importance of each technique are briefly outlined in this chapter with related theory.

3.2 Structural Characterization

A rapidly increasing number of research topics and applications in science and engineering rely on thin films, superlative growth, and pattering down to the sub micrometer scale. In order to understand the structural properties of such nanostructures, a through and detailed structure characterization is required. XRD techniques allow us to probe the internal structure of the layers and the quality of the interfaces between the different materials in a multilayer. XRD provides most definitive structural information.

3.2.1 X-ray Diffraction

X-ray scattering techniques are a family of non-destructive analytical techniques which reveal information about the crystallographic structure, chemical composition, and physical properties of materials and thin films. These techniques are based on observing the scattered intensity of an X-ray beam hitting a sample as a function of incident and scattered angle, polarization, and wavelength or energy-ray diffraction (XRD) is a rapid analytical technique primarily used for phase identification of a crystalline material and can provide information

on unit cell dimensions. The analyzed material is finely ground, homogenized, and average bulk composition is determined. XRD has been used in two main areas, for the fingerprint characterization of crystalline materials and the determination of their structure [1]. Easy crystalline solid has its unique characteristic X –ray powder pattern which may be used as a "fingerprint "for its identification. Once the material has been identified, X –ray crystallography may be used to determine its structure, i.e. how the atoms pack together in the crystalline state and what the inter–atomic distance and angle are etc.

The size and the shape of the unit cell for any compound and can be determined most easily using XRD. X-rays are the electromagnetic waves of wavelength about 1Å. When X-rays are incident on a crystal surface, they are reflected from it figure 3.1.

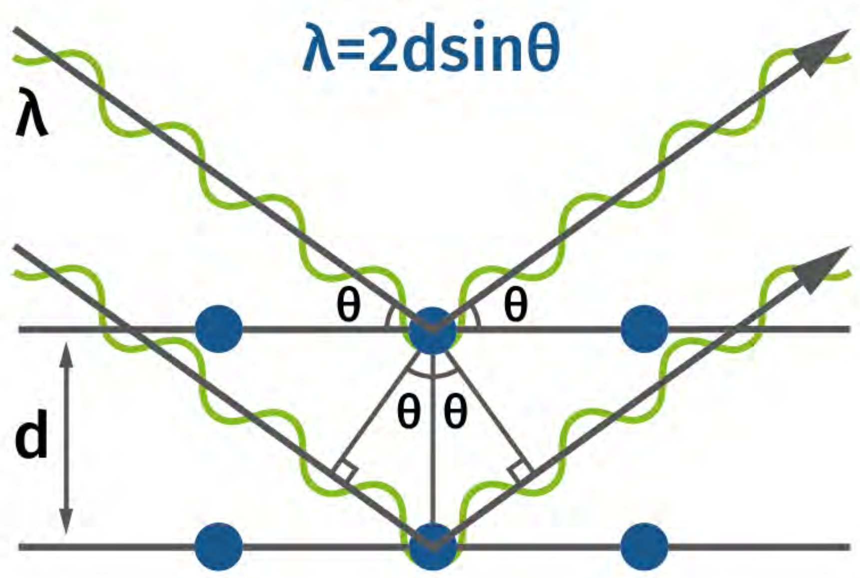

Figure 3.1: Reflection of X-rays from two planes of atoms in a solid.

The reflection obeys the following Bragg's law,

$$2d\sin\theta = n\lambda \tag{3.1}$$

Where d is the distance between crystal planes, θ is the incident angle of X-ray, λ is the wavelength of the X–ray and n is a positive integer. Bragg's law also suggests that the diffraction is only possible when $\lambda < 2d$.

From the width of the diffraction line, it is possible to estimate the average grain size of the thin film [2].

Surface thickness in thin films are about 3000 Å, can be investigated using XRD [3]. Thicker films can be characterized by reflection high-energy electron diffraction (RHEED). Analysis of the diffraction patterns obtained by these techniques and composition with standard ASTM data can reveal the existence of different crystallographic phases in the film, their relative abundance, the lattice parameters and any preferred orientations.

Using' values the set of lattice planes (h k l) are identified from the standard data and the lattice parameters are calculated using the relations. For hexagonal crystal structure the lattice parameters can be determined using the relation,

$$\frac{1}{d^2} = \left[\frac{4}{3}\left(\frac{h^2+hk+k^2}{a^2}\right) + \frac{l^2}{c^2}\right]^{\frac{1}{2}} \tag{3.2}$$

The lattice constants a and c for tetragonal crystal structure are determined from the Eq:

$$\frac{1}{d^2} = \left(\frac{h^2+k^2}{a^2}\right) + \frac{L^2}{c^2} \tag{3.3}$$

Where h, k and l are the indices of the crystal planes, d is the interplanar spacing and β is the full-width half maximum.

Crystallite size (D) is the of the effective crystal domain. It contributes to the peak broadening and as crystallite size decreases, the full width increases. The average D of the film is determined by using Debye Scherrer formula [4].

$$D = \frac{K\lambda}{\beta\, COS\theta} \tag{3.4}$$

Where k is a constant known as shape factor and taken as 0.94, λ is the wavelength of X-rays.

The origin of micro strain (ε) is calculated using the relation [5],

$$\varepsilon = \frac{\beta \cos\theta}{4} \tag{3.5}$$

The dislocation density (δ) is the dislocation lines per unit area of the crystal, can also be evaluated from the crystalline size 'D' using the formula [6],

$$\delta = \frac{1}{D^2} \tag{3.6}$$

3.3 Surface Morphology

Surface morphology is a subset of analytical imaging, which is an advanced form of high spatial resolution imaging that uses sophisticated microscopes to produce images of samples, objects and products that cannot be seen with the naked eye. Such images originate from the exposed surface of the sample or product.

3.3.1 Scanning Electron Microscopy (SEM)

Scanning electron microscope is an instrument that is used to observe the surface morphology of solid sample at higher magnification (>100,000X), higher resolution and greater depth of field up to 100 times that of an optical microscope. It is a type of electron microscope that produces images of a sample by scanning it with a focused beam of high-energy electrons. The electron-sample interactions generate a variety of signals at the surface of solid specimens and carry information about the sample including external morphology (texture), chemical composition, and crystalline structure and orientation of materials making up the sample. The electron beam is generally scanned in a raster scan pattern, and the beam's position is combined with the detected signal to produce an image. In most applications, data are collected over a selected area of the surface (Areas ranging from approximately 1 cm to 5 microns in width) of the sample, and a 2-dimensional image is generated that displays spatial variations in these properties SEM can achieve resolution better than 1 nanometer. Specimens can be observed in high vacuum, in low vacuum, in wet conditions (in environmental SEM), and at a wide range of cryogenic or elevated temperatures [7]. The most common SEM mode is detection of secondary electrons emitted by atoms excited by the electron beam. The number of secondary electrons that can be detected depends, among other things, on specimen topography. By scanning the sample and collecting the secondary electrons that are emitted using a special detector, an image

displaying the topography of the surface is created. Essential components of all SEMs include the following:

- Electron Source ("Gun")
- Electron Lenses
- Sample Stage
- Detectors for all signals of interest
- Display / Data output devices
- Infrastructure Requirements:
  - Power Supply
  - Vacuum System
  - Cooling system
  - Vibration-free floor
  - Room free of ambient magnetic and electric fields

SEMs always have at least one detector (usually a secondary electron detector), and most have additional detectors. The specific capabilities of a particular instrument are critically dependent on which detectors it accommodates [8].

3.3.2 Principles of Scanning Electron Microscopy (SEM)

In SEM, an electron beam is scanned across a sample's surface. The electrons are produced by a thermal emission source, such as a heated tungsten filament, or by a field emission cathode. The energy of the incident electrons can be as low as 100 eV or as high as 30 keV depending on the evaluation objectives. This electron beam generates a number of different types of signals include secondary electrons(SE), back –scattered electrons (BSE), characteristic X-rays, light emitted from the area of the specimen where the electron beam is impinging [9].

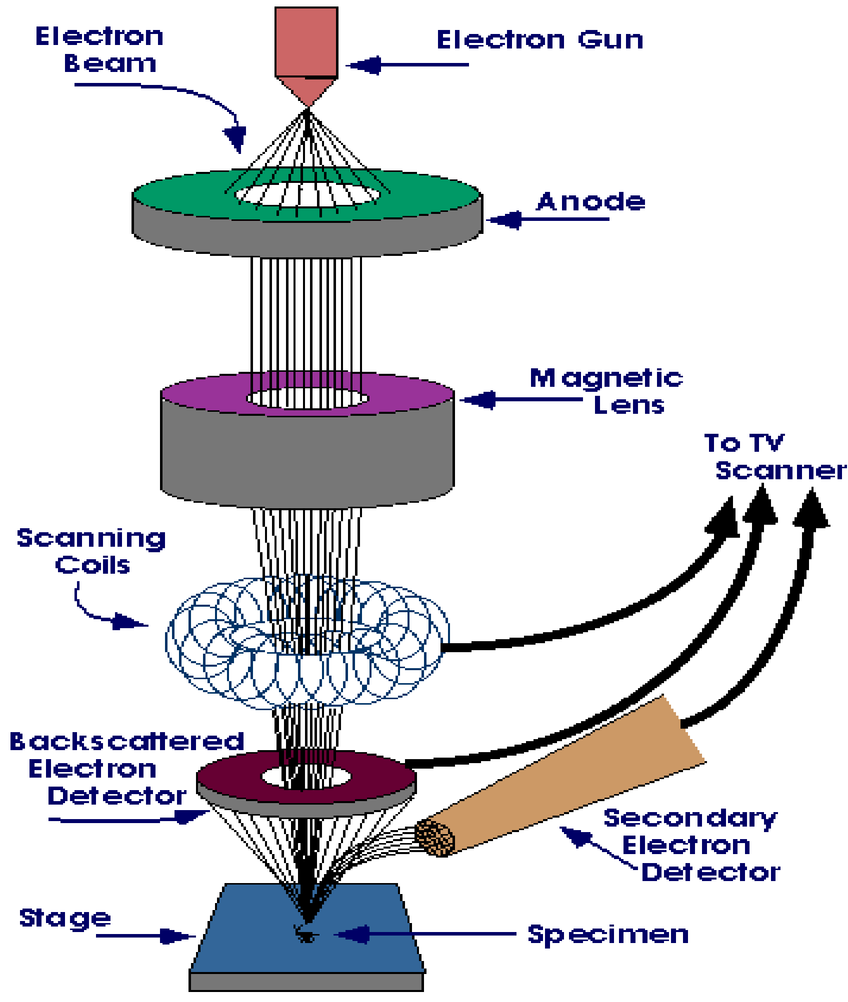

Figure 3.2: Schematic diagram of a scanning electron microscope.

The electrons are focused into a small beam by a series of electromagnetic lenses in the SEM column. The beam passes through pairs of scanning coils or pairs of deflector plates in electron column. The beam passes through pairs of scanning coils or pairs of deflector plates in electron column, typically in the final lens, which deflect the beam in the x and y axes so that it scans in a raster fashion over a rectangular area of the sample surface. When the primary electron beam interacts with the sample, the electrons lose energy by repeated random scattering and absorption within a teardrop-shaped volume of the specimen known

as the interaction volume, which extends from less than 100 nm to approximately 5 μm into the surface. The size of the interaction volume depends on the electron's landing energy, the atomic number of the specimen and the specimen's density. The energy exchange between the electron beam and the sample results in the reflection of high-energy electrons by inelastic scattering and the emission of electromagnetic radiation, each of which can be detected by specialized detectors. The beam current absorbed by the specimen can also be detected and used to create images of the distribution of specimen current. Electronic amplifiers of various types are used to amplify the signals, which are displayed as variations in brightness on a cathode ray tube. The raster scanning of the CRT display is synchronized with the position of the beam on the specimen in the microscope, and the resulting image is therefore a distribution map of the intensity of the signal being emitted from the scanned area of the specimen. The image may be captured by photography from a high –resolution cathode ray tube, but in modern machines is digitally captured and displayed on a computer monitor and also saved to a computer's hard disc [10].

Figure 3.3 represents a thermal field emission gun scanning electron microscope of model JEOL JSM-7600F. This field emission scanning microscope (FESEM) is used in this research work.

Figure 3.3: A field emission scanning electron microscope set up

3.3.3 Atomic Force Microscopy (AFM)

AFM is a very high-resolution type of scanning probe microscopy with demonstrated resolution on the order of fractions of a nanometer, more than 1000 times better than the optical diffraction limit. The precursor of the AFM, the Scanning Tunneling Microscope (STM), was developed by Gerd Binnig and Heinrich Rohrer in the early 1980s at IBM Research – Zurich. They were awarded with the Nobel Prize for Physics in 1986 thanks to the results of their researches. In the same year, Binnig, Quate and Gerber invented the first atomic force microscope which was first placed on the market in 1989. The AFM is one of the foremost tools for imaging, measuring and manipulating matter at the nanoscale. The information is gathered by "feeling" the surface with a mechanical probe. Piezoelectric elements facilitating tiny, accurate and precise movements on (electronic) command enable a very precise scanning. In some variations, electric potentials can also be scanned using conducting cantilevers. In more advanced versions, currents can be passed through the tip to probe the electrical conductivity of the underlying surface. Nevertheless, this is much more challenging with few research groups reporting consistent data.

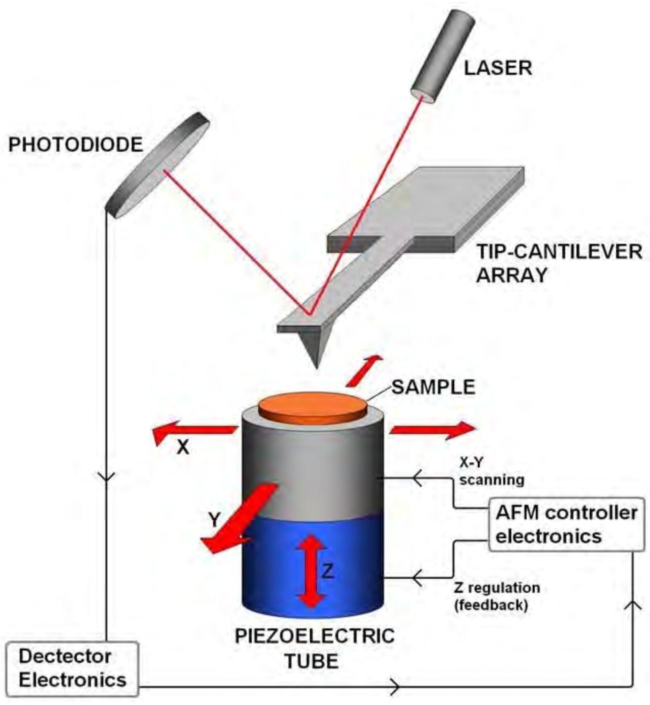

Figure 3.4: Block diagram of atomic force microscope.

The AFM consists of a cantilever with a sharp tip at its end used to scan the specimen surface. The cantilever is usually made by silicon or silicon nitride with a tip radius of curvature on the order of nanometers. When the tip is brought into proximity of a sample surface forces between the tip and the sample lead to a deflection of the cantilever, as per Hooke's law. Depending on the situation, forces that are measured in AFM include mechanical contact force, van der Waals forces, capillary forces, chemical bonding, electrostatic forces, magnetic forces (see Magnetic Force Microscope, MFM), Casimir forces, solvation forces, etc. Along with force, additional quantities may simultaneously be measured through the use of specialized types of probe (see scanning thermal microscopy, scanning joule expansion microscopy, photothermal microspectroscopy, etc.). Typically, the deflection is measured using a laser spot reflected from the top surface of the cantilever into an array of photodiodes. Other methods used include optical interferometry, capacitive sensing or piezoresistive AFM cantilevers. These cantilevers are fabricated with piezoresistive elements acting as a strain gauge. Strain in the AFM cantilever can be measured by using the Wheatstone bridge. Nevertheless, this method is not as sensitive as laser deflection or interferometry. The AFM can be operated in a number of modes depending on the application. In general, possible imaging modes are divided into static (also called “contact”) modes and a variety of dynamic (non-contact or "tapping") modes where the cantilever is vibrated. In static mode, the cantilever is "dragged" across the surface of the sample and the contours of the surface are measured directly using the deflection of the cantilever. In the dynamic mode, the cantilever is oscillated externally at (or close to) its fundamental resonance frequency. The oscillation amplitude, phase and resonance frequency are modified by tip-sample interaction forces. These changes in oscillation with respect to the external reference oscillation provide information about the sample's characteristics.

In tapping mode (also called "AC Mode" or "intermittent contact mode") the cantilever is driven to constantly oscillate vertically closed to its resonance frequency by a small piezoelectric element mounted in the AFM tip holder similar to non-contact mode. However, the amplitude of this oscillation is greater than 10 nm, usually between 100 nm and 200 nm. When the tip comes close to the surface, Van der Waals force, dipole-dipole

interaction, electrostatic forces, etc., cause the amplitude of this oscillation to decrease as the tip gets closer to the sample. An electronic servo uses the piezoelectric actuator to control the height of the cantilever above the sample. The servo adjusts the height to maintain a set cantilever oscillation amplitude as the cantilever is scanned over the sample. A tapping AFM image is therefore produced by imaging the force of the intermittent contacts of the tip with the sample surface [11]. This method of "tapping" lessens the damage done to the surface and the tip compared to the amount done in contact mode. Tapping mode is gentle enough even for the visualization of supported lipid bilayers or adsorbed single polymer molecules (for instance, 0.4 *nm* thick chains of synthetic polyelectrolytes) under liquid medium. With proper scanning parameters, the conformation of single molecules can remain unchanged for hours.

3.4 Optical Characterization

3.4.1 UV-VIS spectroscopy

Ultraviolet (UV) and Visible (VIS) light can cause electronic transitions. When a molecule absorbs UV-VIS radiation, the absorbed energy excites an electron into a higher energy orbital. Ultraviolet radiation has wavelengths of 200-400 nm. Visible light has wavelengths of 400-800 nm.

Wavelength Region (nm)

Far ultraviolet 10-200

Near ultraviolet 200-400

Visible 400-800

Near infrared 800-3000

Middle infrared 3000-30,000

Far infrared 30,000-300,000

Microwave 300,000-1,000,000,000

A diagram (3.5) of the components of a typical spectrometer is shown in the following diagram. The functioning of this instrument is relatively straightforward. A beam of light from a visible and UV light source (colored red) is separated into its component wavelengths by a prism or diffraction grating.

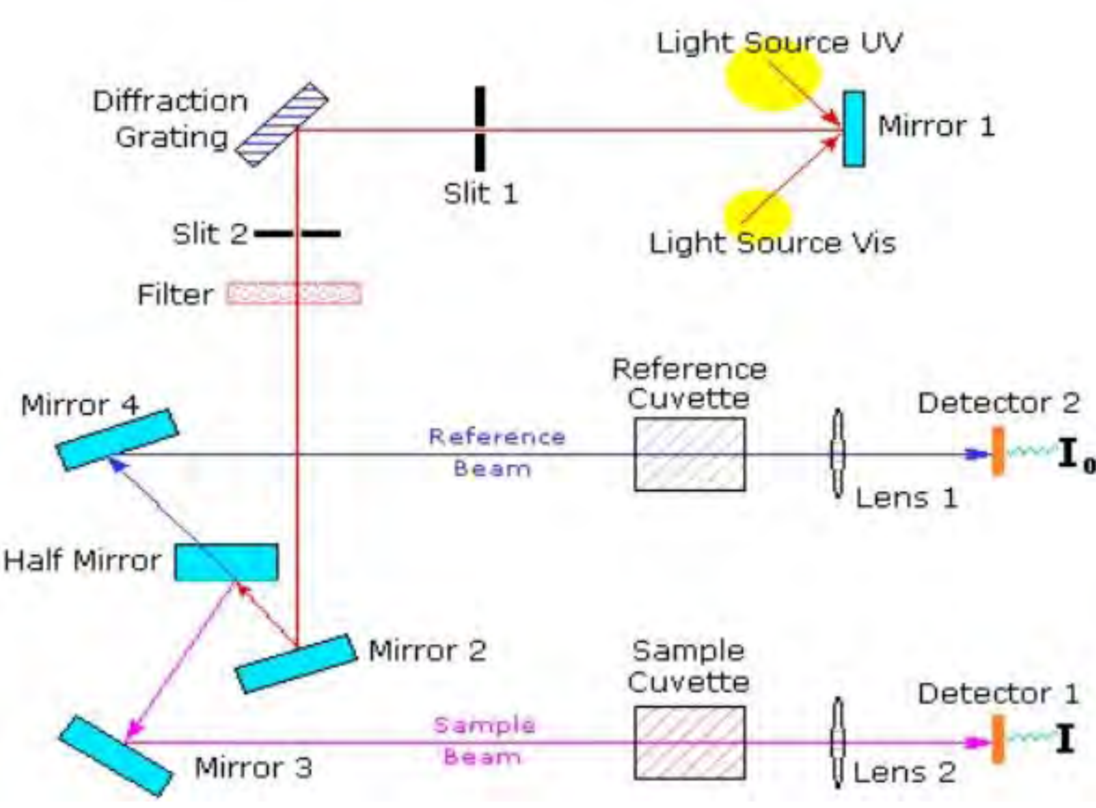

Figure 3.5: The components of a typical spectrometer

Each monochromatic (single wavelength) beam in turn is split into two equal intensity beams by a half-mirrored device. One beam, the sample beam (colored magenta), passes through a small transparent container (cuvette) containing a solution of the compound being studied in a transparent solvent. The other beam, the reference (colored blue), passes through an identical cuvette containing only the solvent. The intensities of these light beams are then measured by electronic detectors and compared [12]. The intensity of the reference beam, which should have suffered little or no light absorption, is defined as I_0. The intensity of the sample beam is defined as I.

3.4.2 Optical characterization of thin films

Optical properties of films have been studied extensively primarily because of their applications in various optical and electro-optical devices. The optical study of a solid

concerns not only with the physical phenomena such as reflection, refraction, transmission, absorption, polarization, interference of light but also the interactions of photon energy with matter and the consequent changes in the electronic states. From reflection, transmission and absorption processes it is possible to evaluate the optical constants refractive index (n), extinction coefficient (k) and absorption coefficient (α) and in turn also the complex dielectric constant (ϵ*) of solid state thin films [12].

3.4.3 Beer-Lambert law

The Beer-Lambert law (or Beer's law) [7] is the linear relationship between absorbance and concentration of an absorbing species. The general Beer-Lambert law is usually written as:

$$A = \alpha bc \tag{3.7}$$

Where A is the measured absorbance, $\alpha(\boldsymbol{\lambda})$ is a wavelength-dependent absorbance coefficient, b is the path length, and c is the analyzed concentration. When working in concentration units of morality, the Beer-Lambert law is written as

$$A = \varepsilon bc \tag{3.8}$$

Where ε is the wavelength-dependent molar absorptivity coefficient with units of $M^{-1}cm^{-1}$. Experimental measurements are usually made in terms of transmittance (T), which is defined as:

$$T = I / Io \tag{3.9}$$

Where I is the light intensity after it passes through the sample and Io is the initial light intensity. The relation between A and T is:

$$A = -log\, T = -\, log\, (I / Io) \tag{3.10}$$

Modern absorption instruments can usually display the data as transmittance, %transmittance, or absorbance. An unknown concentration of an analytic can be determined by measuring the amount of light that a sample absorbs and applying Beer's law. If the absorptive coefficient is not known, the unknown concentration can be

determined using a working curve of absorbance versus concentration derived from standards.

3.4.4 Derivation of the Beer-Lambert law

The Beer-Lambert law can be derived from an approximation for the absorption coefficient for a molecule by approximating the molecule by an opaque disk whose cross-sectional area σ represents the effective area seen by a photon of frequency υ .If the frequency of the light is far from resonance, the area is approximately 0, and if υ is close to resonance the area is a maximum. Taking an infinitesimal slab, dz, of sample (Figure 3.6)

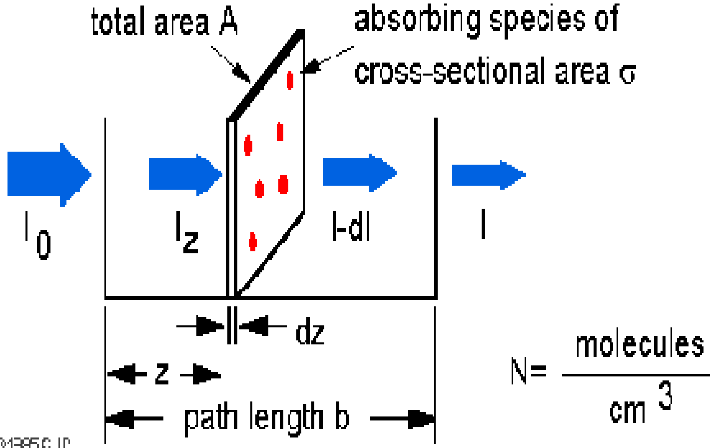

Figure 3.6: Absorption of light by a sample.

I_o is the intensity entering the sample at z = 0, I_z is the intensity entering the infinitesimal slab at z, dI is the intensity absorbed in the slab, and I is the intensity of light leaving the sample. Then, the total opaque area on the slab due to the absorbers is σ× N× A ×dz. Then, the fraction of photons absorbed will be σ×N ×A ×dz /A so,

$$dI\ /\ Iz\ =\ -\ \sigma N dz \qquad (3.11)$$

Integrating this equation from z = 0 to z = b gives:

$$ln(I)\ -\ ln(Io)\ =\ -\ \sigma Nb$$

$$or\ -\ ln(I\ /\ Io)\ =\ \sigma Nb.$$

Since N (molecules/cm^3)×(1 mole / 6.023x1023 molecules)×1000 cm^3 / liter = c (moles/liter) and 2.303 × log(x) = ln(x) then,

$$-\log(I / Io) = \sigma(6.023x1020 / 2.303) \times c \times b$$

$$-\log(I / Io) = A = \varepsilon bc \tag{3.12}$$

Where ε = σ×(6.023x1020 / 2.303) = σ × 2.61x1020, and ε is called absorptivity. Thus, the intensity of the transmitted light can be expressed as $I = Io\ e^{-\alpha d}$ where d is the path length through the sample and α is the absorbance coefficient [13]. This equation can be written as,

$$\alpha = 2.303\left(\frac{A}{d}\right) \tag{3.13}$$

3.4.5 Electronic transitions

The absorption of UV or visible radiation corresponds to the excitation of outer electrons. There are three types of electronic transition which can be considered;

1. Transitions involving π,σ, and n electrons
2. Transitions involving charge-transfer electrons
3. Transitions involving d and f electrons (not covered in this Unit).

When an atom or molecule absorbs energy, electrons are promoted from their ground state to an excited state. In a molecule, the atoms can rotate and vibrate with respect to each other. These vibrations and rotations also have discrete energy levels, which can be considered as being packed on top of each electronic level (Figure3.7).

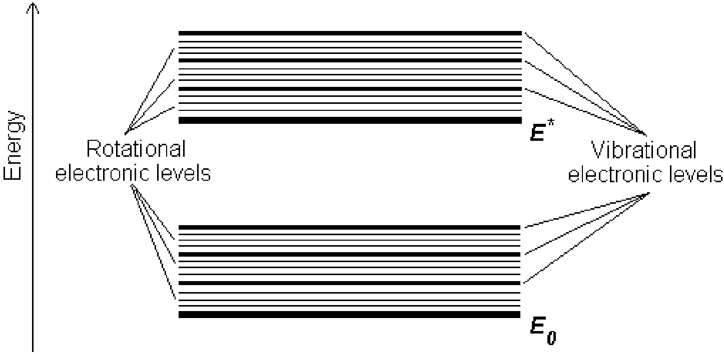

Figure 3.7: Vibrational and rotational energy.

Absorbing species containing π, σ, and n electrons

Absorption of ultraviolet and visible radiation in organic molecules is restricted to certain functional groups (chromophores) that contain valence electrons of low excitation energy. The spectrum of a molecule containing these chromospheres is complex. This is because the superposition of rotational and Vibrational transitions on the electronic transitions gives a combination of overlapping lines. This appears as continuous absorption band. Possible electronic transitions of π, σ, and n electrons are discussed below in figure 3.8

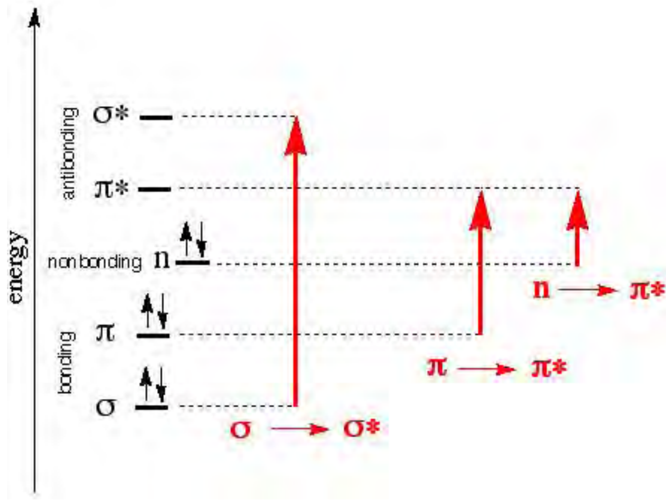

Figure 3.8: Possible electronic transitions

σ → σ* Transitions

An electron in a bonding σ orbital is excited to the corresponding antibonding orbital. The energy required is large. For example, methane (which has only C-H bonds, and can only undergo σ → σ* transitions) shows an absorbance maximum at 125 nm. Absorption maxima due to σ → σ* transitions are not seen in typical UV-Vis. spectra (200 - 700 nm)

n →σ* Transitions

Saturated compounds containing atoms with lone pairs (non-bonding electrons) are capable of n →σ* transitions. These transitions usually need less energy than n →σ* * transitions. They can be initiated by light whose wavelength is in the range 150 - 250 nm. The number of organic functional groups with n →σ* peaks in the UV region is small.

n →σ* and π→π* Transitions

Most absorption spectroscopy of organic compounds is based on transitions of n or π electrons to the π* excited state. This is because the absorption peaks for these transitions fall in an experimentally convenient region of the spectrum (200 - 700 nm). These transitions need an unsaturated group in the molecule to provide the π electrons.

Molar absorbtivities from n →σ* transitions are relatively low, and range from 10 to100 L mol-1 cm-1. π→π* transitions normally give molar absorbtivities between 1000 and 10,000 L mol-1 cm-1. The solvent in which the absorbing species is dissolved also has an effect on the spectrum of the species. Peaks resulting from n →σ* transitions are shifted to shorter wavelengths (blue shift) with increasing solvent polarity. This arises from increased solvation of the lone pair, which lowers the energy of the n orbital. Often (but not always), the reverse (i.e. red shift) is seen for π→π* transitions. This is caused by attractive polarization forces between the solvent and the absorber, which lower the energy levels of both the excited and unexcited states. This effect is greater for the excited state, and so the energy difference between the excited and unexcited states is slightly reduced - resulting in a small red shift. This effect also influences n →σ * transitions but is overshadowed by the blue shift resulting from solvation of lone pairs.

3.4.6 Direct and indirect optical transition

In solid state physics, a band gap, also called an energy gap or band gap, is an energy range in a solid where no electron states exist. For insulators and semiconductors, the band gap generally refers to the energy difference (in electron volts) between the top of the valence band and the bottom of the conduction band. It is the amount of energy required to free an outer shell electron from its orbit about the nucleus to become a mobile charge carrier, able to move freely within the solid material.

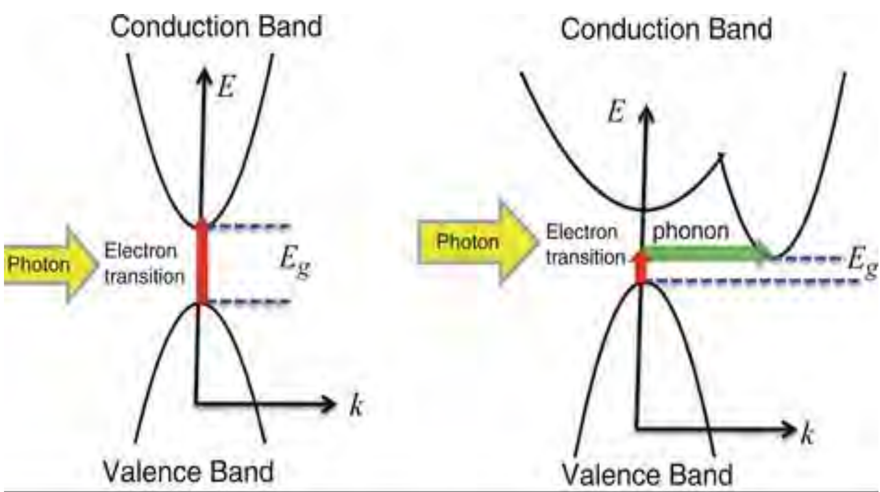

Figure 3.9: Schematic presentation of direct and indirect transitions between valence and conduction band.

In semiconductor physics, the band gap of a semiconductor is always one of two types, a direct band gap or an indirect band gap. The minimal-energy state in the conduction band, and the maximal-energy state in the valence band, are each characterized by a certain k-vector in the Brillouin zone. If the k-vectors are the same, it is called a "direct band gap". If they are different, it is called an "indirect band gap".

The direct and indirect band gap of the material can be obtained from the tauc relation. The tauc relation is given below.

$$\alpha h v = A\,(h v - Eg)^{n} \quad (3.14)$$

where A is a constant or Tauc parameter depending upon the transition probability for direct transitions, n = 1/2 and n = 2 for indirect transitions [8]. Eg is the optical gap.

3.4.7 Refractive index and extinction coefficient

One of the most important optical constants of a material is its refractive index, which in general depends on the wavelength of the electromagnetic wave, through a relationship called dispersion. In materials where an electromagnetic wave, can be lose its energy during its propagation, the refractive index become complex. Refraction of light at the interface between two media of different refractive indices n1 and n2 are shown in figure 3.10

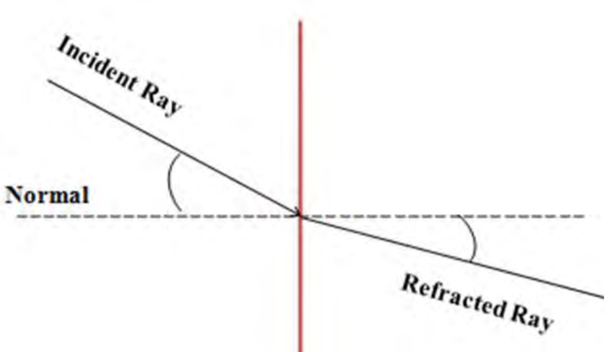

Figure 3.10: Refraction of light at the interface between two different refractive indices media.

The real part is usually the refractive index (n) and the imaginary part is called the extinction coefficient (k). In this section, n and k will be presented in detail along with some common dispersion relations. N of an optical or dielectric medium, is the ratio of the velocity of light (c) in vacuum to its velocity v in the medium, n= c/v . Using the Maxwell's equations, one obtains the well known Maxwell's formula for the refractive index of substance as $n=\sqrt{\varepsilon_r \mu_r}$ where ε is the static dielectric constant or relative permittivity and μ_r the relative permeability. As $\mu_r = 1$ for nonmagnetic substrate, one gets, $n=\sqrt{\varepsilon_r}$, which is very useful in relating the dielectric property to optical properties of materials at any particular frequency of interest. As ε depends on the wavelength of light, n also depends on the wavelength of

light,and this dependence is called dispersion. In addition to dispersion, an electromagnetic wave propagating through a medium, which means it loses its energy, due to various loss mechanisms such as the generation of phonons (lattice wave), photo generation, free carrier absorption, scattering, etc. In such materials, the refractive index becomes a complex function of the frequency of light wave. The complex refractive index, denoted by n*, with real part n, and imaginary part k, called the extinction coefficient, is related to the complex relative permittivity (ε) by:

$$n^* = n - jk = \sqrt{\varepsilon} = \sqrt{(\varepsilon_r - j\varepsilon_i)} \quad (3.15)$$

Where ε_r and ε_i are, respectively, the real and imagination parts of ε. Equation gives

$$n^2 - k^2 = \varepsilon_r \text{ and } 2nk = \varepsilon_i \quad (3.16)$$

In explicit terms, n and k can be obtained as :

$$n = \sqrt{1/2}\,[\sqrt{(\varepsilon_r^2 + \varepsilon_i^2)} + \varepsilon_r]^{1/2} \quad (3.17)$$

$$k = \sqrt{1/2}\,[\sqrt{(\varepsilon_r^2 + \varepsilon_i^2)} - \varepsilon_r]^{1/2} \quad (3.18)$$

the optical constants n and k can be determined by measuring the reflectance from the surface of a material as a function of polarization and the angle of incidence. For normal incidence, the reflective coefficient, r, is obtained as

$$r = (1-n)* /(1+n)* = (1-n+jk)/(1+n+jk) \quad (3.19)$$

The reflectance R is then defined by:

$$R = |r|^2 = |1-n+jk/1+n+jk|^2 = \{(1-n)^2+k^2\}/\{(1+n)^2+k^2\} \quad (3.20)$$

And refractive index can be calculated by using the following equation

$$n = (1+R/1-R) + \sqrt{4R/(1-R)^2 - k^2} \quad (3.21)$$

Notice that whenever k is large, for example over a range of wavelength, the absorption is strong, and the reflectance is almost unity. The light is then reflected, and any light in the medium is highly attenuated. Extinction coefficient can be determined from the relation as follows

$$k = \frac{\alpha\lambda}{4\pi} \tag{3.22}$$

Optical conductivity of thin films is calculated by using the following equation

$$\sigma_{opt} = \frac{\alpha n c}{4\pi} \tag{3.23}$$

3.4.8 Absorption coefficient

When a semiconductor is illuminated by a light, a photon strikes the surface, a fraction of photons are reflected and the remaining photons enter the semiconductor. Some of these are absorbed within the semiconductor and the remainder transmitted into the semiconductor. The absorption of radiation by any medium occurs through the excitation of electrons and photons [14]. For semiconductor, it is convection to consider several types of absorption arising from

I. Electronic transition between different energy bands.
II. Electronic transitions within energy band
III. Electronic transitions to localized states of impurity atoms
IV. Lattice Vibrations
V. Vibrations of impurity atoms

In the fundamental absorption region the transmission T is given by

$$T = A \exp\left(\frac{4\pi\kappa t}{\lambda}\right) \tag{3.24}$$

Where 'A' is a constant, 'k' is the extinction co-efficient and't' is the thickness. For $k^2 << n^2$, the principle variation of T occurs in the exponential term and pre-exponential term A. Therefore

$$T \approx exp\ (-\alpha t) \tag{3.25}$$

Where $\alpha = \frac{4\pi\kappa}{\lambda}$ is the absorption co-efficient of the film. Thus the value of absorption co-efficient may be calculated from the relation

$$\alpha = -\frac{\ln T}{t} \tag{3.26}$$

3.5 Thickness measurement of thin film

Film thickness is defined as the perpendicular distance from any point on a surface to the other end of the film. It plays an important role on the properties of thin film and also it is one of the most significant film parameters. Therefore, the thickness should be measured with great care as far as possible to have an accurate value. There are several methods for thin film thickness measurement, for instance, weighing, X-ray fluorescence, stylus profiler technique and multiple-beam interferometer technique [15]. Multiple-beam interferometer technique is employed for the measurement of thickness of the thin films. In this method two reflecting surface are brought into close proximity to produce interference fringes. Nowadays it is a well-developed and standard method . When two reflecting surfaces are brought into close proximity, interference fringes are produced, the measurement of which makes possible a direct determination of film thickness and surface topography with high accuracy. In this method, two types of fringes are utilized for thickness measurement. The first produces Fizeau fringes of equal thickness, using a monochromatic light source. The second uses a light source and produces fringes of equal chromatic order. The second method is prepared for thinner films. The Fizeau fringes method is used in the present work for the measurement of film thickness. For the experimental set up a low power microscope, a monochromatic source of light, a glass plate and an interferometer are required. To make the Fizeau fringes of equal thickness visible in a multiple beam interferometer formed by a thin absorbing film on a glass substrate, generally and auxiliary reflecting Coating on the film surface is required. But if the experimental sample is transparent with a very smooth surface no such auxiliary coating is necessary. The film whose thickness is to be measured is required to form a step on a glass substrate and over it another plane glass plate is placed. This illuminated with a parallel monochromatic beam of light a fringe system is produced and is viewed with low power microscope [16].

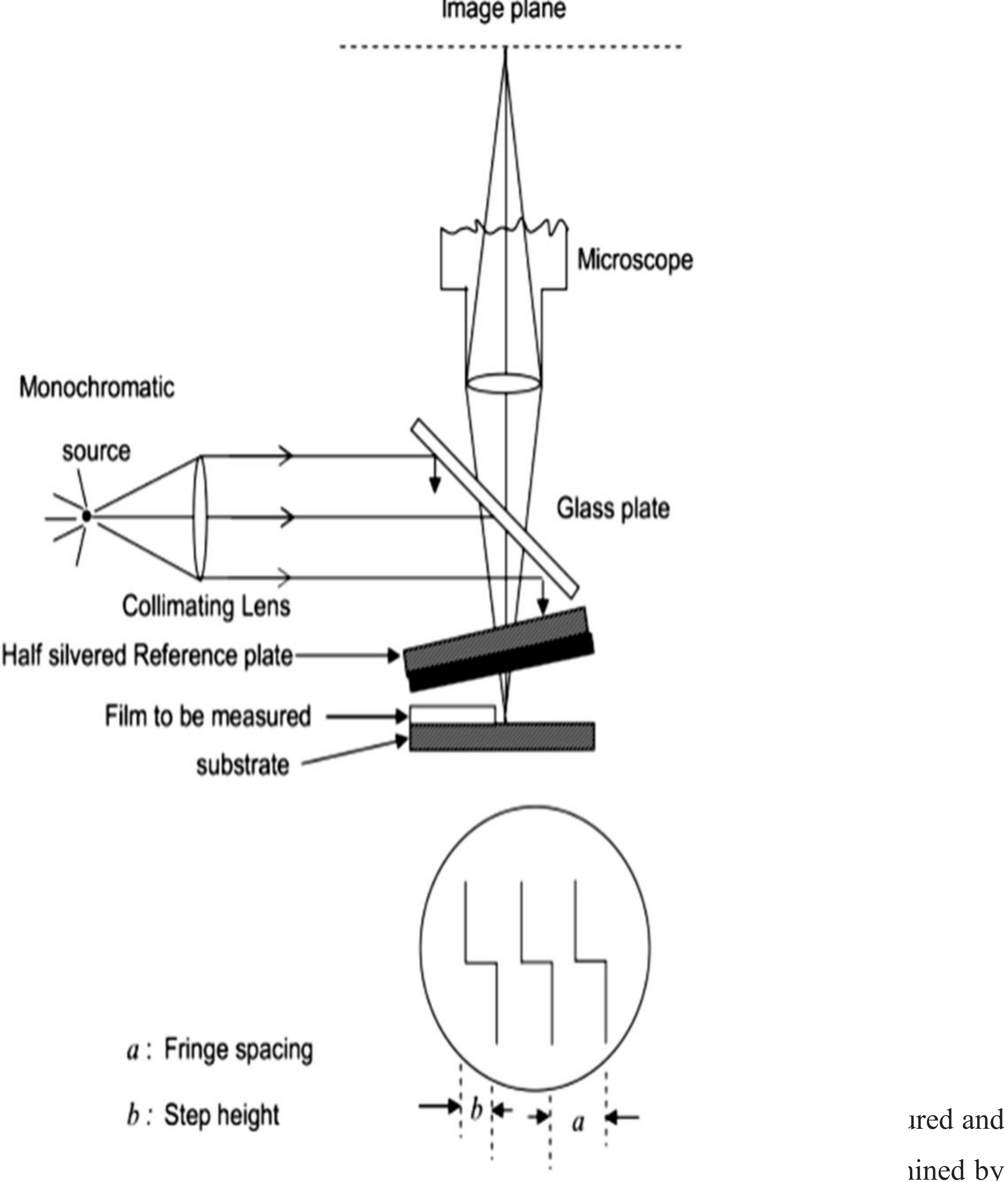

red and

ined by

Figure 3.11: interferometer arrangement for producing refection Fizeau fringes of equal thikness.

$$d = \frac{\lambda}{2} \times \frac{b}{a} \tag{3.26}$$

Where,

λ = wavelength

b = step height

a = fringe spacing

In general, the sodium light is used, for which $\lambda = 5893\ A^0$. Figure 3.5 shows the diagram of multiple –beam interferometer thickness measurement method. From above formula thicknesses of ZnO and SnO_2 single layers are measured. In the case of bilayer thin film this process repeated after second layer deposition because first layer used as a substrate for second layer.

Total thickness of the bilayer thin film – thickness of the first layer of the bilayer thin film = thickness of the second layer of bilayer thin film.

3.6 Electrical Characterization

Electrical characterization methods for the analysis of thin films include the measurement of the electrical resistivity (ρ). ρ is a key physical property of all materials. It is often necessary to accurately measure the value of ρ of a given material. There are four methods commonly used for the measurement of resistivity such as:

I. Direct method
II. Two point probe method
III. Four point probe method
IV. Van der pauw method

3.6.1 Direct method

The resistivity of a thin film can be measured easily by direct method using the relation

$$\rho = R\frac{wt}{L} \tag{3.27}$$

Where w and t are the breath and thickness of the sample. For simplicity, if we consider w = L, the above equation becomes

$$\rho = Rt \quad (3.28)$$

Electrical conductivity of a material is reciprocal of resistivity of the material. Conductivity is denoted by a σ and defined as

$$\sigma = 1/\rho \quad (3.29)$$

Measuring the resistance, R and thickness, t one can easily determine the resistivity and the conductivity.

3.6.2 Two point probe method

It is simple method of measuring resistivity and is illustrated in figure 3.12

In this method, voltage drop V across the sample and current through the sample I are measured. Then the resistivity is given as

$$\rho = \frac{VA}{IL} \quad (3.30)$$

Where L is the specimen length and A is the cross- sectional area of the specimen. This method is useful when the sample has large resistance

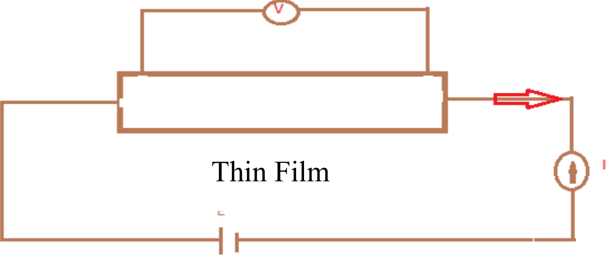

Figure 3.12: Electrical resistivity measurement by two point probe method.

3.6.3 Four point probe method

Four probe apparatus is one of the standard and most widely used apparatus for the measurement of resistivity of semiconductors. This method is employed when the sample is in the form of a thin wafer, such as a thin semiconductor material deposited on a substrate.

The sample is millimeter in size and having a thickness w. It consists of four probe arranged linearly in a straight line at equal distance S from each other. A constant current is passed through the two probes and the potential drop V across the middle two probes is measured. An oven is provided with a heater to heat the sample so that behavior of the sample is studied with increase in temperature.

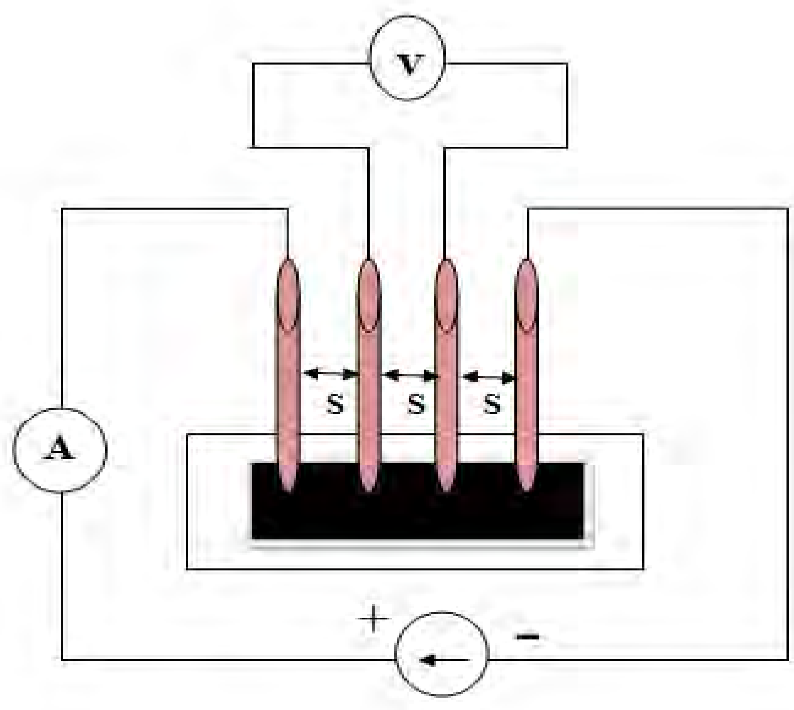

Figure 3.13: The arrangements of four probes that measure voltage (V) and supply current (I) to the surface of the crystal.

In the case of a four point probe on a sheet, the two outside current points represent the dipole. Therefore, the resistivity in this case can be given by

$$\rho = 2\pi S\left(\frac{V}{I}\right) \tag{3.31}$$

Here, the distance between all the four points is equal. I is the current flowing through the sample, V_D is produced voltage across two inner points and S is the distance between the

adjacent points. If the distance between contact points is not equal and it is given as S_1, S_2 and S_3 respectively, then the resistivity is given as

$$\rho = \frac{V}{I}\left[\frac{2\pi}{\left(\frac{1}{S1}+\frac{1}{S2}-\frac{1}{S1+S2}-\frac{1}{S2+S3}\right)}\right] \tag{3.32}$$

Where V is the floating potential difference between the inner probes, and I is the current through outer pair of probes.

3.6.4 Van der pauw method

The van der pauw method, due to its convenience, is widely used in the semiconductor industry to determine the resistivity of sample [17]. The van der pauw method can be used to measure samples of arbitrary shape, although several basic sample condition must be satisfied to obtain accurate measurements, such as the thickness of the sample must be constant , point contacts placed at the edges of the samples must be used for the measurements, and the sample quality has to be homogeneous. Most semiconductor samples satisfy these conditions, so that this convenient measurement method has been widely utilized.

Figure 3.14: experimental arrangements for measuring resistivity by using Van der Pauw method.

At first we select a region on the sample where four electrical contacts were made at four corners, say A, B, C and D as shown in figure 3.10. Silver paste or indium was used to the contact. If a current I_{AB} entering the specimen through the contact A and leaving through the contact, B produces a potential difference V_{DC} between the points C and D then the resistance $R_{AB,CD}$ is defined as

$$R_{AB,CD} = \frac{V_{DC}}{I_{AB}} \qquad (3.33)$$

Similarly, we have

$$R_{CD,AB} = \frac{V_{BA}}{I_{CD}} \qquad (3.34)$$

$$R_{BC,DA} = \frac{V_{AD}}{I_{BC}} \qquad (3.35)$$

$$R_{DA,BC} = \frac{V_{CB}}{I_{DA}} \qquad (3.36)$$

The resistivity of a thin film can be expressed by the equation

$$\rho = \frac{\pi d}{\ln 2}\left[\frac{R_{AB,CD} + R_{BC,DA}}{2}\right] f\left(\frac{R_{AB,CD}}{R_{BC,DA}}\right) \qquad (3.37)$$

$$\rho = 4.53d\left[\frac{R_{AB,CD} + R_{BC,DA}}{2}\right] f\left(\frac{R_{AB,CD}}{R_{BC,DA}}\right) \qquad (3.38)$$

Where d is the thickness of the film and the function f can be evaluated from the equation

$$[\, R_{AB,CD} – R_{BC,DA}/R_{AB,CD} + R_{BC,AD}] = f/\ln 2 \text{ arc cosh } \exp(\ln 2/f)/2 \qquad (3.39)$$

If $R_{AB,CD}$ and $R_{BC,DA}$ is almost equal, f may be approximately equal to unity and then the equation 3.42 takes the form.

$$\rho = 2.265d(R_{AB,CD} + R_{BC,DA})\ \Omega\text{-cm}. \qquad (3.40)$$

3.6.5 Hall Effect Measurement

Hall Effect Principle is one of the most popular theories in magnetic field measurement. This post will discuss Hall Effect Principle, its history, theory explanation, applications and mathematical expressions of Hall Effect Principle including calculations for Hall Voltage, Hall Coefficient, Charge Carrier Concentration, Hall Mobility and Magnetic Field Density Hall Effect Principle explains the behavior of charge carriers when it is exposed to electricity and magnetic fields. This principle can be regarded as an extension to Lorentz Force which is the force acting on the charge carriers (Electrons and Holes) passing through a magnetic field. The sensors working on this Principle are called Hall Effect Sensors. These Hall Effect Sensors are in high demand and have very wide spread applications such as Proximity sensors, Switches, Wheel speed sensors, Positional sensors, etc [18].

Hall Effect Principle

Hall Effect Principle says that when a conductor or semiconductor with current flowing in one direction is introduced perpendicular to a magnetic field a voltage could be measured at right angles to the current path. The effect of getting a measurable voltage, as told above, is called the Hall Effect.

Here are some mathematical expressions which are widely used in Hall Effect calculations:

Hall Voltage

Hall Voltage is represented by V_H. The mathematical Expression for Hall voltage is:-

$$V_H = \frac{IB}{qnd} \tag{3.41}$$

Where

I – Current flowing through the Sensor

B – Magnetic Field Strength

q – Charge

n – number of charge carriers per unit volume

d – Thickness of the Sensor

Hall Coefficient

It is represented by R_H. Mathematical expression for Hall Coefficient (R_H) is **1/(qn)**. The Hall Coefficient (R_H) is positive if the number of positive charge Holes are more than the number of negative charge Electrons. Similarly, The Hall Coefficient (RH) is negative if the number of negative charge Electrons are more than the number of positive charge Holes.

Charge Carrier Concentration

The Charge Carrier Concentration of Electrons is represented by 'n' and Holes is represented by 'p'. The mathematical expression for the Charge Carrier Concentration is:

$$n \ or \ p = \frac{1}{qR_H} \tag{3.42}$$

Hall Mobility

The Hall Mobility for Electrons is represented by 'μ_n' and for Holes is represented by 'μ_p'. The mathematical expression for the Hall Mobility is: –

$$\mu_n \ or \ \mu_p = \sigma n R_H \tag{3.43}$$

Where:

μ_n – Conductivity due to Electrons

μ_p – Conductivity due to Holes

If the Hall Coefficient is negative, it means that the majority charge carriers are Electrons. And as the number of electrons are more compared to Holes in n-type semiconductors, that clearly indicates that the semiconductor being tested is n-type. Similarly, if the Hall Coefficient is positive, it means that the majority charge carriers are Holes. And as the number of Holes are more compared to electrons in p-type semiconductors, that clearly indicates that the semiconductor being tested is p-type [19].

3.6.6 Activation energy

The energy required to transfer charge from one initially neutral island to another is known as activation energy and denoted by ΔE. This is equivalent to the electrostatic binding energy of the charge of the island. When these charge carriers are excited to a least this energy from the Fermi-level, there will be tunneling from one island to another. These islands or small particles are called crystalline. The activation energy is related with film conductivity and given by the relation

$$\sigma = \sigma_0 \exp\left(-\Delta E / 2KT \right) \tag{3.44}$$

Where σ_0 is the conductivity at 273 K, k is the Boltzmann constant and T is the absolute temperature. Equation (3.41) can be written as:

$$ln\sigma = \frac{-\Delta E}{2KT} + ln\sigma_0 \tag{3.45}$$

Equation (3.44) is equivalent to a straight line equation, y = mx + c. So that ΔE can be determined from the slope of the straight line. From the graph of lnσ vs. $\frac{1}{T}$, ΔE can be calculated by using the relation

$$\Delta E = -\frac{\ln \sigma}{\frac{1}{T}} \times 2k\,(eV) \tag{3.46}$$

References

[1] Raviprakash, Y., Kasturi, Bangera, V., Shivakumar, G. k., "Preparation and characterization of $CdZn_{1-x}S$ thin films by spray pyrolysis technique for photovoltaic applications", Solar Energy., Vol. 83, pp. 1645-1651, 2009.

[2] Gupta, B. k. and Agnihoti, O. P., "Structural investigations of spray –deposited CdS films doped with Cu, In, and Ga", Philos. Mag. (b), Vol. 37, pp. 631-633, 1978.

[3] Warren, B. E., "X-ray Diffraction", Addision Wesely Publishing Co.: London, 1969.

[4] Cullity, B. D., "Elements of X-ray Diffraction", Addison-Wesley Publishing Company. Inc. USA, 1959.

[5] Zhao, Y. and Zhang, J., "Microstrain and grain-size analysis form diffraction peak width and graphical derivation of high –pressure thermomechanics", J. Appl. Cryst., Vol. 41, pp. `1095-1108, 2008.

[6] Szekely, F., Groma, I., and Lendvai, J., "Characterization of self-similar dislocation structures by X-ray diffraction", Mater. Sci, Engn., A, Vol. 324, pp.179-182, 2002.

[7] Barrett, C. S., Massalski, T. B., "Structure of Metals", McGraw-Hill Book Company: New York, 1966.

[8] Maissel, L. I., Glang, R., "Handbook of Thin Film Technology" McGraw-Hill Book Company: New York, 1970.

[9] Hirsch, P. B., Howie, A., Nilcholson, R.B., Pashly, D.W., Whelan, M.J., Electron "Microscopy of Thin Crystals", Butterworths: Washington D. C., 1965.

[10] Howland, R., Benatar, L., "A Practical guide to Scanning Probe Microscopy", Park Scientific Instruments, 1996.

[11] Jagtap, R. N., & Ambre, A. H., "Overview literature on atomic force microscopy (AFM): Basics and its important applications for polymer characterization", Indian Journal of Engineering & Materials Sciences Vol. 13, pp. 368-384, 2006.

[12] Islam M. R., and Podder J., "Optical Properties of ZnO nano fiber thin films grows by spray pyrolysis of zince acetate precursor" Cryst. Res. Technol., Vol. 44, No.3, pp. 286-292, 2009.

[13] Swinehart, D. F., "The Beer-lambert law", J. Chem. Edu., Vol. 39(7), pp. 333-335, 1962.

[14] Davies, E. A., and Mott, N. F., “Conduction in non-crystalline system, optical absorption and photoconductivity in amorphous semiconductor”, Philos. Mag.,Vol. 22, pp. 903-922, 1970.

[15] Pliskin, W. A., and Stelvio, J. Z., “Thin Film Technology”, McGraw Hill New York, 1970.

[16] Tolanasky, S., “Multiple Beam Interferometry”, Oxford University Press, London, 1948.

[17] Singh, Y., “Electrical resistivity measurement: a review”, Int. J. Mod. Phys.: Conf. Series, Vol. 22, pp. 745-756, 2013.

[18] Van der Pauw, L. J., “A method of measuring specific resistivity and hall effect of discs of arbitrary shape”, Philips. Res. Report., Vol. 13(1), pp. 1-9, 1958.

[19] Gutitrrez, F. J., Arks, L., Robla, J. I., Getino, J. M., Horrillo, M. C., Sayago, I., and de Agapito, J. A., “Hall coefficient of temperature measurements for SnO_2, doped sensors, as a function and atmosphere”, Sensors and Acrua~ors B, Vol. 15-16, 98-104, 1993.

CHAPTER FOUR

EXPERIMENTAL DETAILS

CHAPTER FOUR

EXPERIMENTAL DETAILS

4.1 Preparations of Thin Films

A thin film can be defined as a quasi-two-dimensional material created by condensing, atomic/molecular/ionic species of mater. Thin film preparation is a sequential process. Spray pyrolysis is the most commonly used technique adopted for the synthesis of thin film of transparent, conducting, etc. compounds. Spray pyrolysis (SP) is one of the most common techniques used for deposition of thin films. In this work, pure ZnO, pure SnO_2 and bilayer ZnO/SnO_2 thin films are prepared by using a locally fabricated SP deposition (SPD) unit. This chapter includes a brief discussion of the SPD unit and various steps of preparation of bilayer ZnO/SnO_2 thin films with thickness variation of SnO_2 layers on glass substrate by SPD technique.

4.2 Experimental details

4.2.1 Preparation of masks

In order to study the various properties of thin film, it is necessary that they must be properly patterned. The direct deposition of thin film pattern requires a suitably shaped aperture, commonly referred to as a mask. For the purpose of various experimental studies, film of specific size and shape are required. Mask was made from stainless steel plate with the desired pattern cut into it. The aperture was made in a bath machine. All mask should be thoroughly cleaned and inspected before use.

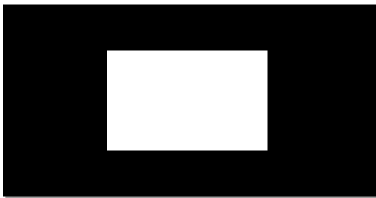

Figure 4.1: Mask for the sample

Regardless of mask material and fabrication process all masks should be thoroughly cleaned and inspected before use. Surface contaminants, particularly oil, grease or other organic materials may become volatile when the mask is heated and then be absorbed by the substrate and this may be a cause of weak film adhesion. The mask is placed in proximity to the substrate, thereby allowing condensation of the evaporated only in the exposed substrate areas. The mask is prepared in such a way that the edge of the mask is smooth so that it is helpful for determining the film thickness accurately. Mask used for film are shown in (Figure 4.1).

4.2.2 Heater

The heater "H" is an ordinary hot plate 2kW michrome wire heater. The top of the plate is covered with a piece of asbestos sheet having a small open area at the center where a mica sheet is attached. A thick stainless steel plate "G" (figure 4.3) is placed on this mica sheet. Substrate is placed on this susceptor plate 'G' to have a uniform temperature throughout the substrate surface. An electrical voltage variac controls the heater power. The temperature of the heater was measured by copper constantan thermocouple tightly attached to the substrate surface placed on the heater susceptor.

4.2.3 The design of the reactor

The design of the reactor is shown in figure 4.2. It is a vertical batch type reactor composed of a galvanized iron enclosure 'E', heater 'H' and heat susceptor 'G'. For the rapid expulsion of the by-product gases there are opening at the side and at the top of the reactor. It helps focusing the incoming sprayed solution towards the substrate 'S' and also provides a chimney action to the exhaust gas upwards.

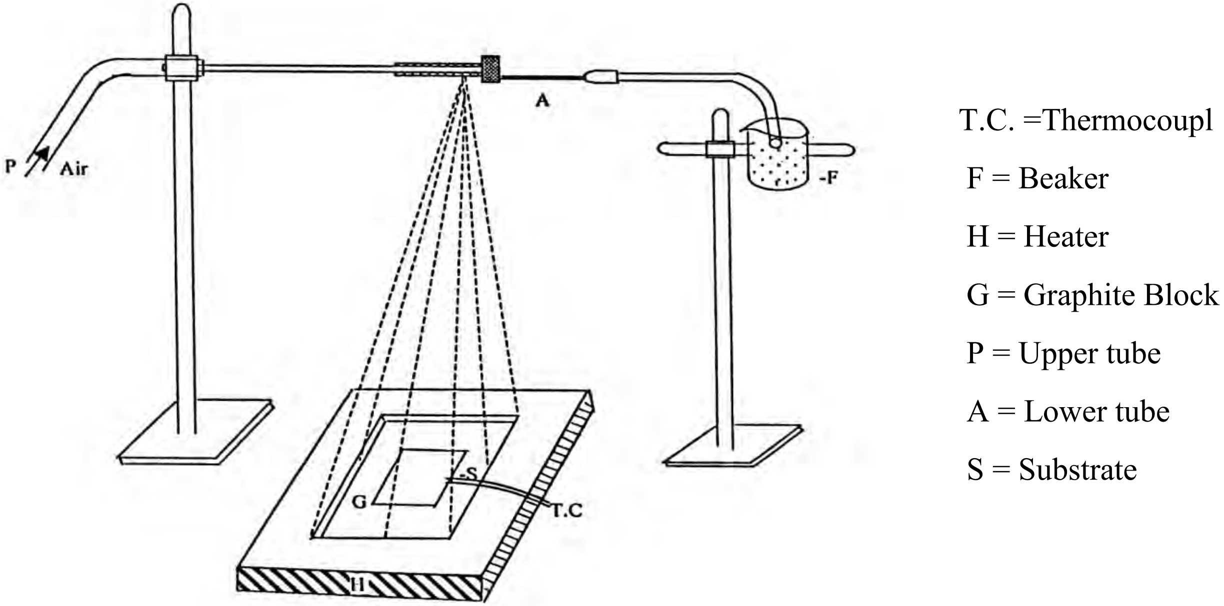

Fig. 4.2**:** Experimental setup of spray pyrolysis technique

4.2.4 The fume chamber

It is a large type chamber with a slanting top and is provided with a chimney. There is an exhaust fan fitted at the mouth of the chimney to remove the unused gases from the chamber. The slanting top and the sidewalls are made of glass and wood. There are airtight doors in the front side. The chamber has purging facilities. The whole spray system and the reactor are kept inside the fume chamber at the time of film deposition because of the safety grounds and to check air current disturbances at the deposition site. These two points just stated are very important for the spray process when deposition is carried out in open air atmosphere.

4.2.5 Air compressor

An air compressor is a device that converts power usually from an electric engine into kinetic energy by pressurizing and compressing air, which is then released in quick bursts. It is reservoir type electrical air compressor. A rotary pump in this section mode draws atmospheric air and keeps it reserved in a large capacity air tank. At the outlet of the tank

a pressure gauge is attached which records the pressure of the air at the time of supplying it from the tank. There is a bypass control valve which can keep the output pressure constant.

4.2.6 Spray nozzle

The single spray nozzle consists of capillary tubes (stainless steels) fitted perpendicular to the other tube as shown in Figure 4.3. When compressed air is passed rapidly through the upper tube ‘P’ in direction tangential to the mouth of the lower tube ‘A’ a partial vacuum is created at the front part of the tube ‘A’ whose other end is kept immersed in the spray liquid. Due to this partial vacuum the liquid rises up through the tube ‘A’ and the compressed air drives it away in the form of fine spray particles. The thinner spray nozzle would give the finer spray particles. A very fine needle shaped capillary tube was used for the spray nozzle and it may vary from nozzle to nozzle.

4.3 Substrate and Substrate Cleaning

Several types of substrates are used for thin film deposition. Substrate may influence various the properties of thin films [1]. Generally, glass, quartz, plastic and ceramic substrates are used for polycrystalline films. However, in the present work, thin films are deposited on glass substrates. The most commonly microscope glass slides having 5 cm long, 2 cm wide and 0.1 cm thickness are used. These are fine smooth high quality microscope glass slides. The cleaning of substrate has a major influence on the properties of the thin film deposited onto them. Surface contaminations manifest it in pinholes, which can cause open resister or localized high resistance. The following procedures are used for substrate cleaning. The gross contamination of each of the substrate are first removed by warm aqueous solution carbonate and then washed with distilled water. After washing in distilled water, the substrate was washed by ultrasonic bath. Finally, these are dried in hot air and preserved for use. During the whole process the substrates are always held by slide holding forceps.

4.4 Working Solution

The working solution for SnO_2 layer was prepared by taking tin (1I) chloride dihydrate [$SnCl_2.2H_2O$] as a source material dissolved into ethanol (CH_3CH_3OH) and water (H_2O). Aqueous solutions were prepared by mixing 0.1 M of [$SnCl_2.2H_2O$] and (CH_3CH_3OH) for pure SnO_2 thin film. To enhance the solubility of prepared solution, a few drops of HCI were added. The working solution for ZnO layer was prepared by taking zinc acetate dihydrate [$Zn (CH_3COO)_2. 2H_2O$] as a source material. The most commonly used solvents are distilled water and ethanol. As $Zn (CH_3COO)_2. 2H_2O$ dissolves in water at room temperature, water is taken as solvent. Since, the spray system used in the present experiment operates via a partial vacuum path as the mouth of the spray nozzle, the concentration of the solution prepared by the solvent is made in such a way that it could be at least be drawn by the nozzle. If the solution concentration is high the spray rate will be low. A typical value of solution concentration 0.1 M is used in this work.

4.5 Deposition Parameters

In the spray pyrolysis technique the structure, composition and other characteristics of the deposited thin films depend on a number of process variables (deposition parameters). The deposition parameters such as the substrate temperature (T_S), type and concentration of the solution (C), flow rate of the solution (S_r), deposition time (t_d), quality of the substrate material, size of atomized particles, carrier air pressure (P_a) and substrate to spray outlet distance (d_s), etc. affect the properties of the thin films. It is obvious that T_s is the most important deposition parameter and it must be controlled with great care.

The deposition parameters S_r, d_s, P_a and C are kept constant when ZnO and SnO_2 thin films are deposited onto glass substrates. The temperature for deposition of ZnO thin film is 300°C and for deposition of SnO_2 is 450°. SnO_2 layers are deposited at various deposition time (T_d). For first layer glass slides are used as substrate but for the second layer deposited first layer used as a substrate. The effect of these two combined double layer film parameters on the structural, optical and electrical properties are studied in this work.

4.6 Rate of deposition

The rate of flow of the working solution can be controlled to a better accuracy by suitably designing the nozzle A and adjusting the air flow rate. In preparing ZnO, SnO_2 and bilayer ZnO/SnO_2 films, the solution flow rate of 0.5ml/min was used for the present experiment.

4.7 Thickness control

Thickness plays an important role in the properties of thin films unlike a bulk material [2-4].In the present spray deposition process, the deposition time is the main factor for the thickness control, provided the other parameters, remain constant for ZnO layer and it varies for SnO_2 layer to get different thicknesses. Since the deposition is carried out in normal atmosphere a direct and inside control of thickness is not so easy. To control the film thickness therefore calibration chart may be used. These charts are generally plots of deposition time vs. thickness, and can be prepared at different constant substrate temperatures prior to the preparation of particular experimental samples using the same solution and deposition variables.

4.8 Steps of thin film processes

There are four sequential steps are followed when a thin film is grown on a substrate. A source of film material is provided, the material is transported to the substrate, deposition takes place, so the film is subsequently annealed, and finally it is analyzed to evaluate the process. The results of the analysis are then used to adjust the condition of the steps for film property modification.

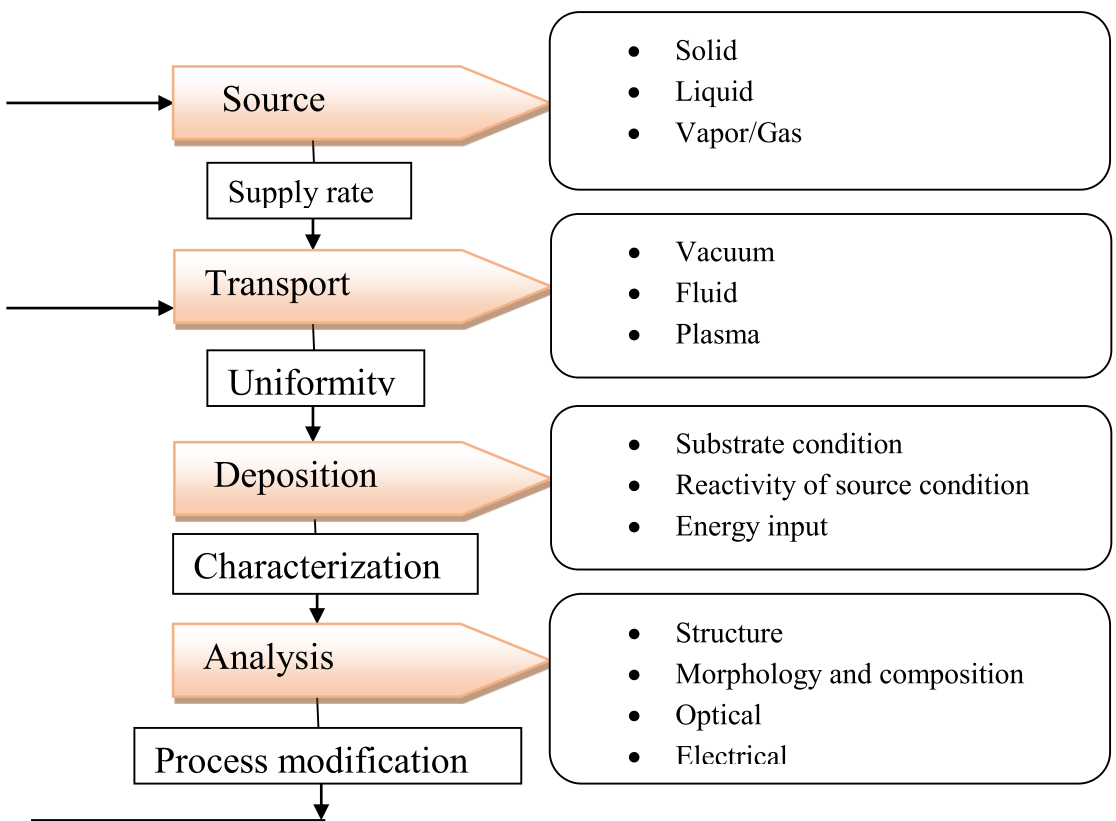

Figure 4.3**:** Steps of thin film processes

4.9 Sample Deposition

It has been stated earlier that spray pyrolysis method for preparing both zinc oxide and tin oxide thin films is an economically attractive method [5-7]. The apparatus needed to carry out the chemical spray process consists of a device to atomize the spray solution and a substrate heater. Figure 4.4 shows a schematic diagram of SPD unit and Figure 4.4 shows a typical experimental setup for SPD used in this work. A considerable amount of 100 ml solution taken in the container 'F' fitted with the spray nozzle 'A'. The clean substrate with a suitable mask was put on the susceptor of the heater 'H'. The distance between the tip of

the nozzle and the surface of the glass substrate was kept 25 cm. Before supplying the compressed air the substrate temperature 'T_s' was to be kept at a level slightly higher than the required substrate temperature because at the onset of spraying a slight fall of temperature is likely. The temperature of a substrate was controlled by controlling the heater power using a variac. The substrate temperature was measured by placing a copper constituent thermocouple on the substrate. When compressed air is passed through 'P' at constant pressure (0.5 bar), a fine SnO_2 was produced and automatically carried to the reactor zone where bottom SnO_2 layer was deposited on the heated substrate [8-10]. The solution is adjusted such that about 10,12, 14, 16 minutes of spray produces SnO_2 thin films of thickness about 200-350 nm. Similarly, ZnO top layer was deposited on SnO_2 layer for constant deposition time 10 minutes at temperature 300°C.

Figure 4.4: Experimental set up of Spray Pyrolysis unit at the Department of Physics, BUET

The main reaction that leads to the formation of SnO_2 first layer is

$$SnCl_2 + H_2O \rightarrow SnO + 2HCL$$

$$SnO + \frac{1}{2} O_2 \rightarrow SnO_2$$

And the reaction to the formation of ZnO second layer on the SnO_2 first layer is

$$Zn(CH_3COO)_2 \rightarrow 4Zn(CH_3COO)_2 + H_2O \rightarrow Zn_4O(CH_3COO)_6 + 2CH_3COOH$$

$$Zn_4O(CH_3COO)_6 \rightarrow 4ZnO \text{ (Film)} + 6CH_3COOH \text{ (Gas)}$$

Figure (4.5) shows the deposited SnO_2 thin films with different thicknesses. SnO_2 films were deposited on glass substrate at 450°C and figure (4.6) shows deposited bilayer ZnO/SnO_2 thin films with different thicknesses. For bilayer formation ZnO precursor solution was sprayed over the preheated SnO_2 layers in order to get ZnO/SnO_2 bilayer films at 300°C [11-13].

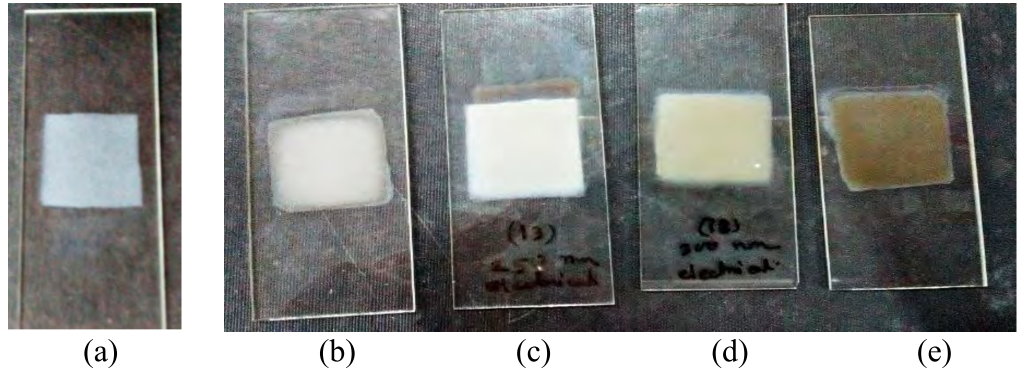

(a) (b) (c) (d) (e)

Figure 4.5: Deposited single layer thin films (a) ZnO(200nm) (b) SnO_2 (200nm) (c) SnO_2 (250nm) (d) SnO_2 (300nm) and (e) SnO_2 (350nm)

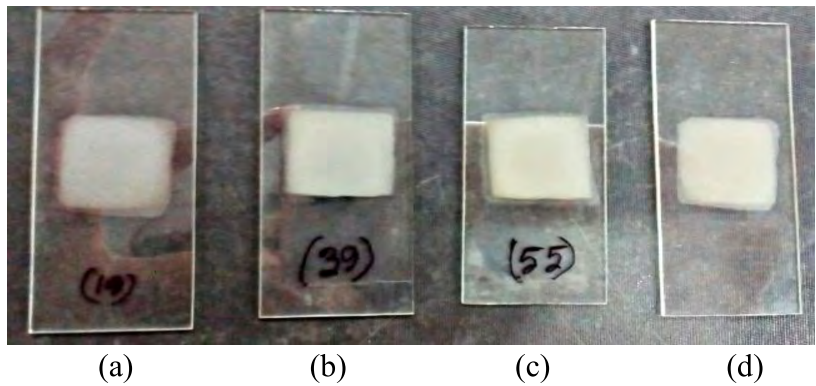

(a) (b) (c) (d)

Figure 4.6: Deposited bilayer thin films (a) ZnO/SnO_2 (400nm) (b) ZnO/SnO_2 (450nm)

(c) ZnO/SnO_2 (500nm)) (d) ZnO/SnO_2 (550nm)

References

[1] Antonaia, P., Menna, M. L., Addonzio, and Crocchilo, "Transparent properties of polycrystalline tin oxide films" Sol. Energy Mater, Vol. 28, pp. 167-173, 1992.

[2] Mohammad, T. M., "Performance and characteristics of L-PbS/SnO_2: F selective coating system for photothermal energy conversion" Sol. Energy Mater, Vol. 20, pp. 297-305, 1990.

[3] Choudhury, C., Sehgal H. K., "Properties of spray deposited cobalt oxide selective coating on aluminum and galvanized iron substrate", Appl. Energy, Vol. 10, pp. 313-324, 1982.

[4] Kadam, L. D., Patil P. S., "Thickness dependent properties of sprayed cobalt oxide thin films" Mat. Chem. Phys., Vol. 68, pp. 225-232, 2001.

[5] Abdelkrim, A., Rahmane, S., Abdelouahab, O., Hafida, A., and Nabila, K., "Optoelectronic properties of SnO_2 thin films sprayed at different deposition times", Chin. Phys. B Vol. 25, pp. 046801, 2016.

[6] Islam, M. R., Podder J., "Optical properties of ZnO nanofiber thin films grown by spray pyrolysis of zinc acetate precursor, Cryst. Res. Technol., Vol. 44(3), pp. 286-292, 2009.

[7] Affreen, S., Balamurugan D., Jeyaprakash B.G., "Thickness dependent physical property of spray deposited $ZnFe_2O_4$ thin film" J. Appl. Sci., Vol. 12, pp. 1636-1640, 2012.

[8] Chamberlin, R. R., Skarman J. S., "Chemical spray deposition process for inorganic films", J. Electrochem. Soc., Vol. 113(1), pp. 86-89, 1996.

[9] Altiokka, B., Akasy S., "Optical properties of CulnS2 films produced by spray pyrolysis method," J. Phys., Vol. 36(3B), pp. 1042-1045, 2006.

[10] Riveros R., Romero E., Gordillo G., "Synthesis and characterization of highly transparent and conductive SnO_2:F and In_2O_3:Sn thin films deposited by spray pyrolysis," Braz. J. Phys., Vol. 36(3B), pp. 1042-1045, 2006.

[11] Elangovan, E., Rsmamurthi K., "Studies on optical properties of polycrystalline SnO_2:Sb thin films prepared using $SnCl_2$ precursor," Cryst. Res. Technol. Vol. 38(9), pp. 779-784, 2003.

[12] Yadav, S. C., Uplane M. D., "Synthesis and properties of boron doped ZnO thin films by spray CVD technique at low substrate temperature," Int. J. Engr. Sci. Technol., Vol. 4(12), pp. 4893-4898, 2012.

[13] Anandhi, R., Ravichandran, K., Mohan, R., "Conductivity enhancement of ZnO:F thin films by the deposition of SnO_2:F over layers for optoelectronic applications", Materials Science and Engineering B, Vol. 178, pp. 65– 70, 2013.

CHAPTER FIVE

RESULTS AND DISCUSSION

CHAPTER FIVE
RESULTS AND DISCUSSION

5.1 Introduction

The objective of this study is to synthesis and characterize films by home fabricated spray pyrolysis system. Here, films deposited by the reduced of the preparation cost and made it economical1y feasible. In this chapter the results and discussion of the various experimental studies viz., surface morphology, structural, optical and electrical properties of pure ZnO, pure SnO_2 and bilayer ZnO/SnO_2 thin films have been presented and discussed step by step.

5.2 Surface Morphology

Scanning electron microscopy is a convenient technique widely used to obtain the surface morphological information of thin films. Surface morphology of pure ZnO, pure SnO_2 and ZnO/ SnO_2 bilayer thin films on glass substrate were studied by field effect scanning electron microscopy (SEM).

5.2.1 Pure ZnO

Figure (5.1a) shows the surface morphology of asdeposited ZnO thin film at X10k magnification.

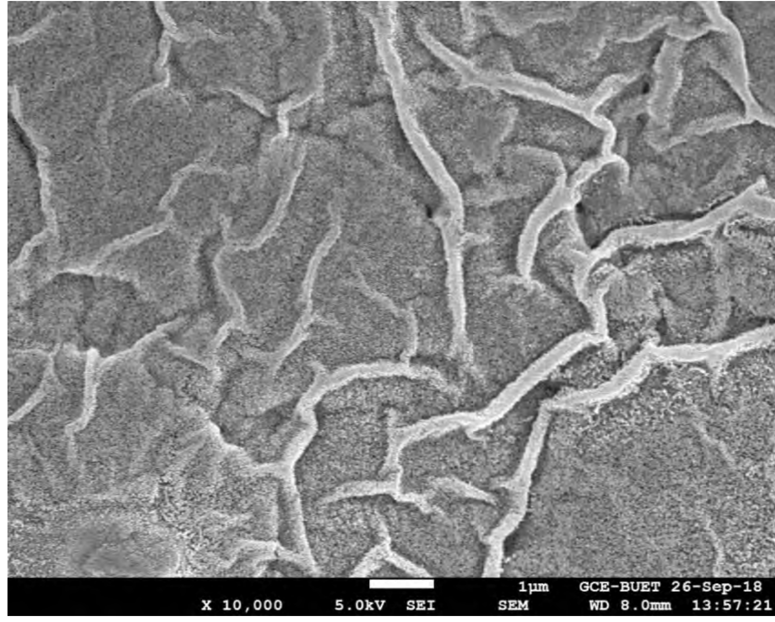

Figure 5.1(a): FESEM image (X10 k) of ZnO thin film deposited at the Ts of 300 °C.

The FESEM micrographs reveal that sprayed particles have covered the whole substrates uniformly. In 10k magnification, it is seen in Figure 5.1(a) that the scanned area is nicely covered with fibrous and non-fibrous ZnO thin films [1].

5.2.2 Pure SnO_2

FESEM images Fig. 5.1(b) for SnO_2 thin film is shown that the surface of the film is uniform, homogeneous and well covered on the glass substrate surface. FESEM images discovered that sprayed particles are adsorbed on the glass substrate into clusters as the primary stage of nucleation [2].

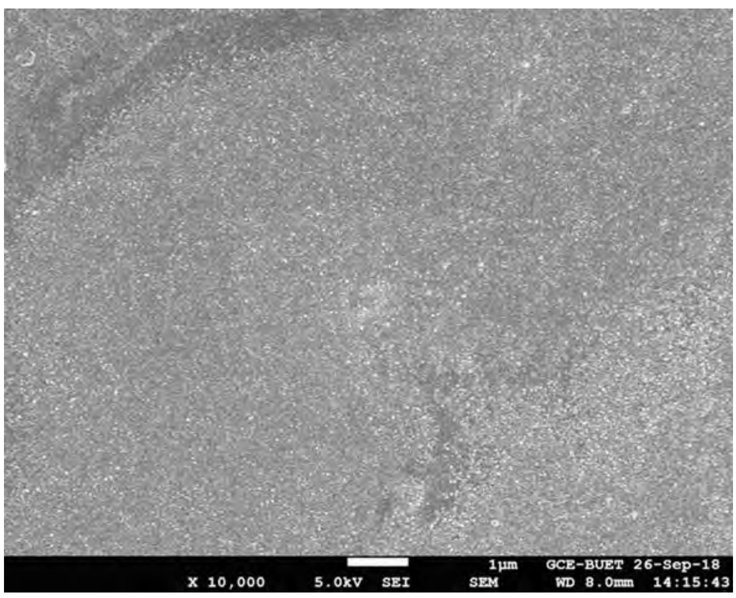

Figure 5.1(b): FESEM image (X10 k) of SnO_2 thin film deposited at the Ts of 450 °C.

5.2.3 Bilayer ZnO/SnO_2

The FESEM images of bilayer ZnO/SnO_2 thin films with constant thickness of ZnO(200nm) and different thicknesses of SnO_2 (200nm; 250nm; 300 and 350nm) are shown in Figures 5.2(a-d). The FESEM image of ZnO/SnO_2 thin films shows the presence of tightly packed small grains with smooth and transparent surface and the nanocrystals are uniformly distributed on the glass substrate. In the case of bilayer ZS_1 (for ZnO=200 nm; SnO_2=200nm thicknesses) the nanofibers become more compact and at bilayer ZS_2 (for ZnO=200 nm;

SnO_2=200nm thicknesses) some branches are broken and grains are formed. Due to porous surface of SnO_2 layers ZnO are filled with SnO_2 layers and most of the fiber has broken which transformed into grain shown in figure 5.2 (b). But at higher thickness of SnO_2 in the case of ZS_3 (for ZnO=200 nm; SnO_2=200nm thicknesses), ZS_4 (for ZnO=200 nm; SnO_2=200nm thicknesses) all the fiber has broken and whole surface transform into agglomerated grain shown in figure 5.2 (c-d). This tendency may be caused by the agglomeration of crystallites due to increase the thickness of SnO_2 layers [3].

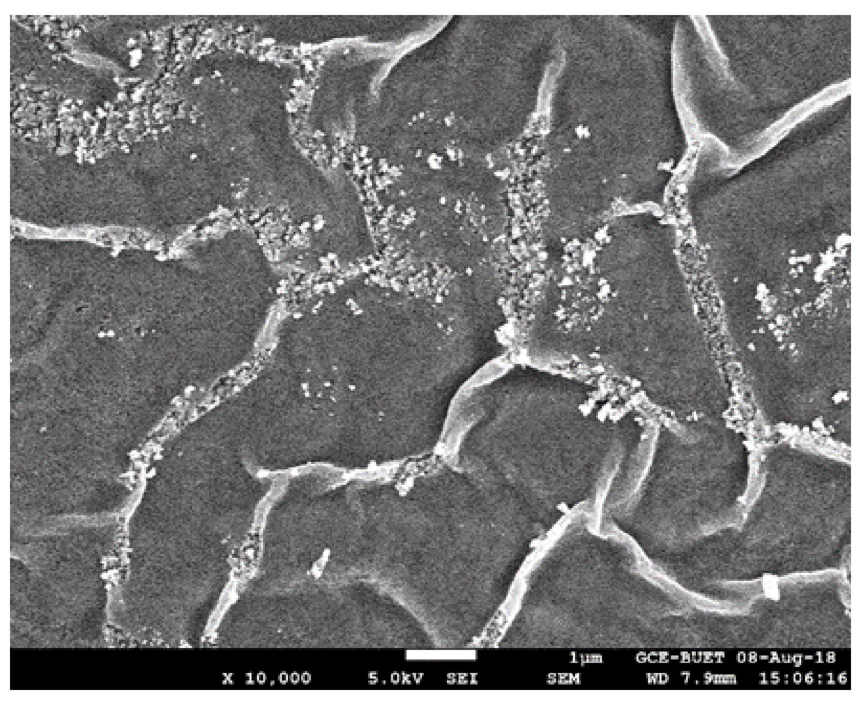

Figure 5.2(a): FESEM image (X10 k) of bilayer ZS_1 (for ZnO=200 nm; SnO_2=200nm thicknesses) thin film.

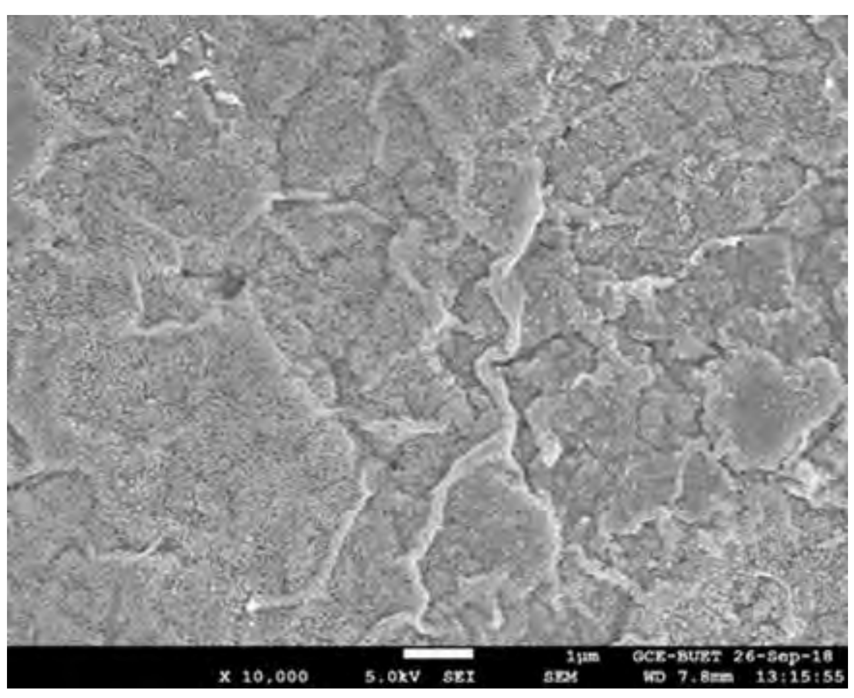

Figure 5.2(b): FESEM image (X10 k) of bilayer ZS_2 (for ZnO=200 nm; SnO_2=250nm thicknesses) thin film

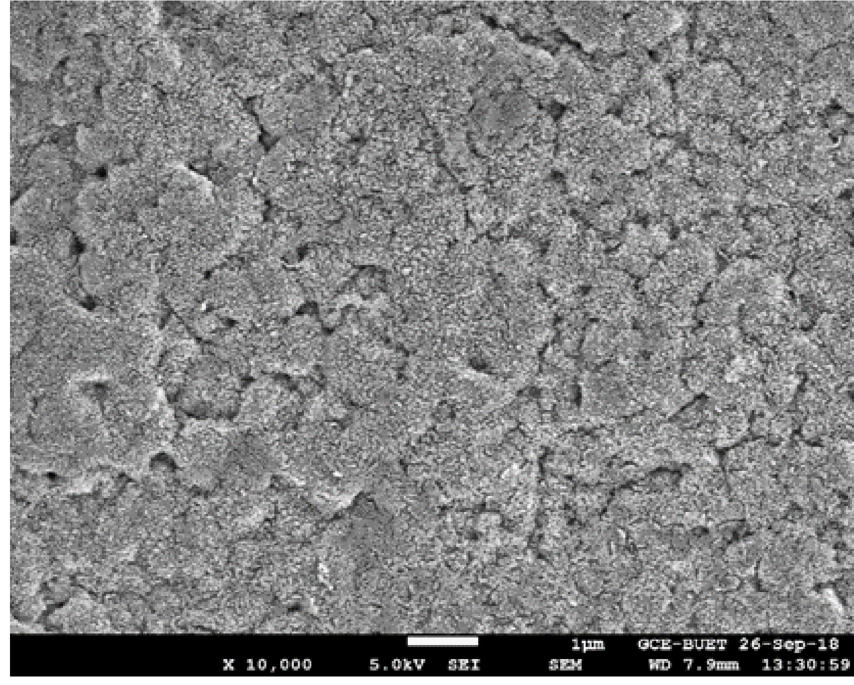

Figure 5.2(c): FESEM image (X10 k) of bilayer ZS_3 (for ZnO=200 nm; SnO_2=300nm thicknesses) thin film

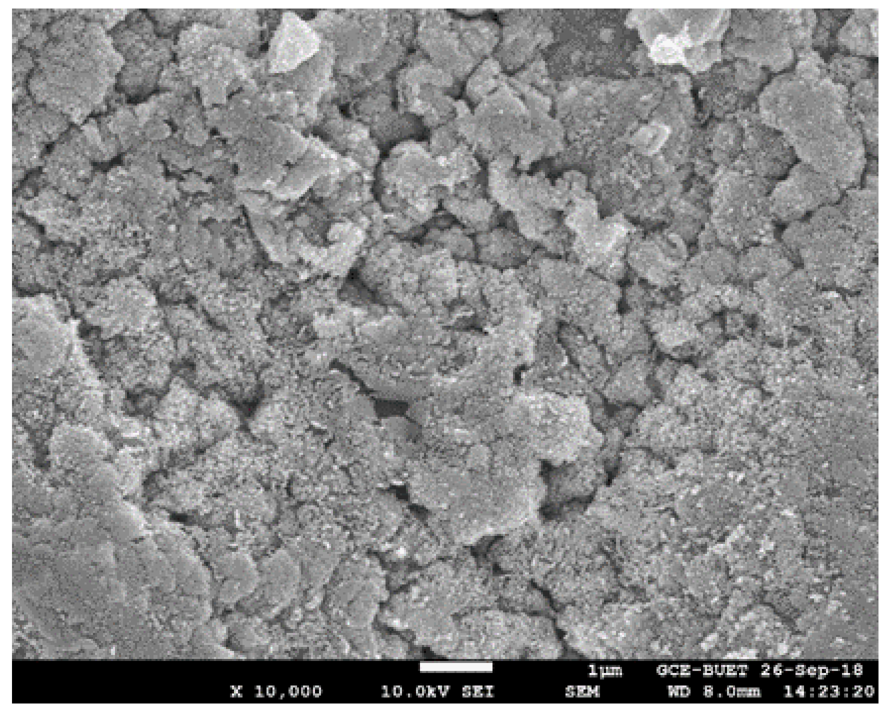

Figure 5.2(d): FESEM image (X10 k) of bilayer ZS_4 (for ZnO=200 nm; SnO_2=350nm thicknesses) thin film

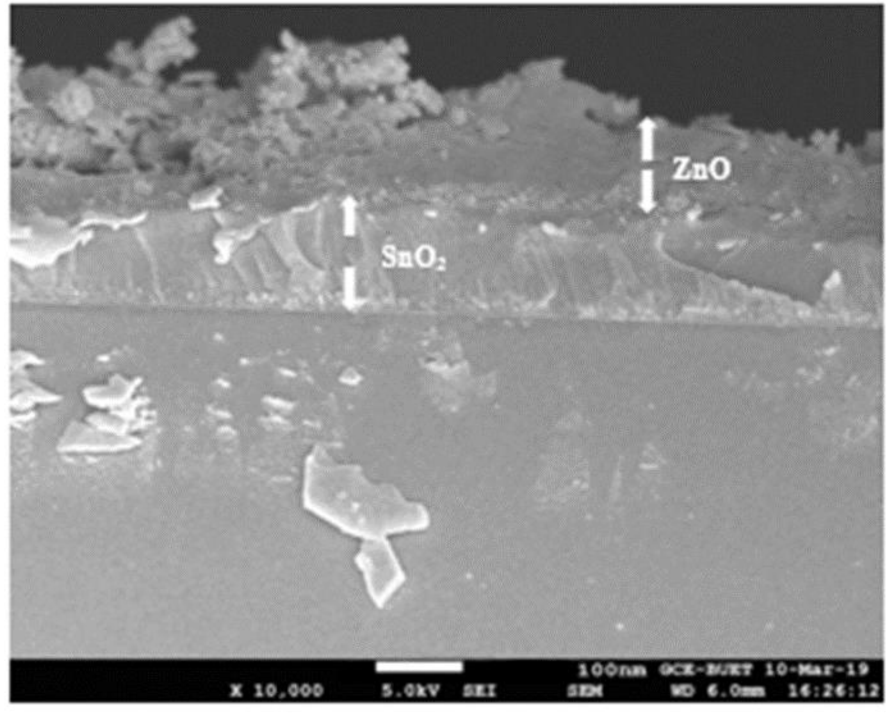

Figure 5.3(a): Cross-sectional FESEM image (×10 k) of bilayer ZS_1 thin film

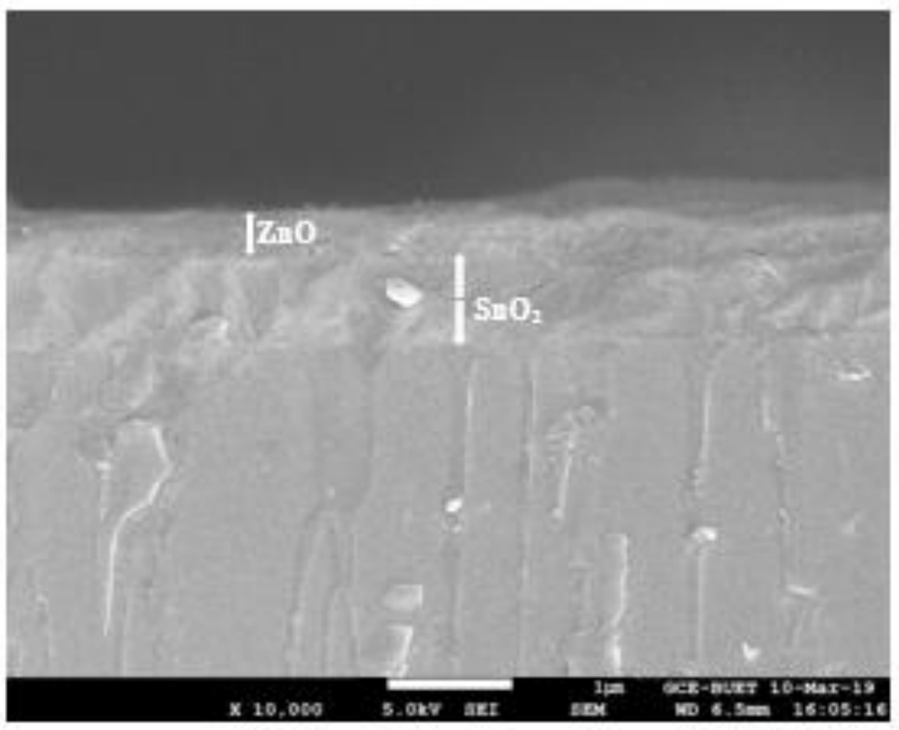

Figure 5.3(b): Cross-sectional FESEM image (×10 k) of bilayer ZS_2 thin film

A thin continuous ZnO layer was formed on SnO_2 as a result of the low surface energy of the SnO_2, and it could completely bridge the gap at the interface. Both the SnO_2 and ZnO layers exhibited clear lattice fringes that separated one another from the atomically sharp interface shown in figure 5.3(a-b). When ZnO is grown over the SnO_2 layers, the ZnO coating is conformal; moreover, even though SnO_2 layers are initially porous, no porosity is evidenced in the final layers [Figure-5.3(b)]

5.3 X-ray Diffraction Analysis

The structural properties of pure ZnO, pure SnO_2 and bilayer ZnO/SnO_2 thin films on glass substrates are investigated by X-ray diffraction patterns. The XRD patterns of the thin films were taken using CuK_α (λ= 1.54178 Å) source, scanning speed 2 degree/min, starting from 10° and ending at 80° to ensure the information of the single phase nature of the sintered product. Peak intensities are recorded corresponding to their 2Θ values.

The XRD patterns of pure ZnO thin films deposited at T_s of 300 °C is presented in Figure-5.4 (a). The film show polycrystalline nature. The reflections are observed for (100), (002), (101), (110) and (112) planes indicating hexagonal wurtzite type of crystal structure of the film (JCPDS card No.36-1451) [4]. Among these peaks first four are well defined, but (112) peak is less intense one. The lattice constant values of a and c and the c/ a ratio of ZnO thin film are presented in Table-5.1. The lattice constants are comparable to the standard values for ZnO [5]. The lattice constants a and c for hexagonal phase structure are determined from the Eq:

$$\frac{1}{{d^2}_{hkl}} = \left[\frac{4}{3}\left(\frac{h^2 + hk + k^2}{a^2}\right) + \frac{l^2}{c^2}\right]^{\frac{1}{2}}$$

Figure -5.4(a): XRD pattern of pure ZnO

The XRD pattern of pure SnO_2 thin film deposited at Ts of 450 °C is presented in figure-5.4-(b). The analysis of XRD pattern reveal that the SnO_2 film has polycrystalline nature with a tetragonal rutile phase of tin oxide (JCPDS card No.041-1445), which belongs to the space group P42/mnm (number 136). It is perceptible from the XRD pattern of figure-5.4(b)

that the matching of the observed values with standard'd' values confirms that the deposited film is of SnO_2 film with a cassiterite tetragonal structure. The (110) is the most intense peak and other peaks assigned as (101), (200), (111), (210), (211), (220), (002) and (112) orientations are also observed. This can be attributed to the density of the atoms in the (110) plane, which is the highest in the atom densities in all planes of the rutile crystal structure; therefore, the surface energy of the (110) plane is the lowest [6].

Figure -5.4(b): XRD patterns of pure SnO_2 thin films

The lattice constants a and c for tetragonal phase structure are determined from the Eq:

$$\frac{1}{d^2} = \left(\frac{h^2 + k^2}{a^2}\right) + \frac{L^2}{c^2}$$

where d is the interplaner distance; h, k, l are Miller indices. The calculated a and c values are slightly higher than those given in JCPDS card No: 41-1445 ($a_0 = b_0 = 4.7382$ A°, $c_0 = 3.1871$ A°) are presented in Table-5.1. The grain sizes of the films are calculated from the highly textured (110) peaks from the Scherer formula:

$$D = \frac{0.9\lambda}{\beta cos\theta}$$

where D is the grain size of nano-particle, b is the full width at half of the peak maximum (FWHM) in radian and β is the Bragg angle.

In ZnO/SnO_2 bilayer thin films, the combined double layer film also shows crystallites of the two metal oxide compounds [Figure- 5.4(c)]. There is a gradual rise in the predominance of the (110) plane as the thickness of the SnO_2 bottom layer increases. It indicates that the growth pattern of ZnO/SnO_2 bilayer is different when compared with that of SnO_2 on the bare glass substrate. When the thickness of SnO_2 layer is high, the intensity of (110) peak of SnO_2 substantially increases indicating the good crystalline property of the double layered films.

Figure 5.4(c): XRD patterns of bilayer ZnO/SnO_2 thin films

The higher value (39.86 nm) obtained for the crystallite size in the case of ZnO/SnO_2 (400nm) bilayer when compared with the single layer films, suggests the better crystallinity of the bilayers [Table-5.1]. This enhancement in the crystallite size can be

explained on the basis of the fact that when the thickness increases, surface energy decreases, and surface mobility of the species and grain boundary migration increases resulting in the enhancement of crystallite size. The misfit strain is one of the most important factors adversely affecting the structural properties, which results from the geometric mismatch at inter phase boundaries between crystalline lattices of films and substrate. These stresses can cause strains in the films. The strain (ε) value of SnO_2 film for the (110) peak is calculated from the following formula:

$$\varepsilon = \frac{bcos\theta}{4}$$

where b is the full-width at half-maximum of the preferential peak; the calculated values for (110) peak are given in [Table-5.1]. It is observed that the strain decreases with the increase of deposition time [7]. The dislocation density (δ) is defined as the length of dislocation line per unit volume (lines/nm2). The dislocation density (δ) of the film is estimated from the following equation:

$$\delta = \frac{1}{D^2}$$

Figure 5.5 shows the variations of grain size, strain and dislocation density with film thickness. We note an inverse relationship between the crystal size and dislocation density. This explains the dislocation density contribution to the smash grain. It is noted that the strain has an inverse variation to that of the grain size, due to the corresponding increase of the grain boundaries.

Figure- 5.5(a): variations of grain size and strain with bilayer film thickness.

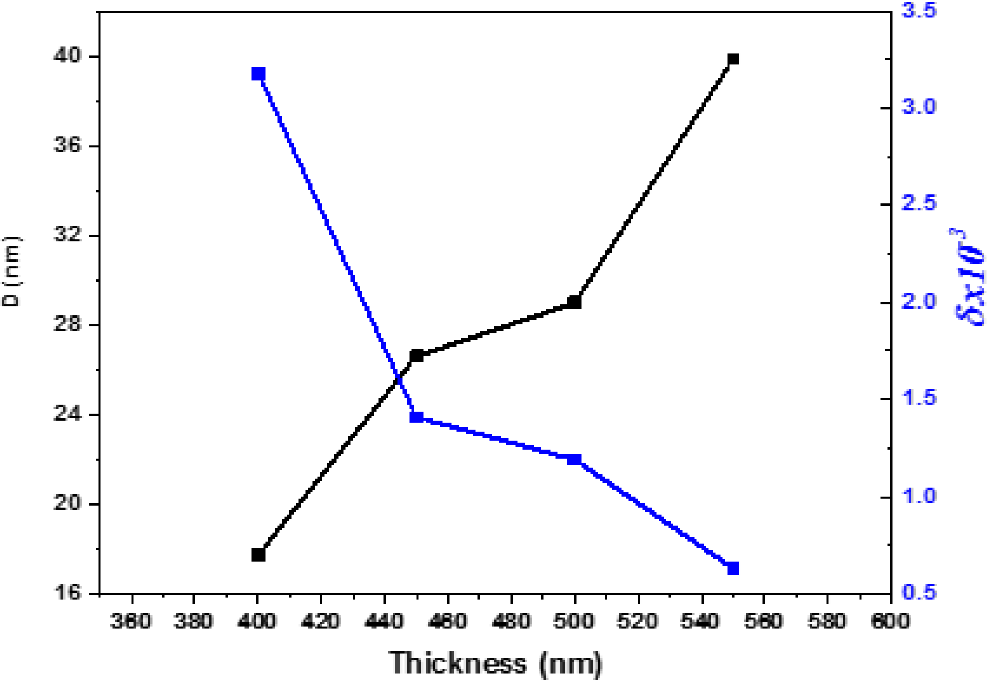

Figure- 5.5(b): variations of grain size and dislocation density with bilayer film thickness

Table 5.1: Structural parameters of pure ZnO, pure SnO_2, bilayer ZnO/SnO_2 thin films					
Sample	Thickness (nm)	Peak Position (2θ)	Crystalline size, D (nm)	Dislocation density (δ)$\times10^{-3}$ Line/nm^2	Microstain (ε)$\times10^{-3}$
ZnO	200	34.29	10.16	9.69	3.41
SnO_2	200	26.51	22.79	1.92	1.52
ZnO/SnO_2	400	26.78	17.73	2.51	1.73
ZnO/SnO_2	450	26.75	19.95	1.41	1.30
ZnO/SnO_2	500	26.72	28.99	1.18	1.19
ZnO/SnO_2	550	26.71	39.86	0.62	0.87

5.4 Atomic Force Microscopy (AFM)

The surface morphology of ZnO, SnO_2 and ZnO/SnO_2 thin films was analyzed using atomic force microscope. Using AFM data, the surface roughness (rms) values on the surface of ZnO, SnO_2 and ZnO/SnO_2 were determined. In Fig. 5.6(a–f), the AFM images of ZnO, SnO_2 and ZnO/SnO_2 thin films are presented, respectively. Two dimensional view shows that the ZnO, SnO_2 and ZnO/SnO_2 film surface is covered uniformly by fine grains. The three dimensional view shows that the growth of film takes place with closely placed sharp peaks and valleys [8-9]. The values of surface roughness are listed in Table-5.2. The surface roughness of the film increases with increasing thickness of SnO_2

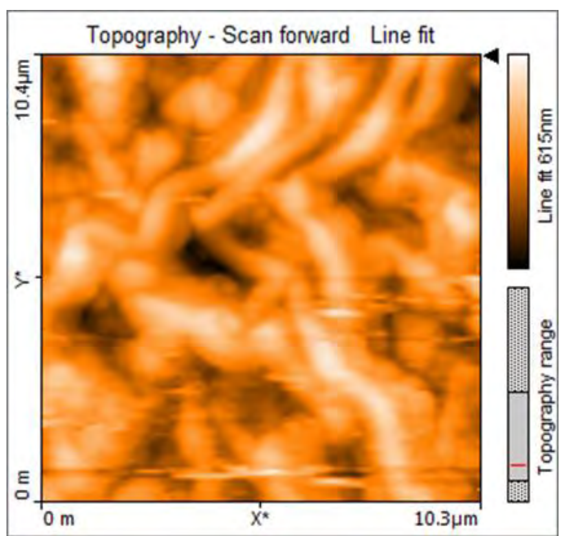

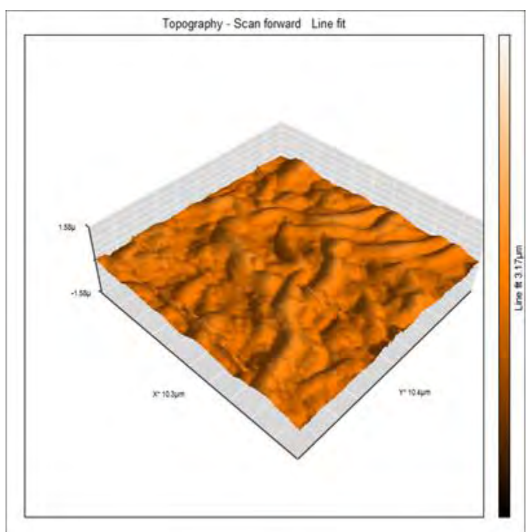

Figure-5.6.1: AFM image of pure ZnO

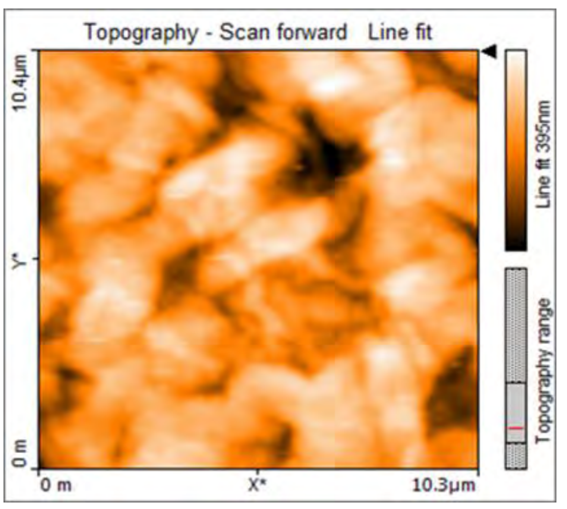

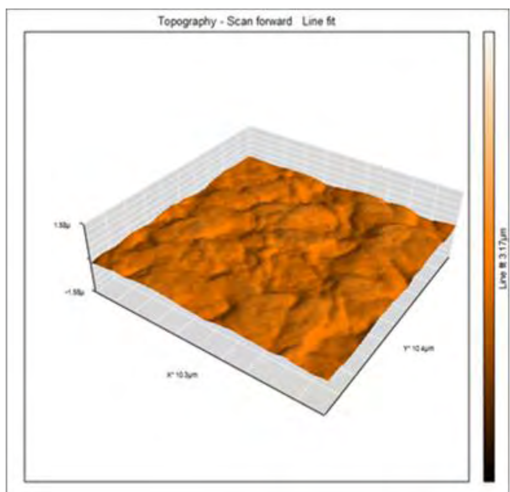

Figure-5.6.2: AFM image of pure SnO_2

AFM image of pristine sample ZnO and SnO_2 surface roughness (RMS) of 45.28 nm and 56.02nm respectively.

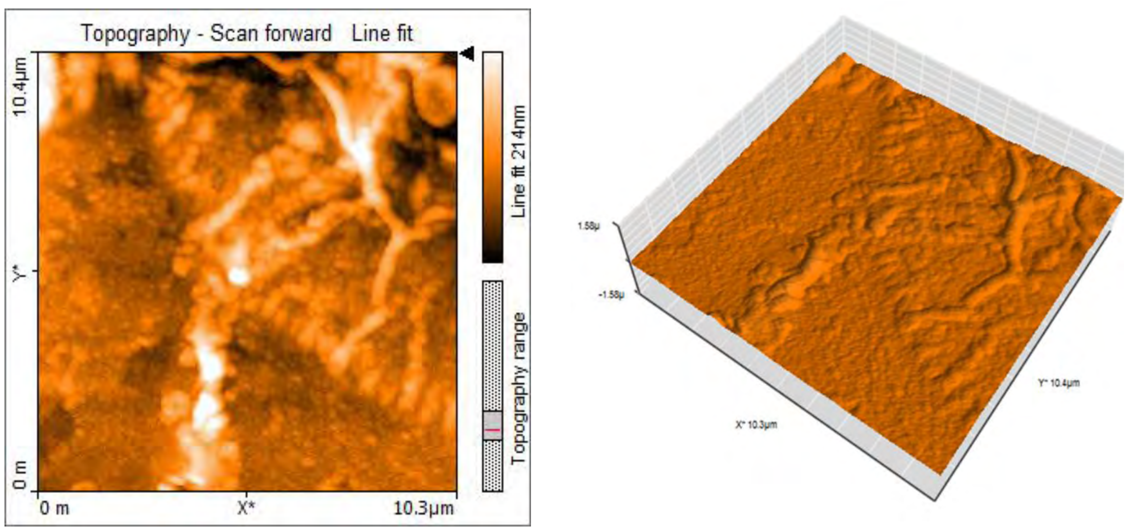

Figure-5.6.3: AFM image of bilayer ZnO/SnO_2 for (ZnO=200; SnO_2=200) thickness

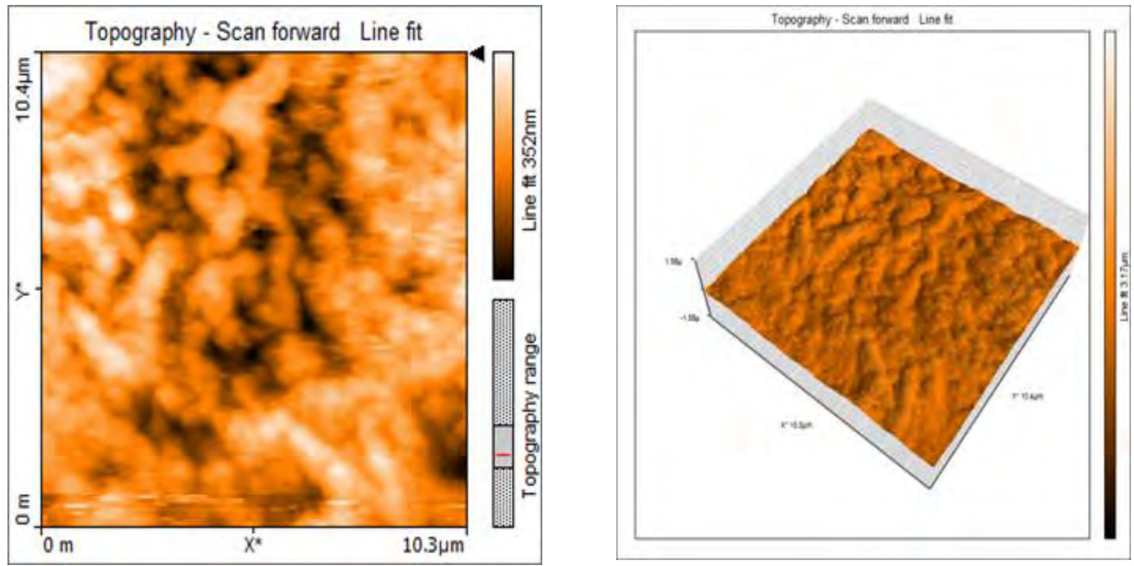

Figure-5.6.4: AFM image of bilayer ZnO/SnO_2 for (ZnO=200; SnO_2=250) thickness

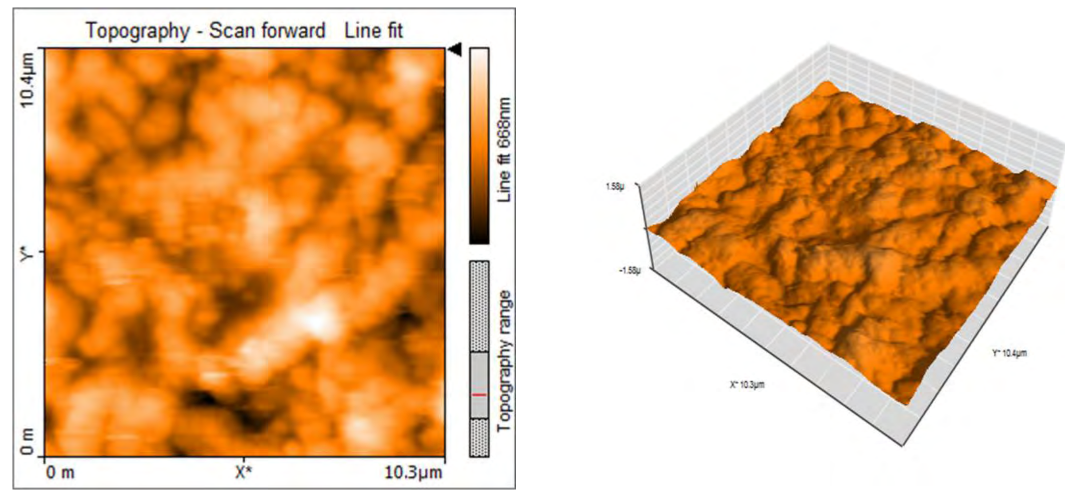

Figure-5.6.5: AFM image of bilayer ZnO/SnO_2 for (ZnO=200; SnO_2=300) thickness

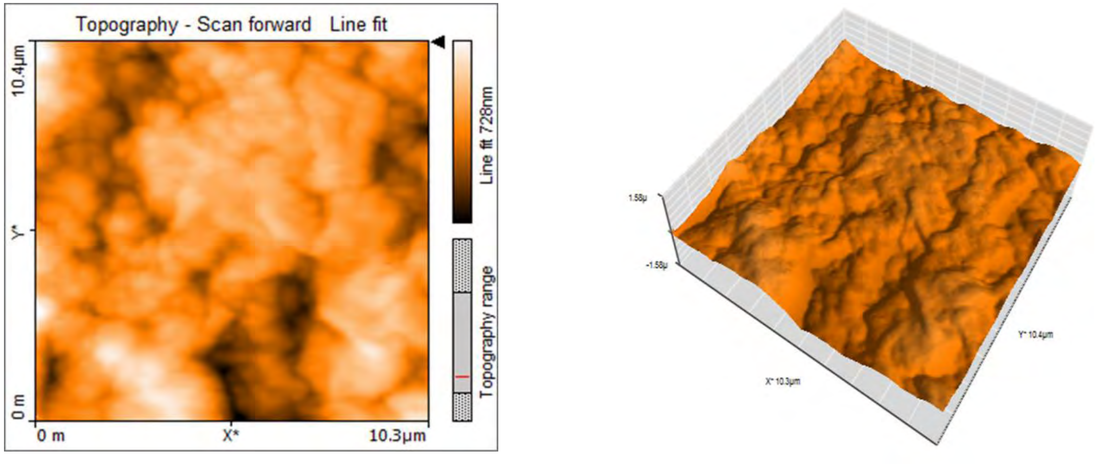

Figure-5.6.6: AFM image of bilayer ZnO/SnO_2 for (ZnO=200; SnO_2=350) thickness

From figure-(5.83) to figure-(5.86) shown that for different thickness of ZnO/SnO_2 layers the growth rate seems to be different among grains and overlapping grains are also observed. The behavior is strongly reflected in the dependence of RMS values on the film thickness. The surface roughness increases drastically from 50.24nm to 60.99nm. RMS roughness increased for thicker samples due to the stacking of successive layers possessing oriented in different directions with respect to the substrate normal [10].

Table 5.2: Roughness vaues of pure ZnO, pure SnO_2, bilayer ZnO/SnO_2 thin films		
Sample	Thickness (nm)	RMS Roughness R_q (nm)
Pure ZnO	200	45.28
Pure SnO_2	200	56.02
Bilayer ZnO/SnO_2	400	50.24
Bilayer ZnO/SnO_2	450	52.31
Bilayer ZnO/SnO_2	500	57.59
Bilayer ZnO/SnO_2	550	60.99

5.5 Optical properties

5.5.1 Transmittance

The optical transmission spectra of pure ZnO, pure SnO_2 and bilayer ZnO/SnO_2 thin films are shown in Fig. 5.7 with wavelength range 250 nm-1100 nm. The figure shows Pure ZnO and SnO_2 films are highly transparent in the visible range and near infrared regions of the electromagnetic spectrum with transmittance value up to 91 % for ZnO and 83% for SnO_2. In the case of bilayer ZnO/SnO_2 thin films figure shows the variation of transmittance with different thicknesses of SnO_2 layers. In the visible region, the all the films show good transparency and bilayerd thin films have average transmittance value 69%. These spectra show high transmittance in the wavelength range from 500 nm -1100 nm. Below 500 nm there is a sharp fall of transmittance of the films [11].

Fig. 5.7: Transmittance vs. wavelength of pure ZnO, pure SnO_2 and bilayer ZnO/SnO_2 thin films.

5.5.2 Absorbance

Figure 5.8 shows the absorbance (A) for the pure ZnO, pure SnO_2, and bilayer ZnO/SnO_2 thin films. The value of absorbance (A) is highest for the ZnO/SnO_2 (ZnO=200nm; SnO_2=350nm) thin films in the wavelength range of 300-1100 nm as shown in figure 5.8. The absorption starts at wavelength ~ 400nm. From the figure 5.8 it is clear that A decrease for all of films with the increase in wavelength. This decrease in the absorption indicates that the presence of optical band gap in the materials.

Fig. 5.8: Absorbance vs. wavelength of pure ZnO, pure SnO_2 and bilayer ZnO/SnO_2 thin films.

5.5.3 Absorption coefficient

The absorption coefficient (α) was calculated from the transmission spectra using the relation,

$$\alpha = \frac{\ln(\frac{1}{T})}{t}.$$

Figure 5.9 the variation of absorption coefficient (α) with wavelength for all the samples. It is observed that in the higher wavelength region the absorption coefficient decrease very slowly. It is also seen that the absorption coefficient slightly increase with the increase of the thickness of bilayer thin films. It is well known that the absorption coefficient depends on the film thickness, impurity state and doping concentration as well. Therefore it may be

implied that the observed variation in (α) is due to the variation of thickness of bilayer thin films.

Figure 5.9: Variation of absorption coefficient with wavelength for pure ZnO, pure SnO_2, and bilayer ZnO/SnO_2 thin films.

5.5.4 Determination of optical band gap

The optical transmittance spectra of the deposited film with respect to plain glass substrate were taken using double beam UV spectrophotometer for wavelength range 200 to 1100 nm. From transmittance spectra, the absorption coefficient and optical band gap were calculated for pure ZnO, pure SnO_2 and bilayer ZnO/SnO_2 thin films. The optical transmission data were analyzed using the classical relation for near edge of the optical absorption using the relation (for $\alpha > 10^4$ cm^{-1})

$$\alpha h\nu = B(h\nu - E_g)^n$$

Where B is a constant in the optical frequency range and E_g is the optical band gap, and n is an index related to the density of state curves for the energy band. This n is determined by the nature of the optical transition involved in the absorption process. Analyses of the data have been made using both n = 1/2. The energy gap in a semiconductor is responsible for the fundamental optical absorption edge. A plot of $(\alpha h\nu)^2$ vs. hν for (direct transition) pure ZnO, pure SnO_2 and bilayer ZnO/SnO_2 are shown in Fig.5.10. The direct band gap energy of pure ZnO, pure SnO_2 and bilayer ZnO/SnO_2 thin films have been obtained from intercept on the energy axis after extrapolation of the straight line section of $(\alpha h\nu)^2$ vs. hν curve. Optical band gap obtained for pure ZnO, pure SnO_2 and bilayer ZnO/SnO_2 are given in the Table 5.3.The optical direct band gap for pure ZnO is 3.38, for pure SnO_2 is 3.68 and for bilayer thin films bandgap varies from 3.47 to 3.64 eV. These values are very close to the reported values. From the figure it is seen that for bilayer thin films band gap is decreased with increasing thickness of SnO_2 layers. Increase of band gap (Eg) may be attributed the Burstein-Moss shift [12], i.e. due to increase in carrier concentration, the absorption edge shifts to higher energy level.

Figure 5.10: Plots of $(\alpha h\upsilon)^2$ vs. $h\upsilon$ of pure ZnO, pure SnO_2 and bilayer ZnO/SnO_2 thin films

Table-5.3: Bandgap of pure ZnO, pure SnO_2 and bilayer ZnO/SnO_2 thin films		
Sample	Thickness (nm)	Direct band gap energy E_g in eV
Pure ZnO	200	3.38
Pure SnO_2	200	3.68
ZnO/SnO_2	400	3.45
ZnO/SnO_2	450	3.49
ZnO/SnO_2	500	3.53
ZnO/SnO_2	550	3.64

5.5.5 Extinction coefficient

The extinction coefficient (also called molar absorptivity) is parameters defining how strongly a substance absorbs light at a given wavelength, per mass density or per molar concentration, respectively. The extinction coefficient (k) has been calculated using the equation

$$K = \frac{\alpha\lambda}{4\pi}$$

Where α is the absorption coefficient and λ is the wavelength. The extinction coefficient is the imaginary part of the complex index of refraction, which also relates to light absorption [13]. The variation of k with wavelength for deposited thin films is shown in figure 5.11. The rise and fall in k is directly related to the absorption of light. Since the extinction coefficient describes the attenuation of light in a medium and increase of k with wavelength indicates the probability of raising the electron transfers across the mobility gap with wavelength. Higher values of k represents the greater attenuation of light in a thin film and

also the higher probability of raising the electron transfer across the mobility gap with the wavelength.

Figure 5.11: Variation of extinction coefficient with wavelength for pure ZnO, pure SnO_2 and bilayer ZnO/SnO_2 thin films

5.5.6 Refractive index

The refractive index or index of refraction n of a material is a dimensionless number that describes how light propagates through that medium**.** The refractive index (n) has been calculated using the equation

$$n = \left(\frac{1+R}{1-R}\right) + \sqrt{\left(\frac{4R}{(1-R)^2} - K^2\right)}$$

Where k is the extinction coefficient and R is the optical reflectance. The variation of n with wavelength for pure ZnO, pure SnO_2 and bilayer ZnO/SnO_2 thin films are shown in figure 5.12. It is observed that the refractive indices are high at 400 to 500 nm wavelength and

refractive index decreases for pure ZnO and SnO_2 thin films. Lower value of n reveals that light moves faster through the films.

Figure 5.12: Variation of refractive index with wavelength for pure ZnO, pure SnO_2 and bilayer ZnO/SnO_2 thin films

5.6 Electrical Properties

5.6.1 Hall effect measurement

Conductivity measurements in semiconductors cannot reveal whether one or both types of carriers are present, nor distinguish between them. However, this information can be obtained from Hall Effect measurements, which are a basic tool for the determination of mobilities. Hall effect measurement values for pure ZnO, pure SnO_2 and bilayer ZnO/SnO_2 are given in the Table 5.4. All of the films have n-type carrier concentration. In the case of bilayer thin films carrier concentration increase with increasing thickness of SnO_2 layer [14]. The change of ρ is related to the change in the Eg values.

Table-5.4: Hall effect measurement of pure ZnO, pure SnO_2 and bilayer ZnO/SnO_2 thin films				
Sample	Thickness (nm)	Carrier concentration, n_c (10^{19} cm^{-3})	Mobility μ ($cm^2V^{-1}s^{-1}$)	Carrier type
ZnO	200	0.18	0.19	n-type
SnO_2	200	0.42	0.42	n-type
ZnO/SnO_2	400	0.45	0.18	n-type
ZnO/SnO_2	450	0.61	0.52	n-type
ZnO/SnO_2	500	1.42	0.44	n-type
ZnO/SnO_2	550	2.06	0.13	n-type

5.6.2 Variation of Resistivity and Conductivity with temperature

Electrical resistivity of pure ZnO, pure SnO_2 and bilayer ZnO/SnO_2 thin films are measured by four point probe method and data are taken as a function of temperature. Figure 5.13 shows that the resistivity decreases with the increase of temperature that confirms the semiconducting nature of the films. It is also seen that the resistivity of the bilayer samples decreases with increasing the thickness of SnO_2 layer. This might be caused by the increase of carrier concentration or carrier mobility.

The conductivity (σ) of all the deposited samples has been calculated from resistivity data. The plot of conductivity as a function of temperature for pure ZnO, pure SnO_2 and bilayer ZnO/SnO_2 thin films are shown in figure 5.14. From this figure it is clear that the conductivity is inversely related to the resistivity ($\sigma = 1/\rho$) [15]. The conductivity was found to increase with increase of temperature and with increase of thickness of SnO_2 layer in the case of bilayer thin films as well.

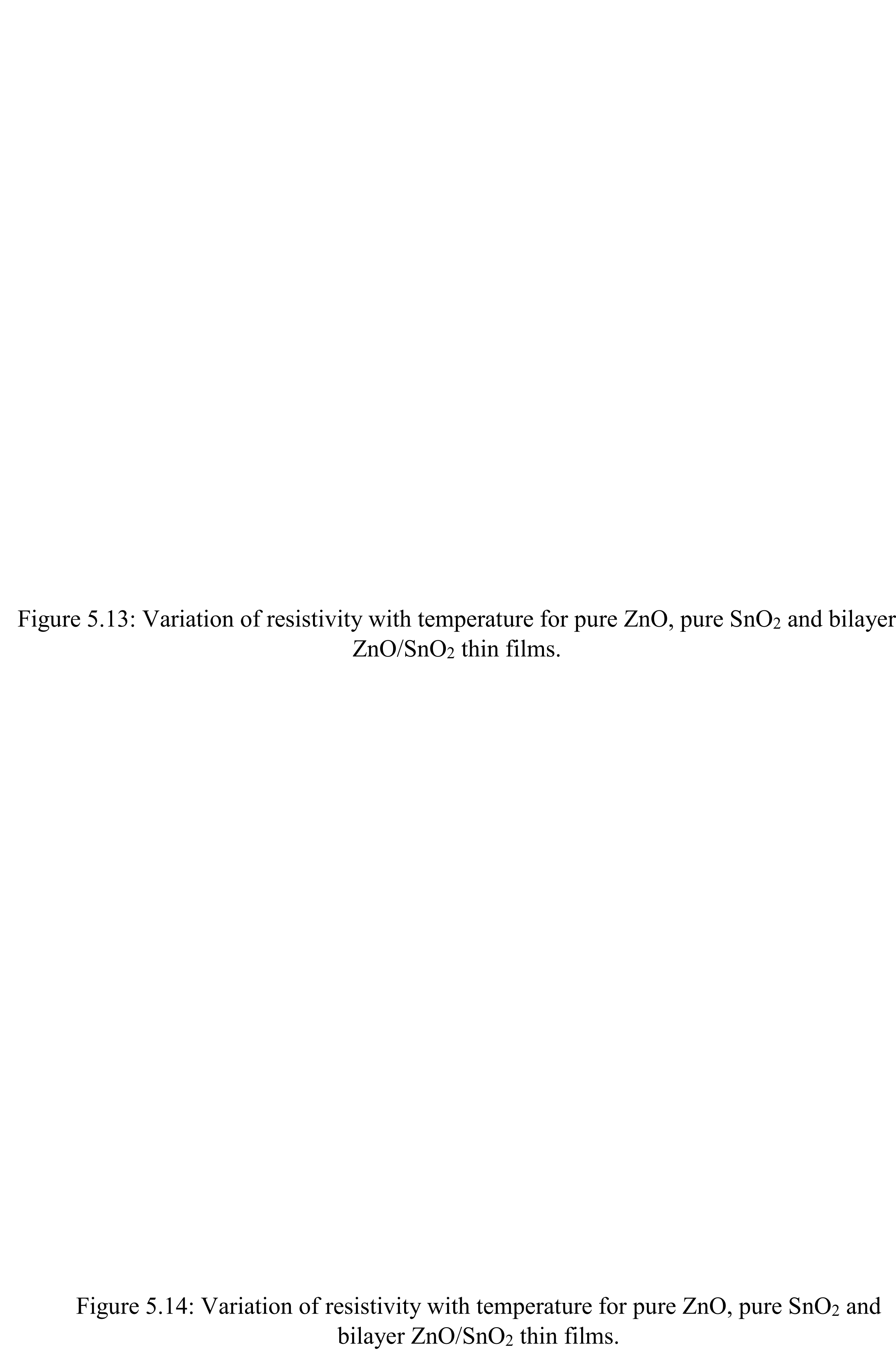

Figure 5.13: Variation of resistivity with temperature for pure ZnO, pure SnO_2 and bilayer ZnO/SnO_2 thin films.

Figure 5.14: Variation of resistivity with temperature for pure ZnO, pure SnO_2 and bilayer ZnO/SnO_2 thin films.

5.6.3 Variation of sheet resistance with temperature

Sheet resistance is a measure of resistance of thin films that are nominally uniform in thickness. Sheet resistance is applicable to two-dimensional systems in which thin films are considered two-dimensional entities. The sheet resistance can be calculated using the equation

$$R_S = \frac{\rho}{t}$$

Here ρ is the resistivity of the deposited thin films and t is the thickness. The sheet resistances of the deposited bilayer thin films are decreases with increasing the thickness of the SnO_2 layer as sheet resistance is inversely proportional to the thickness. Another reason is incorporation of Zn into SnO_2 layers imcrease carrier concentration of the film [16-17].

Figure 5.15: Variation of sheet resistance with temperature for pure ZnO, pure SnO_2 and bilayer ZnO/SnO_2 thin films.

References

[1] Kaneva N. V., and Dushkin C. D., “Preparation thin films of ZnO by sol-gel dip coating” Bulgarian Chem. Com., Vol. 43, pp. 259-263, 2011.

[2] Papadopoulos N. D., Tsakiridis P. E., Hristoforou E., "Structural and electrical properties of undoped SnO_2 films developed by a low cost CVD technique with two different methods: comparative slo.dy", Journal of Optoelectronics and Advanced Materials Vol. 7, pp. 2693 – 2706, 2005.

[3] Cai, Y., Li, X., Liu, Y., Du, S., Cheng, C., Liu, F., Shimanoe, K., Yamazoe, N., and Lu, G., “Hollow cylinder ZnO/SnO_2 nanostructures synthesized by ultrasonic spray pyrolysis and their gas-sensing performance”, Cryst. Eng. Comm., Vol. 16(27), pp. 6135, 2014.

[4] Özgür, Ü., Alivov, Y.I., Liu, C., Teke, A., Reshchikov, M. A., Dogan, S., Avrutin, V., Cho, S.J., Morko, H., “A comprehensive review of ZnO materials and devices”, J. Appl. Phys., Vol. 98, pp. 041301, 2005.

[5] Tewari S., and Bhattacharjee A., “Structural, electrical and optical studies on spray-deposited aluminium-doped ZnO thin films” Pramana J. Phys., Vol. 76, pp. 153–163, 2011.

[6] Komteenkov G., Maesaooy V., Tolstoy V., Brinzari Y., Scbwok J. and Fag1ia G, "Structural and gas response characterization of nano-size $Sn0_2$ films deposited by SILO method", Sensors and Actuators B: Chemical, Vol. 96, 3, pp. 602-609, 2003.

[7] Prabhu, M., Marikkannan, M., Mayandi, J., Soundararajan, N., and Ramachandran, K, “Heterojunction Thin Films Based On Multifunctional Metal Oxides For Photovoltaic Application”, AIP Conference Proceedings, Vol. 1591, pp. 930, 2014.

[8] Mariappan, R., Ponnuswamy, V., Suresh, P., Ashok, N., Jayamurugan, P., Chandra Bose, A., “Influence of film thickness on the properties of sprayed ZnO thin films for gas sensor applications”, Superlattices and Microstructures, Vol. 71, pp. 238–249, 2014.

[9] Paraguay-Delgado, F., Miki-Yoshida, M., Antunez, W., González Hernández, J., Vorobiev, Y.V., Prokhorov, E., “Morphology and microstructure of textured SnO_2 thin films obtained by spray pyrolysis and their effect on electrical and optical properties”, Thin Solid Films, Volume 516, pp. 1104-1111, 2008.

[10] Kim, S., Kang, D., Sichanugrist, P., and Konagai, M., “Amorphous solar cell on multilayer of SnO_2/ZnO TCO substrate for full spectrum splitting solar cell application”, Can. J. Phys. Vol. 92, pp. 917–919, 2014.

[11] Shinde, S. S., Shinde, P. S., Bhosale, C. H., and Rajpure, K. Y., “Optoelectronic properties of sprayed transparent and conducting indium doped zinc oxide thin films”, J. Phys. D: Appl. Phys., Vol. 41, 105109 (6pp), 2008.

[12] Abdelkrim, A., Rahmane, S., Abdelouahab, O., Hafida, A., and Nabila, K., “Optoelectronic properties of SnO_2 thin films sprayed at different deposition times”, Chin. Phys. B, Vol. 25, pp. 046801, 2016.

[13] Ravichandran, K., Anandhi, R., Sakthivel, B., Swaminathan, K., Ravikumar, P., Jabena Begum, N., and Snega, S., “Thickness Dependence of FTO Over-Layer on Properties of FTO/FZO Bilayer”, Materials and Manufacturing Processes, Vol. 28, pp. 1322–1326, 2013.

[14] Min, B. S., Park, Y. H., and Lee, C. S., “Fabrication and Characterization of SnO_2/ZnO Gas Sensors for Detecting Toluene Gas”, J. Nanosci. Nanotechnol., Vol. 14, 2014.

[15] Pant, R., Patel,N., Nanda, K. K., and Krupanidhi, S. B., “Negative differential resistance and resistive switching in SnO_2/ZnO interface”, Journal of Applied Physics, Vol. 122, pp. 125303, 2017.

[16] Wang, D., Wu, C., Luo, W., Guo, X., Qu, B., Xiao, L.,and Chen, Z., “ZnO/SnO_2 Double Electron Transport Layer Guides Improved Open Circuit Voltage for Highly Efficient $CH_3NH_3PbI_3$-Based Planar Perovskite Solar Cells”, Appl. Energy Mater., Vol. 1, pp. 2215−2221, 2018.

[17] Ravikumar, P., Ravichandran, K., and Sakthivel, B., “Effect of Thickness of SnO_2:F over Layer on Certain Physical Properties of ZnO:Al Thin Films for Opto-electronic Applications”, J. Mater. Sci. Technol., Vol. 28(11), pp. 999-1003, 2012.

CHAPTER SIX

CONCLUSIONS AND SUGGESTION FOR FUTURE WORK

CHAPTER SIX

CONCLUSIONS AND SUGGESTION FOR FUTURE WORK

6.1 Conclusions

In this research work, pure ZnO, pure SnO_2 and bilayer ZnO/SnO_2 thin films are deposited on glass substrate at substrate temperature 450°C for SnO_2 layer and 300°C for ZnO layer by spray pyrolysis technique. Thickness of the bilayer films is in the range of 400 to 550 nm. The effects of thickness variation of SnO_2 bottom layer on structural, optical and electrical properties of bilayer ZnO/SnO_2 thin films are investigated. The results of the present work are summarized and the following noteworthy conclusions are drawn.

The FESEM micrographs reveal that ZnO sprayed particles are covered the whole substrates uniformly and the scanned area is nicely covered with fibrous and non-fibrous ZnO thin films. For SnO_2 thin film is FESEM shown that the surface of the film is uniform, homogeneous and well covered on the glass substrate surface. FESEM images discovered that sprayed particles are adsorbed on the glass substrate into clusters as the primary stage of nucleation. The FESEM image of ZnO/SnO_2 thin films shows the presence of tightly packed agglomareted grains are uniformly distributed on the glass substrate. With the thickness increment of SnO_2 layers, the fibrous surface disappears gradually due to porous surface of SnO_2 layers. Cross sectional image shown that both the SnO_2 and ZnO layers exhibited clear lattice fringes that separated one another from the atomically sharp interface.

The XRD patterns of pure ZnO thin films deposited at T_s of 300 °C shown polycrystalline nature. The reflections are observed for (100), (002), (101), and (110) planes indicating hexagonal wurtzite type of crystal structure of the film. The XRD pattern of pure SnO_2 thin film deposited at Ts of 450 °C reveal that the SnO_2 film has polycrystalline nature with a tetragonal rutile phase of tin oxide. The (110) is the most intense peak and other peaks assigned as (101), (200), (111), (210), (211), (220), (002) and (112) orientations are also observed. This can be attributed to the density of the atoms in the (110) plane, which is the highest in the atom densities in all planes of the rutile crystal structure; therefore, the surface energy of the (110) plane is the lowest. In ZnO/SnO_2 bilayer thin films, the combined double layer film also shows crystallites of the two metal oxide compounds and there is a gradual

rise in the predominance of the (110) plane as the thickness of the SnO_2 bottom layer increases. It indicates that the growth pattern of ZnO/SnO_2 bilayer is different when compared with that of SnO_2 on the bare glass substrate. When the thickness of SnO_2 layer is high, the intensity of (110) peak of SnO_2 substantially increases indicating the good crystalline property of the double layered films.

From AFM two dimensional view shown that the ZnO, SnO_2 and ZnO/SnO_2 film surface is covered uniformly by fine grains. The three dimensional view shown that the growth of film takes place with closely placed sharp peaks and valleys. The surface roughness of the film increases with increasing thickness of SnO_2.

Form the UV-visible spectroscopy measurements it is seen that all the synthesized films are transparent in the NIR region. The direct band gap is highest for pure SnO_2 thin film about 3.68 eV. In the case of bilayer thin film band gap increases with increasing thickness of SnO_2 bottom layer. The refractive index for bilayer thin film n is decreasing with increasing thickness.

From Hall effect measurement values for pure ZnO, pure SnO_2 and bilayer ZnO/SnO_2 are given in the Table 5.3. All of the films have n-type carrier concentration. In the case of bilayer thin films carrier concentration increase with increasing thickness of SnO_2 layer.

From the electrical data it has been shown that the resistivity decreases with the increase of temperature that confirms the semiconducting nature of the films. It is also seen that the resistivity of the bilayer samples decreases with increasing the thickness of SnO_2 layer. This might be caused by the increase of carrier concentration or carrier mobility. The sheet resistances of the deposited bilayer thin films are decreases with increasing the thickness of the SnO_2 layer as sheet resistance is inversely proportional to the thickness. Another reason is incorporation of Zn into SnO_2 layers imcrease carrier concentration of the film.

In this study, the results obtained from surface, structural, optical and electrical characteristics of bilayer ZnO/SnO_2 nanocomposite thin films are found to be in good agreement with the previous reported data by other researchers. The bi-layered films were found to have better electrical and optical properties than single layer films. The Eg value of the ZnO/SnO_2 bi-layer was found to be well within the range of wide band gap of TCOs

generally used in photovoltaic and other optoelectronic applications. The sheet resistance value of bi-layer ZnO/SnO_2 film was found to be morelesser than that of the single layered films. It was seen from AFM images that the bi-layer film showed a surface with good packing density and homogeneity. The optical, electrical and surface morphological studies showed that the bi-layered ZnO/SnO_2 film was found to be suitable for gas sensing application and other opto-electronic devices more effectively.

6.2 Suggestions for future work

This is the first time that bi-layer ZnO/SnO_2 thin films have been prepared in our laboratory. We have deposited bi-layered ZnO/SnO_2 thin films on glass substrate at 300°C (ZnO) and 450 °C (SnO_2) substrate temperature and studied some of their morphological, structural, electrical and optical properties. More investigations are needed to explain different characteristics elaborately, which will help to reveal the suitable applications of bi-layered ZnO/SnO_2 thin films, such as:

1. To study higher resolution image by transmission electron microscopy (TEM)
2. To study the gas sensitivity measurement.
3. To study the variation of the structural, optical and electrical properties of the bi-layered ZnO/SnO_2 thin films with annealing temperature.
4. To study the bi-layered ZnO/SnO_2 thin films at high temperature for thermal stability.